Studies on Energy Feedback and Collective Dynamics of Hindmarsh-Rose Neuron Model with Electrical, Chemical and Field Couplings

Thesis submitted to the University of Calicut

in partial fulfillment of the requirements

for the award of the degree of

Doctor of Philosophy in Physics

Under the Faculty of Science

Usha K.

Department of Physics

University of Calicut

Malappuram Dt., Kerala. 673 635

October 2018

CERTIFICATE

Certified that the work presented in this thesis entitled 'Studies on Energy Feedback and Collective Dynamics of Hindmarsh-Rose Neuron Model with Electrical, Chemical and Field Couplings' is a bonafide work done by Mrs. Usha K. under my guidance in the Department of Physics, University of Calicut and that this work has not been included in any other thesis submitted previously for the award of any degree.

Farook College
October 2018

Dr. P. A. Subha
(Supervising Guide)

DECLARATION

I hereby declare that the work presented in this thesis entitled 'Studies on Energy Feedback and Collective Dynamics of Hindmarsh-Rose Neuron Model with Electrical, Chemical and Field Couplings' is based on the original work done by me under the guidance of Dr. P. A. Subha, Department of Physics, Farook College, University of Calicut, and has not been included in any other thesis submitted previously for the award of any degree.

University of Calicut

October 2018 Usha K.

Acknowledgements

First and foremost, I wish to express my heartfelt gratitude to my mentor, guide and teacher, Dr. P. A. Subha, Head of the Department of Physics, Farook College, University of Calicut, for introducing me to this exciting field. Her supervision, valuable help with appropriate questions and support helped me to complete this work successfully. She taught me to think critically, to select problems, to solve them and to present their solutions. I hereby record my indebtedness to her for guiding me with so much patience and affection.

I express my sincere gratitude to Prof. (Dr.) P. P. Pradyumnan, Head of the Department of Physics, University of Calicut, for his support and cooperation. I thankfully remember his valuable suggestions in all matters associated with the submission of the thesis. I am also thankful to the former Heads of the Department, Prof. (Dr.) George Varghese, Prof. (Dr.) Antony Joseph, Prof. (Dr.) M M Musthafa for their help and support. I am deeply indebted to Dr. Mohamed Shahin T., my co-guide, for his kindness and encouragements. I would like to thank all the other faculties of Department of Physics for their support and inspiration. I am thankful towards the library and office staffs of this department for the helps they rendered during the entire course of my research.

It's a pleasure to acknowledge Prof. E. P. Imbichikoya, former Principal, Farook college and Dr. K. M. Naseer, Principal, Farook college, for their support to complete my research work. Dr. K. K. Abdullah, former Head of the Department of Physics, Farook college, deserves special mention for his interests in my research.

I am indebted to all the faculties of Department of Physics, Farook College, for their cooperation. I owe greatly to the staffs in the informatics centre, Farook College, for providing the technical support.

I am deeply indebted to Dr. Chitra R. Nayak, Assistant Professor, Department of Physics, Tuskegee University, USA, for the effective discussions and helps at various stages of fledgling. Her valuable suggestions helped me a lot to tackle the problem and to do the numerical simulations. It's a pleasure to share my love and respect for her. I am expressing my deep love and gratitude to Mrs. Suneera T. P., Head of the Department of Physics, Govt. College Madappalli, for extending a helping hand whenever I needed. I thankfully remember her constant support, motivation and help during the numerical works. My special thanks to Prof. A. Sreekumar, former Principal, Sri Vyasa NSS College, for his keen interest and motivation in my research work.

Special thanks to Raheena K. K. and Sreepriya M. K. for their active involvement during the initial stages of work. Thanks to VidyaRajan and Sebastian Koothottil for their constant support. I express my deep sense of gratitude to T. Remi for her valuable helps. I also thank N. M. Mussammil and K. Aysha Muhsina for their helps offered during this period. My special thanks to S. Leo Kingston and Sunsu Kurian for the fruitful discussions. I express my love and gratitude to all the research scholars, Mphil and Msc students of Calicut University for the delightful moments we enjoyed together in the university campus and hostel.

I would also like to acknowledge the financial support provided by the University Grants Commission, New Delhi, in the form of Junior Research Fellowship.

I thank my family members and friends for their constant support and encouragement throughout my research career.

Usha K.

Contents

List of Figures

Preface

Nonlinear physics finds its own unique requirement to study natural systems where linear systems are mere approximations. Nonlinear systems exhibit complex dynamics and such systems are modelled using nonlinear differential and difference equations. In effect, the solutions of nonlinear equations do not obey the principles of superposition and proportionality. A nonlinear system is said to be chaotic if its behaviour is highly sensitive to the initial conditions. In such systems, two orbits starting near to each other will diverge exponentially as the system evolves in time. This makes long term predictions impossible. Chaotic behaviour is common in electronics, photonics, superconductivity, chemical reactions and biological systems.

Nonlinear models are widely used to study biological phenomena such as population dynamics, heart rhythms and electrical brain activity. The epileptic seizures and the cardiac rhythm observed in electrocardiogram exhibit chaotic behaviour. Chaos in a pacemaker neuron with bursting dynamics has been reported. Hodgkin and Huxley approached the problem of propagation of action potentials in neurons by developing a set of differential equations for the parameters that govern the ion channel states, known as the Hodgkin-Huxley (HH) equations. Later Hindmarsh and Rose proposed a neuron model which is capable of exhibiting spiking and bursting behaviour of membrane potential observed in experiments. The analysis of Hindmarsh-Rose (HR) model is of significant interest because of its ability to produce both simple and complex oscillations by varying the external stimulus.

An average human brain consists of nearly 10^{11} neurons. They communicate

with one another at junctions known as synapses. Based on the mode of impulse transmission, synapses are classified as electrical and chemical. To perform a specific function, large number of neurons are interconnected to form networks. Global, lattice, nonlocal and star are some important network topologies. The transmission of nerve impulse is an energy demanding process. A major portion of the total energy consumed by brain is utilised for this. Therefore it is interesting to investigate the energy aspects of neurons during information encoding. The control of chaotic trajectories by applying a negative feedback in the Hamilton energy function is also an interesting area with vast applications.

This thesis presents a theoretical study of the energy aspects and collective dynamics of HR neuron model with electrical, chemical and field couplings. The structure of the thesis is as follows. **Chapter 1** gives a basic introduction to nonlinear systems, nonlinear biological systems, neuron models, HR neuron model, coupling topologies and methods of analysis. In **Chapter 2**, a unidirectional star network with electrical coupling has been studied. Controllers have been used to produce synchronisation and other collective behaviours. Interesting dynamics like Drum head mode (DHM), Mixed oscillatory state (MOS), desynchrony and multi cluster states have been formed before settling to complete synchrony in the presence of modified controllers. **Chapter 3** discuss the dynamics of chemically coupled HR neurons in unidirectional and bidirectional star topology. The synchronisation transitions are verified by plotting the Transverse Lyapunov exponents (TLEs). The synchronised, desynchronised and DHM regions have been observed, when the neurons are connected in unidirectional and bidirectional coupling configurations. A detailed analysis of the time evolution of membrane potential corresponding to each region has been presented. The annihilation of synchronised region and the expansion of DHM region in bidirectional coupling have been discussed using parameter space.

In **Chapter 4**, we have analysed single and two coupled HR neurons with field effects. Memristors are used to model the relations between magnetic flux of the electromagnetic field and the membrane potential of interacting neurons.

The bifurcation analysis has been carried out by varying the modulation intensity of induced current on the membrane potential. The two coupled system with electrical, chemical and field couplings has been studied. Important dynamical behaviours such as synchrony, desynchrony, Amplitude Death (AD), anti-phase oscillations, coexistence of resting and spiking state and near death rare spikes are observed. In all cases the TLEs are plotted to observe the point of transition from desynchrony to synchrony.

Chaos control via energy feedback in modified HR neuron model with different external stimuli have been studied in **Chapter 5**. The Hamilton energy of the system has been derived. The time evolution of membrane potential and the rate of change of energy function have been analysed. The dependence of Hamilton energy function on system parameters is used to control and stabilise chaotic trajectories by giving a negative energy feedback. The energy aspects of two HR neurons with synaptic coupling and field effects have also been studied in **Chapter 5**. The study has been extended to a star network of HR neurons with electrical, chemical and field couplings in **Chapter 6**. The collective behaviour and the energy aspects have been discussed. The electrically coupled network with field effects shows desynchronised and synchronised regions, whereas in the presence of chemical coupling and field effects, the system exhibits desynchrony, synchrony and DHM region. The parameter space has been plotted to explain the transition from desynchronised to synchronised state and DHM region. The time evolution of membrane potential in the absence of synaptic coupling reveals that, the field coupling regulates the electrical modes of the system. The energy aspects of the network with synaptic coupling and field effects have been analysed. In electrically coupled star network with field effects, the energy returns to its initial uncoupled value in the synchronised state. The average energy variations of chemically coupled system with field effects have also been analysed.

Chapter 7 summarises the findings of the thesis and describes future prospects of this work.

Papers Published

1. **K. Usha**, P. A. Subha, Chitra R. Nayak, The route to synchrony via drum head mode and mixed oscillatory state in star coupled Hindmarsh-Rose neural network. Chaos, Solitons, and Fractals, 108, 25-31, 2018.

2. **K. Usha**, P. A. Subha, Star-coupled Hindmarsh-Rose neural network with chemical synapses. International Journal of Modern Physics C, 29, 1850023, 2018.

3. **K. Usha**, P. A. Subha, Hindmarsh-Rose neuron model with memristors. BioSystems, 178, 19, 2019.

4. **K. Usha**, P. A. Subha, Energy feedback and synchronous dynamics of Hindmarsh-Rose neuron model with memristor. Chin. Phys. B, Vol. 28, No. 2, 020502, 2019

5. **K. Usha**, P. A. Subha, Collective dynamics and energy aspects of star-coupled Hindmarsh-Rose neuron model with electrical, chemical and field couplings. Nonlinear Dyn, 96, 2115-2124, 2019.

Conference Presentations

1. **K. Usha**, K. K. Raheena, P. A. Subha, Dynamics of coupled bursting neuron model driven by a periodic force. 8^{th} Conference on nonlinear systems and Dynamics, IIT Indore, December 2013.

2. **K. Usha**, K. K. Raheena, P. A. Subha, Synchronisation of coupled Hindmarsh-Rose neuron model. 26^{th} Kerala Science Congress, Wayanad, January 2014.

3. **K. Usha**, M. K. Sreepriya, P. A. Subha, Energy consumption in conductance based neuron models exposed to an electromagnetic radiation of varying frequency and amplitude. National Conference on Modern Optics and Material science, Farook College, University of Calicut, December 2015.

4. **K. Usha**, P. A. Subha, Synchronisation of Hindmarsh-Rose Neural Network with linear gap junction coupling. National Seminar on Dynamical Systems and Chaos. St. Mary's College, University of Calicut, January 2016.

5. **K. Usha**, M. K.Sreepriya, P. A. Subha, Energy consumption in Hodgkin-Huxley type fast spiking neuron model exposed to an external electric field. International Conference on Engineering and Material Science (ICEMS), Jaipur, Rajasthan, March 2016.
   Conference paper - Perspectives in Science, **8**, 132-134, 2016 (ISSN: 2213-0209).

6. **K. Usha**, P. A. Subha, Chitra R. Nayak, Synchronisation of electrically coupled HR neurons. International Conference on Nonlinear Physics: Theory and Experiment. Farook College, University of Calicut, December 2016.

7. **K. Usha**, P. A. Subha, Combined effect of electrical and chemical synapses in star coupled Hindmarsh-Rose neural network. Annual Physics Symposium: St. Teresa's College, Ernamkulam, December 2017.

List of Abbreviations

IF	Integrate and Fire
HH	Hodgkin-Huxley
ML	Morris-Lecar
FHN	FitzHugh-Nagumo
HR	Hindmarsh-Rose
DHM	Drum Head Mode
MOS	Mixed Oscillatory State
OD	Oscillation Death
AD	Amplitude Death
LE	Lyapunov Exponent
LLE	Largest Lyapunov Exponent
TLE	Transverse Lyapunov Exponent
EEG	Electroencephalography
MEG	Magnetoencephalography
fMRI	functional Magnetic Resonance Imaging
NDE	Near Death Experience
ISI	Inter Spike Interval

Chapter 1

Basic Concepts and Thesis Outline

1.1 Introduction

The time evolution of physical systems depend on the nature of force acting on them and the initial state and are generally classified as linear and nonlinear. Nonlinear physics finds its own unique requirement to study natural systems where linear systems are mere approximations. The behaviour of a nonlinear system composed of several components cannot be fully understood and predicted by dividing the components and studying out their individual characteristics. The output of such a system is not proportional to its input and they do not obey the principles of superposition and proportionality. In such systems, small changes in initial condition causes drastic and unpredictable results. It is something like changing the rules of a game depending upon its current status thus generating surprises.

A nonlinear system is said to be chaotic if its behaviour is highly sensitive to the initial conditions. In such systems, two orbits starting close to each other will diverge exponentially as the system evolves in time. This makes long term predictions impossible. Nonlinear phenomena find its applications in almost all

fields such as electronics, photonics, superconductivity, chemical reactions and biological systems. Differential equations and iterated maps (difference equations) serve as useful tools for analysing chaotic systems. Differential equations express the time evolution of systems in continuous time, whereas difference equations are applied in situations where time is discrete [1]. Some well known examples of nonlinear systems modelled using differential equations and maps are given below.

Lorenz System:

Edward Lorenz proposed a nonlinear, three-dimensional, non-periodic and deterministic model to study the atmospheric convection in 1963. The governing equations are of the form:

$$\begin{aligned} \dot{x} &= \sigma(y - x), \\ \dot{y} &= x(\rho - z) - y, \\ \dot{z} &= xy - \beta z. \end{aligned} \tag{1.1}$$

The variables x, y and z denote the rate of convection, horizontal temperature variation and vertical temperature variation respectively. The system posses chaotic solutions for suitable parameter values and initial conditions [2].

Rössler System:

In 1976, Otto Rössler designed the Rössler system consisting of three coupled nonlinear differential equations,

$$\begin{aligned} \dot{x} &= -y - z, \\ \dot{y} &= x + ay, \\ \dot{z} &= b + z(x - c). \end{aligned} \tag{1.2}$$

The system has three variables x, y and z and three parameters a, b and c. It contains only one quadratic term and its chaotic attractor has a single lobe [3].

Logistic Map:

The logistic map is generally used in population biology. It maps the population dynamics with a single first order difrerence equation having the form:

$$x_{(n+1)} = Ax_n(1 - x_n) \tag{1.3}$$

where x_n and $x_{(n+1)}$ are the populations of the n^{th} and $(n + 1^{th})$ generations respectively. A represents the growth rate [1].

Nonlinear problems are of interest to scientists of all disciplines because of its promising applications in physical, chemical, social, economic and biological systems.

1.2 Nonlinear Biological Systems

Biological systems are well known for their complex behaviours. Nonlinear models are widely used to explore the intriguing dynamics of such systems. Some examples of biological systems modelled using nonlinear equations are population dynamics, heart rhythms and electrical brain activity. The epileptic seizures and the cardiac rhythm observed in electrocardiogram exhibit chaotic behaviour [4]. Chaos in a pacemaker neuron with bursting dynamics was reported [5, 6]. Experimental data from intact swimming lampreys and isolated spinal cords reveal the existence of unstable periodic orbits in the phase space of the systems [7]. Complex neural networks also exhibit chaotic behaviour [8]. The dynamics of ion channels and the exchange of ions influence the properties of neurons. This thesis analyses neurons as nonlinear dynamical system.

1.2.1 Brain and Neurons

Brain, neurons and sense organs constitute the control network of our body. An average human brain contains approximately 10^{11} neurons that carries information around the body in the form of electrical impulses. Electrical signals from the sense organs shoot along the nerves and propagate towards the brain. A

typical nerve cell has one large fibre called 'axon' that carries outgoing electrical signals and a large number of smaller fibres termed as 'dendrites' that receive incoming signals.

1.2.2 Spike Generation Mechanism in Neurons

The difference in voltage across the nerve membrane is termed as the membrane potential. In neurons, the dendrites, axon and cell body show different electrical properties due to the presence of different types of ion channels. This leads to the generation of an action potential called 'nerve impulse' or 'spike' and a sequence of such spikes are called a 'spike train' [9]. The membrane potential has two important states. One is the resting potential that a cell maintains if nothing perturbs it and the other is a higher value called the threshold potential. In a typical neuron, the resting and threshold potentials are around $-70mV$ and $-55mV$ respectively. A stimulus induces some potential variations in the nerve membrane. Action potentials are triggered when enough depolarisation accumulates to bring the membrane potential up to a threshold. After reaching the threshold, the membrane potential rapidly increases and then shoots back downwards, sometimes ending below the resting potential value. A shematic diagram of spike generation in neuron is represented in Fig. 1.1. In bursting state, the neuron repeatedly fires separate groups of spikes where each burst is followed by a quiescent period. Bursting neurons are important for motor pattern generation and synchronisation [10]. Hodgkin and Huxley approached the problem of propagation of action potentials in neurons by developing a set of differential equations. These equations form the foundation for most of the studies and for the formulation of other models.

1.3 Neuron Models

The mechanism of impulse transmission in neuron is studied through modelling the dynamical nature of its electrical properties.

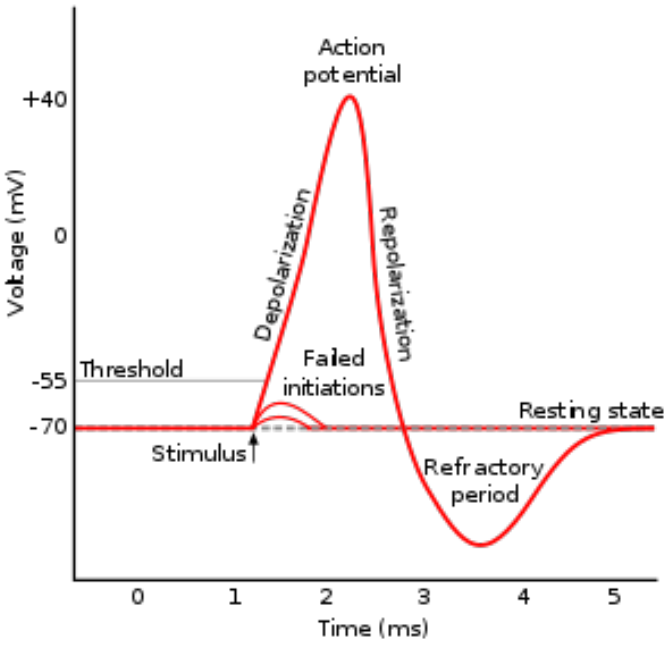

Figure 1.1: Schematic diagram of spike generation in neuron.

The variables describing neurons can be classified as follows [10].

- Membrane potential
- Excitation variables: The variables that denote the activation of a Na^+ current and are responsible for the upstroke of the spike.
- Recovery variables: Regulates the inactivation of Na^+ current and the activation of K^+ current which are responsible for the down stroke of the spike.
- Adaptation variables: Denotes the activation of Ca^{2+} dependent currents. This can affect the excitability of the system.

Some important neuron models are listed below.

1.3.1 Integrate and Fire (IF) Model

IF model is one of the simplest model, consisting of only one differential equation. When an input current is applied, the membrane potential increases until it

reaches a threshold V_{th}, then a delta function spike occurs and the voltage resets to its resting potential [11]. The model exhibits limited outputs, usually tonic spiking activity only.

1.3.2 Hodgkin-Huxley (HH) Model

HH model is a conductance based model that describes the generation and propagation of action potentials in neurons. Based on the data from the squid giant axon, the model connects the ion currents crossing the neuron and the membrane voltages. The model consists of four differential equations and has many tunable coefficients [12]. Hodgkin and Huxley were awarded the 1963 Nobel prize in physiology for this model.

1.3.3 Morris-Lecar (ML) Model

The voltage oscillations observed in barnacle muscle fibers lead Morris and Lecar to propose an accurate bio-physical model. In ML model each variable has some biological relevance. Output exhibits spiking activity but bursting dynamics is not observed [13].

1.3.4 FitzHugh-Nagumo (FHN) Model

The model describes regenerative self-excitation by a nonlinear positive feedback membrane potential and recovery by a linear negative feedback gate voltage. The resulting model is more analytically and numerically tractable and it maintains certain biophysical meaning. This model explains dynamical mechanism of spiking, the excitation phenomenon and the post-inhibitory spikes. However, there are some disadvantages. The FHN model is not capable of explaining the firing threshold and tonic bursting exactly [14].

1.3.5 Hindmarsh-Rose (HR) Neuron Model

Hindmarsh and Rose proposed a neuron model consisting of three coupled first order differential equations which is capable of exhibitting spiking and bursting behaviour of membrane potential observed in experiments. The model has the form:

$$\begin{aligned} \dot{x} &= y + ax^2 - x^3 - z + I, \\ \dot{y} &= 1 - bx^2 - y, \\ \dot{z} &= r(R(x - x_e) - z), \end{aligned} \tag{1.4}$$

where x denotes the membrane potential. y is the recovery variable representing the rate of change of fast current of K^+ or Na^+ ions and z denotes the adaptation variable which capture the slower dynamics of other ion channels (e.g., Ca^+). The parameter a denotes activation of the fast ion channel. 'a' regulates the switching between bursting and spiking dynamics and controls the spiking frequency. The parameter b describes inactivation of the fast ion channel. R and x_e describe the activation and the inactivation of the slow ion channel. A unitary value of R determines spiking dynamics without accommodation and subthreshold adaptation, whereas $R = 4$ give strong accommodation. x_e sets the resting potential of the system. The speed of variation of z is controlled by the parameter r [15, 16]. When the model exhibits spiking behaviour, r regulates the spiking frequency, whereas in the case of bursting, it affects the number of spikes per burst. The parameter I represents the external stimulus that reaches the neuron. The model describes the firing behaviour of neurons and can be decomposed into a slow fast system and the slow oscillations of z drive the fast subsystem (x, y) through periods of quiescent and oscillatory behaviour. Real neurons show a variety of dynamical behaviours, according to the values of biophysical parameters. If the parameters of the model in Eq. 1.4 are chosen as $a = 3.0$, $b = 5.0$, $R = 4.0$, $r = 0.006$ and $x_e = -1.61$ [17],

the model exhibits resting state, regular spiking, regular bursting and chaotic bursting by varying I. For low I values, the trajectories are stabilised. As I is increased, the behaviour of the system changes from periodic spiking to periodic bursting/ chaotic state [18], i.e., the HR model reproduces all the dynamical behaviours exhibitted by real neurons.

The HR model is widely studied because of the following characteristics.

- Low dimensional nature.
- Produces spiking and bursting property of neurons.
- Describes the generation of action potentials.
- Exhibits simple and complex oscillations.

This is the selected neuron model for our study.

1.4 Electrical, Chemical and Field Couplings

A synapse is a structure that permits a neuron to pass a signal to another neuron. Electrical and chemical synapses are the two major forms. Electrical synapses connects the cytoplasm of nearby neurons directly, as a result the transmission of electrical impulses occur quickly [19]. The speed of transmission is of great advantage in the tail muscles of crayfish and other organisms which show escape mechanism where a rapid response is needed [20]. In chemical synapse the transmission of information takes place via the release of a neurotransmitter. Recent studies show that synaptic dysfunction leads to major neurodevelopmental diseases like epilepsy, down syndrome and autism and neurodegenerative diseases such as Parkinson's and Alzheimer's disease. Understanding the common reasons of disease associated synaptic dysfunction can offer significant clues towards synapse based treatments for neurological and neuropsychiatric disorders [21].

Recent studies also focus on the effect of field coupling in information transmission. In nerve cells the fluctuation in concentration of ions across the nerve

membrane creates an electromagnetic field and modulates the induced currents. Memristor is used to bridge the membrane potential of interacting neuron and magnetic flux associated with the field. The field coupling can contribute greatly towards signal transmission between neurons [22].

1.5 Coupling Topologies

To study the collective dynamics of neurons suitable coupling topologies can be employed. Global, nearest neighbour, star and nonlocal couplings are widely studied with unidirectional and bidirectional connections. In globally coupled networks each oscillator is coupled to all others in the network [23]. In the case of nearest neighbour coupling, each oscillator is connected to its nearest ones only. If there is no connection between the first and the last oscillator, it is known as nearest neighbour coupling with fixed ends (chain). If there exist a connection between the first and last one, the configuration is named as ring type nearest neighbour coupling of oscillators [24]. Neuronal networks are often structured in topologies where strong interconnections are found within a range, but much fewer connections exist at longer distances, which is termed as nonlocal coupling [25]. In star coupling, all oscillators are connected to only one common oscillator in the network. A peculiar feature of star topology is the usage of fewer number of connections compared to other coupling schemes [26]. Schematic diagram of some coupling topologies are shown in Fig. 1.2. Recent studies also focus on networks of networks called multilayered networks which take into account the interacting real world networks. Metabolic network, gene regulation network and protein interaction network can be connected in multilayer topology [27].

1.5.1 Collective Dynamics

The emergence of various collective dynamics strongly depend on the properties of individual cells, type of coupling and network topology [28, 29]. One of the central topics of network dynamics is synchronisation. Christiaan Huygens was

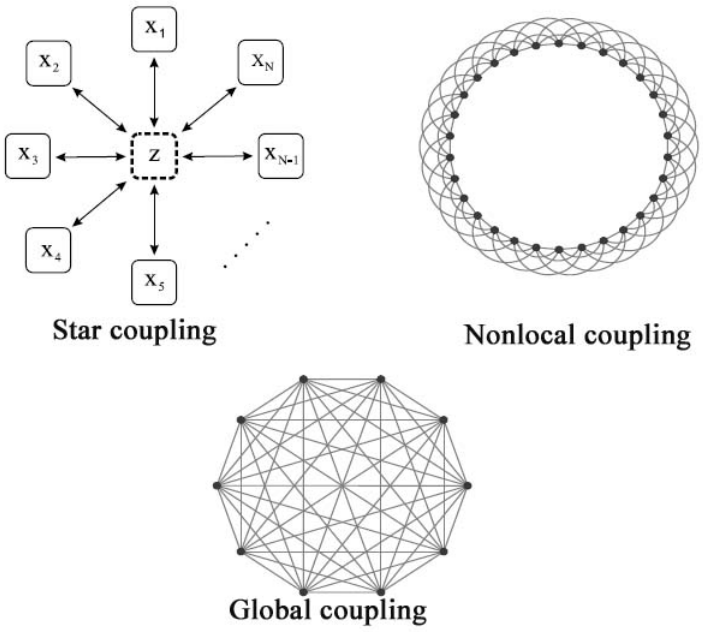

Figure 1.2: Star, nonlocal and global coupling of oscillators.

the first one to observe the synchronisation of two coupled pendulum clocks in 16^{th} century [30]. The mean field approach to synchronisation was developed by Winfree in 1967 [31] and the analysis of pulse coupled oscillators to study cardiac cells were carried out by Peskin in 1975 [32]. Motivated by the dynamics of chemical and biological oscillators, Kuramoto *et al.* proposed a model which describes the synchronisation of a large array of coupled oscillators [33]. Circadian rhythm, uterus contractions at the time of delivery, insulin oscillators and glycolytic oscillators are some examples of biological processes where synchronisation plays the major role. During the transition to sleep the thalamocortical neurons show synchronised bursting activity, whereas they exhibit desynchronised tonic spiking in waking state [34]. The tremor associated with Parkinson's disease originates as a result of the synchronised firing of sensory-motor nuclei [35]. Different kinds of synchronisation have been reported in literature, which include, complete synchronisation characterised by the equality of state variables of coupled oscillators [36]. The phases of unsynchronised chaotic oscillators become locked as the coupling strength is increased and it is termed as phase synchronisation [37–39]. Generalized, lag and frequency synchronisation are also

well studied in literature [40–42].

Other than synchronous firing, the network also exhibits various kind of attracting patterns, which include, Drum Head Mode (DHM), Mixed Oscillatory State (MOS), cluster formation and chimera state [25, 29, 43]. When the neurons control the oscillatory behaviour of each other through interaction, oscillation quenching in the form of Oscillation Death (OD) and Amplitude Death (AD) are also observed. In AD, all oscillators are stabilised to a single equilibrium, whereas in OD the coupled systems are stabilised to multiple equilibria [44]. This phenomena can be used as an effective control method to suppress unwanted oscillations [45]. Anti phase oscillations are of great interest, because it helps to distinguish different functional regions of brain [46]. Near death rare spikes are also observed when memristor effects are considered.

1.6 Methods of Analysis

1.6.1 Stability Analysis

Stability theory plays a central role in system analysis. A stable system means its output is bounded within an admissible limit. Consider a dynamical sytem described using a differential equation of the form:

$$\dot{X} = F(X). \tag{1.5}$$

Where $X = (x, y, z)$ and $F = (f_1, f_2, f_3)$. The solution to the function $F(X) = 0$ i.e., ($\dot{x} = 0$, $\dot{y} = 0$ and $\dot{z} = 0$) is defined as the fixed point (equilibrium point). Fixed points are considered as the organising centers of the system's phase space dynamics [47]. It is always possible to build up an approximate local phase portrait by identifying the fixed points and drawing the phase curve in their neighbourhood [48]. Once the equlibrium points are identified, their stability can be determined by examining the evolution of some small displacement $(\delta x, \delta y, \delta z)$

about the equilibrium point(x_0, y_0, z_0). The disturbed system has the form:

$$\begin{bmatrix} \delta\dot{f}_1 \\ \delta\dot{f}_2 \\ \delta\dot{f}_3 \end{bmatrix} = \begin{bmatrix} \frac{\partial f_1}{\partial x} & \frac{\partial f_1}{\partial y} & \frac{\partial f_1}{\partial z} \\ \frac{\partial f_2}{\partial x} & \frac{\partial f_2}{\partial y} & \frac{\partial f_2}{\partial z} \\ \frac{\partial f_3}{\partial x} & \frac{\partial f_3}{\partial y} & \frac{\partial f_3}{\partial z} \end{bmatrix} \begin{bmatrix} \delta x \\ \delta y \\ \delta z \end{bmatrix}$$

$$\begin{bmatrix} \delta\dot{f} \end{bmatrix} = \begin{bmatrix} J \end{bmatrix} \begin{bmatrix} \delta f \end{bmatrix}$$

Where J is the Jacobian matrix of the system. The eigenvalues are the roots of the equation,

$$det|J - \lambda I| = 0. \tag{1.6}$$

By identifying the sign of the eigenvalues, we can predict the stability of fixed point. If all the eigenvalues are negative, the fixed point is stable, otherwise unstable [47].

1.6.2 Lyapunov Exponent (LE)

To characterise the rate of divergence or convergence of infinitesimally close trajectories in the phase space, LEs are used. A positive value for LE indicates chaotic dynamics. Consider a nonlinear dynamical system represented as $\dot{X} = F(X(t))$, where $X(t) = (x_1(t), x_2(t), x_3(t), ...)$ represents the state variables of the system and $F(X(t))$ is the nonlinear function that regulates the time evolution of the system. Let $X(0)$ be the initial point of $X(t)$ and $X(0)+\delta X(0)$ is the starting point of a nearby trajectory. The separation between these two trajectories with time is represented as $\delta X(t)$, then the LE of the system can be expressed as,

$$\lambda = \lim_{t\to\infty} \frac{1}{t} log \frac{||\delta(X(t))||}{||\delta(X(0))||}. \tag{1.7}$$

We apply the algorithm proposed by Wolf *et al.* to evaluate the LEs in this thesis [49].

1.6.3 Transverse Lyapunov Exponent (TLE)

In a coupled system, identical synchronisation is achieved under suitable circumstances (like increasing the coupling strength). Then coordinates of the coupled system are restricted to a low dimensional hyperplane. For a dynamical system having variables x_1 and y_1 coupled to another system with variables x_2 and y_2, the condition for identical synchronisation is $x_1 = x_2$ and $y_1 = y_2$. If the motion is in the synchronised state, the coordinates transverse to the synchronisation manifold becomes zero. The stability of synchronisation can be quantified using the master stability approach developed by Pecora and Carroll [50]. The synchronisation is stable if the master stability function is negative at each of the transverse eigenvalues [42]. On the completely stable synchronisation manifold, the LE associated with the system for the space transverse to the synchronisation manifold should be negative. The analytical expressions for estimating the synchronisation threshold for diffusively coupled continuous and discrete time chaotic systems have been reported [51].

1.6.4 Bifurcation

The sudden change in the qualitative behaviour of the system for specific values of the control parameters are called bifurcation. The dynamics may change from periodic to quasiperiodic/chaotic state via different routes. During a bifurcation the equilibrium points may gain or lose its stability leading to the appearance, disappearance or replacement of the attractors. The bifurcation diagram can be plotted by taking the consecutive maxima of a single variable from the time series for every possible values of the control parameter. If the system is in the periodic regime, it is indicated by a single point in the bifurcation diagram. If the system is chaotic, then the time series may contain several maxima and it is represented by large number of points in the plot. Depending upon the magnitude of injected current, each cell may jump from resting to regular spiking/regular bursting/chaotic state. Information transmission in neuron not only depends on

the electrophysiological properties, but also on its dynamical properties. Based on the bifurcation dynamics, the neurons in the same area of the nervous system showing similar properties may respond to the same input in completely different ways [10]. Hence the study of dynamical properties of neurons are much useful.

1.6.5 Controllers

Regulating network properties by the application of controllers is well studied in literature [52, 53]. The control laws serve as a bridge for the estimation of unknown or abnormal parameters of the model which may indicate disease condition in the case of biological neurons and are used to create a bridge between the abnormal and the normal network [54]. The probability of neurotransmitter release of unreliable synapses has been estimated by constructing control inputs by Xue *et al.* [55]. The method proposed by Li *et al.* can be used to derive the control inputs for fractional order chaotic systems designed for prescribed performance [56]. Using Lyapunov principle of fractional differential equations the control inputs for fractional fuzzy cellular neural networks to obtain synchronisation criteria have been derived [57].

Consider two coupled dynamical systems as follows:

$$\dot{x_1} = f_1(x_1, y_1) + k(x_1, x_2),$$

$$\dot{y_1} = g_1(x_1, y_1), \tag{1.8}$$

$$\dot{x_2} = f_2(x_2, y_2) + k(x_1, x_2) + U(x),$$

$$\dot{y_2} = g_2(x_2, y_2) + U(y), \tag{1.9}$$

where, $k(x_1, x_2)$ is the coupling term. In eqn (1.9) control inputs are denoted using $U(x)$ and $U(y)$. For multilayered systems in star topology, the coupling term can be written as $k_1(x_{11}, x_{1N}) + k_2(x_{1N}, x_{2N})$. Here the first term represents connection among first and N^{th} neurons in the same network and the second term denotes the connection between the hubs of two networks. The error states are

defind as $e_x = x_2 - x_1$ and $e_y = y_2 - y_1$. Then the error dynamics takes the form $\dot{e_x} = \dot{x_2} - \dot{x_1}$ and $\dot{e_y} = \dot{y_2} - \dot{y_1}$. The Lyapunov function of the form $V = \frac{1}{2}(e_x^2 + e_y^2)$ is used to derive the controllers, where $\dot{V}$ has the form:

$$\dot{V} = e_x\dot{e_x} + e_y\dot{e_y}. \tag{1.10}$$

Now the problem of synchronisation of drive and response oscillators are transformed into a problem of realising the asymptotical stabilisation of the error variables of the system. The $U(x)$ and $U(y)$ are selected as such $\dot{V}$ remains negative on applying the controllers.

1.6.6 Hamilton Energy Function

Consider an autonomous dynamical system of the form: $\dot{x} = f(x)$, $x \in R^n$ and $f : R^n \longrightarrow R^n$ is a smooth function [58, 59]. According to Helmholtz's theorem the velocity vector field $f(x)$ can be written as,

$$f(x) = f_c(x) + f_d(x). \tag{1.11}$$

The f_c component of the vector field is conservative. It does not contribute to the energy change along any trajectory of the system and satisfies the following equation,

$$\nabla H^T f_c(x) = 0. \tag{1.12}$$

The function $H(x)$ is the generalized Hamiltonian for the conservative system as long as it can be rewritten in the form $\dot{x} = J(x)\nabla H$, where J is a skew symmetric matrix that satisfy Jacobi's closure condition [60]. The dissipative component, f_d is composed of velocity dependent terms and contribute to the divergence. The dissipation of energy due to the f_d part obeys the relation:

$$\nabla H^T f_d(x) = \dot{H}. \tag{1.13}$$

Eq. (1.13) implies that, the energy is dissipated, actively or passively, due to the f_d part of the vector field [61].
In this thesis, we use this approach to study the energy aspects and feedback of the HR neuron model.

1.6.7 Fourth Order Runge-Kutta Method

The method helps to calculate the function y, at $y(x_n + h)$, if we know the value of the function as well as its derivatives at x_n. Here h represents the step size. In Runge-Kutta method, the x values are iterated by simply adding h at each iteration. The y iteration formula is the weighted average of four values k_1, k_2, k_3, and k_4.

$$k_1 = f(x_n, y_n),$$

$$k_2 = f(x_n + \frac{1}{2}h, y_n + \frac{1}{2}k_1),$$

$$k_3 = f(x_n + \frac{1}{2}h, y_n + \frac{1}{2}k_2),$$

$$k_2 = f(x_n + h, y_n + k_3).$$

The Runge-Kutta formula has the form:

$$y_{n+1} = y_n + \frac{h}{6}(k_1 + 2k_2 + 2k_3 + k_4). \tag{1.14}$$

1.7 Outline of the Thesis

The energy aspects and collective dynamics of HR neuron model with Electrical, chemical and field couplings have been studied in this thesis. In Chapter 2, the electrically coupled star network of HR neurons with unidirectional connections has been discussed. The condition for synchronisation has been evaluated using Lyapunov function method. The dynamics of the system in the presence of controllers have also analysed. The control input generate interesting behaviours which consist of clusters of spatially coherent domains depending on the cou-

pling strength. DHM, MOS, desynchrony and multi cluster states are formed and cluster reduction takes place before settling to complete synchrony. The parameter values which lead to stable cluster formation has also discussed.
Chapter 3 is an extension of the work to chemically coupled HR neurons. A two coupled system has been studied for synchronisation by varying the coupling strength and the parameter describing the dynamics of the fast ion channel. The synchronised, desynchronised and DHM regions have been observed, when the neurons are connected in unidirectional and bidirectional star configurations. A detailed analysis about the time evolution of membrane potential corresponding to each region has been presented.

In Chapter 4, single and two coupled HR neurons in the presence of time varying electromagnetic field modelled using memristor has been analysed. The bifurcation analysis of HR neuron has been carried out by varying the modulation intensity of induced current on the membrane potential. Many important dynamical behaviours such as synchrony, desynchrony, amplitude death, anti-phase oscillations, coexistence of resting and spiking state and near death rare spikes have been observed when the neurons are coupled using electrical and chemical synapses.

The energy feedback and synchronous dynamics of HR model with memristor have been discussed in Chapter 5. The energy function for uncoupled neuron has been derived. The dynamics has been analysed in the presence of various external stimuli. The bursting mode of the system has been changed with external stimuli. The negative feedback in Hamilton energy function has been effectively used to control the chaotic trajectories and the phase space. The energy aspects during the synchronous dynamics of electrically and chemically coupled neurons have also discussed in this chapter.

In Chapter 6, the energy aspects and the collective dynamics of star coupled HR neuron model with memristor have been presented. In the presence of electrical coupling and field effects, the system exhibits desynchrony and synchrony, whereas a chemically coupled network with field effects shows desynchronised,

synchronised and DHM states. The parameter space has been plotted to explain the transition from a desynchronised to synchronised/DHM states as a function of the coupling strength and modulation intensity of electromagnetic field. The time evolution of the membrane potential in the absence of synaptic coupling has revealed that, the field coupling regulates the electrical modes of the system. The variations in average energy with synaptic coupling strength and its connection with various transitions in parameter space have been discussed.

Chapter 7 concludes the study and the future plan of work have also been discussed.

Bibliography

[1] S. H. Strogatz. *Nonlinear Dynamics And Chaos: With Applications To Physics, Biology, Chemistry And Engineering.*

[2] E. N. Lorenz. *J. Atmospheric Sciences*, 20(2):130–141, 1963.

[3] O. E. Rössler. *Phys. Lett. A*, 57(5):397–398, 1976.

[4] H. Hayashi and S. Ishizuka. *J. Theor. Biol.*, 156:269–291, 1992.

[5] M. I. Rabinovich and H. D. I. Abarbanel. *Neuroscience*, 87:5–14, 1998.

[6] A. O. Komendantov and N. I. Kononenko. *J. Theor. Biol.*, 183:219–230, 1996.

[7] S. Lesher, M. L. Spano, N. M. Mellen, L. Guan, S. Dykstra, and A. H. Cohen. *Ann. N. Y. Acad. Sci.*, 860:486–491, 1998.

[8] T. Elbert, W. J. Ray, Z. J. Kowalik, J. E. Skinner, K. E. Graf, and N. Birbaumer. *Physiol. Rev.*, 74:1–47, 1994.

[9] J. Wang, L. Chen, and X. Fei. *Chaos, Solitons & Fractals*, 31:247–256, 2007.

[10] E. M. Izhikevich. *Dynamical systems in neuroscience: The geometry of excitability and bursting.* The MIT Press, Cambridge, 2007.

[11] N. Burkitt. *Biol. Cybern*, 95:1–19, 2006.

[12] A. L. Hodgkin and A. F. Huxley. *J. Physiol. (Lond.)*, 117:500–544, 1952.

[13] C. Morris and H. Lecar. *Biophys. J.*, 35:193–213, 1981.

[14] R. FitzHugh. *Biophys. J.*, 1:445–466, 1961.

[15] J. L. Hindmarsh and R. M. Rose. *Proc. R. Soc. Lond. B*, 221:87–102, 1984.

[16] R. M. Rose and J. L. Hindmarsh. *Proc. Roy. Soc. Lond. B*, 225:161–193, 1985.

[17] V. N. Belykh, I. V. Belykh, and E. Mosekilde. *Phys. Rev. E*, 63:036216, 2001.

[18] X. Shi and Z. Wang. *Nonlinear Dyn*, 69:2147–2153, 2012.

[19] A. E. Pereda. *Nat Rev Neurosci.*, 15:250–263, 2014.

[20] R. D. Veenstra. *Cell Physiology.* Fourth edition, 2012.

[21] K. Lepeta et. al. *J. of Neurochem*, 138:785–805, 2016.

[22] Y. Xu, Y. Jia, J. Ma, T. Hayat, and A. Alsaedi. *Scientific Reports*, 8:1349, 2018.

[23] X. Zhang, A. Pikovsky, and Z. Liu. *Scientific Reports*, 7(2104), 2017.

[24] H. F. El-Nashar, Y. Zhang, H. A. Cerdeira, and A. F. Ibiyinka. *Chaos*, 13: 1216, 2003.

[25] D. M. Abrams and S. H. Strogatz. *Phys. Rev. Lett.*, 93(17):174102, 2004.

[26] H. B. Chen, Y. T. Sun, J. Gao, C. Xu, and Z. G. Zheng. 12(120504), 2017.

[27] G. Menichetti, L. Dall'Asta, and G. Bianconi. *Scientific Reports*, 6(20706), 2016.

[28] A. Pikovsky and M. Rosenblum. *Chaos*, 25:097616, 2015.

[29] L. M. Pecora and T. L. Carroll. *Int. J. Bifurcat. Chaos*, 10(2):273–290, 1999.

[30] M. Bennett, M. F. Schatz, H. Rockwood, and K. Wiesenfeld. *Proc. R. Soc. London*, 458, 2002.

[31] A. T. Winfree. *The Geometry of Biological Time*. Springer, second edition edition.

[32] C. S. Peskin. *Mathematical aspects of heart physiology*. Courant Institute of Mathematical Sciences, New York University, 1975.

[33] Y. Kuramoto and I. Nishikawa. *J. Statist. Phys*, 49, 1987.

[34] J. L. Noebels, editor. *Jasper's Basic Mechanisms of the Epilepsies*. National Center for Biotechnology Information (US), 4 edition, 2012.

[35] S. Postnova, K. Voigt, and H. A. Braun. *J Biol Phys*, 33:129–143, 2007.

[36] R. Roy and Jr. K. S. Thornburg. *Phys. Rev. Lett.*, 72(13), 1994.

[37] U. Parlitz, L. Junge, W. Lauterborn, and L. Kocarev. *Phys. Rev. E.*, 54(2): 2115–2118, 1996.

[38] D. Y. Tang, R. Dykstra, M. W. Hamilton, and N. R. Heckenberg. *Phys. Rev. E*, 57(3):3649–3651, 1998.

[39] C. Schafer, M. G. Rosenblum, J. Kurths, and H. H. Abel. *Nature*, 392: 239–240, 1998.

[40] L. Kocarev and U. Parlitz. *Phys. Rev. Lett.*, 74(5028), 1995.

[41] S. Boccaletti, J. Kurths, G. Osipov, D. L. Valladares, A. S. Pikovsky, and C. S. Zhou. *Phys. Rep*, 366(1), 2002.

[42] L. M. Pecora. *Phys. Rev. E*, 58:347–360, 1998.

[43] J. Hizanidis, V. Kanas, A. Bezerianos, and T. Bountis. *Int. J. Bifurcat. Chaos*, 24:1450030, 2014.

[44] S. K. Thottil and R. P. Ignatius. *Nonlinear Dyn.*, 87:1879–1899, 2017.

[45] A. Sharma and M. D. Shrimali. *Phys. Rev.*, 85:057204, 2012.

[46] D. Li and C. Zhou. *Front Syst Neurosci.*, 5:100, 2011.

[47] M. Tabor. *Chaos And Integrability In Nonlinear Dynamics.* 1989.

[48] Y. Yong-Bin, Z. Hong-Bin, Z. Feng-Li, Y. Jue-Bang, and L. Xiao-Feng. *Commun. Theor. Phys.*, 51:869875, 2009.

[49] A. Wolf, J. B. Swift, H. L. Swinney, and J. A. Vastano. *Physica D*, 16: 285–317, 1985.

[50] L. M. Pecora and T. L. Carroll. *Phys. Rev. Lett.*, 80:2109–2112, 1998.

[51] A. Stefanski, J. Wojewoda, and T. Kapitaniak. *Phys. Rev. E*, 70:026217, 2004.

[52] W. Jiang, B. Deng, and F. Xiangyang. *Chaos, Solitons & Fractals*, 27: 1272–1278, 2006.

[53] B. Deng, W. Jiang, and F. Xiangyang. *Chaos, Solitons & Fractals*, 29: 182–189, 2006.

[54] C. Jia, J. Wang, B. Deng, X. Wei, and Y. Che. *Chaos*, 21:013109, 2011.

[55] M. Xue, J. Wang, C. Jia, H. Yu, B. Deng, X. Wei, and Y. Che. *Chaos*, 23: 013109, 2013.

[56] Y. Li, H. Lv, and D. Jiao. *AIP ADVANCES*, 7:035106, 2017.

[57] W. Ma, C. Li, Y. Wu, and Y. Wu. *Chaos*, 27:103106, 2017.

[58] F. J. Torrealdea, A. d'Anjou, M. Grana, and C. Sarasola. *Phys. Rev. E*, 74: 011905, 2006.

[59] C. Sarasola, F. J. Torrealdea, A. d'Anjou, A. Moujahid, and M. Grana. *Phys. Rev. E*, 69:011606, 2004.

[60] S. Xin-Lin, J. Wu-Yin, and M. Jun. *Chin. Phys. B*, 24(12):128710, 2015.

[61] F. J. Torrealdea, C. Sarasola, and A. d'Anjou. *Chaos, Solitons & Fractals*, 40:60–68, 2009.

Chapter 2

Electrically Coupled HR Neurons in Star Network Topology

2.1 Introduction

The electrical coupling in neurons is characterised by its symmetric structure. The pre and post synaptic nerve membranes are very close to each other and enable a rapid transmission of impulses, both unidirectionally and bidirectionally. The synaptic junction provides a low resistance pathway for ion exchange without any leakage to the extracellular space. They play a significant role in the synchronisation of large networks of neurons [1]. The network topology strongly influences the collective response and the emergence of various patterns like synchronisation, chimera state and cluster formation. For strong coupling, the globally coupled chaotic maps show a transition from desynchrony to synchrony via the formation of clusters, i.e., all oscillators within one cluster will fire in exact synchrony. Synchronous clusters are obtained when oscillators synchronise with the members in the same group with no synchronisation among the groups [2]. Cluster formation in neural network is a mesoscale phenomenon which includes the cooperative rhythms of neuronal subpopulations, whereas synchronisation is a macroscale phenomenon with large scale patterns of activity. Cluster synchrony

is highly dependent on the structure and symmetries of the network [3]. Belykh *et al.* have reported the cluster synchronisation of nonlocally coupled oscillators [4]. Clustering in a mean-field coupled Rosenzweig-Mac Arthur model has been reported by Arumugam *et al.* [5]. In star coupled oscillators, Pecora and Carroll have reported an important desynchronisation bifurcation in which the nodes on the spokes show synchrony, while the hub exhibits different dynamics termed as DHM [6]. An interesting novel type of dynamics called MOS has been identified recently in HR neurons with nonlocal coupling [7].

In star network topology, the common oscillator is called the hub and the oscillators on the spokes of the star are termed as nodes. Star-type configuration of coupling can be realized in three versions, i.e., mutual interaction (type 1) and unidirectional coupling to the central node (type 2) or from the central node (type 3). The experimental realisation of spoke hub distribution paradigm and the importance of unidirectional coupling in human brain have been widely investigated. Identifying the hub regions and their pivotal role in the coordination of brain activities is of great importance. Hubs can be classified as provincial and connector hubs. The provincial hub occupies the middle of a single functional cluster and the connector hub links the multiple functional parts like visual and sensorimotor areas of brain [8]. The contribution of individual brain regions within the cerebral cortex to overall brain activity has been established in cat and macaque [8]. The electroencephalography (EEG), magnetoencephalography (MEG) and functional magnetic resonance imaging (fMRI) studies have also revealed the functional role of individual brain regions in integrating the overall information processing [9]. The recent studies on the synchronisation between the heart signals and EEG frequency bands have revealed that, a strong unidirectional coupling from brain to heart exists during all sleeping stages (stages 1-4) [10]. The EEG and MEG analysis on the cortical activation patterns have shown that, a remarkable unidirectional coupling from contralateral motor cortex to muscles exist in the swing leg during treadmill stereotyped walking [11]. The breathing and heartbeat generators act like two weakly coupled oscillators

and their synchronisation is enhanced by an uncorrelated noise from brain. This coupling has unidirectional nature, with a coupling direction from breathing to heart beat [12]. In communication systems, this type of network structure is important because the hub acts as a driver which controls the entire network. In computer networks, the hub in star topology can be considered as a server and the nodes as the clients.

In this chapter, we have discussed the type 2 unidirectional coupling. In section 2.2, the star coupled HR model and the collective behaviour of the network by varying the values of coupling strength and the parameter describing the dynamics of the fast ion channel have been analysed. The control inputs for synchronising the system have been evaluated using Lyapunov function method in section 2.3. DHM, MOS, cluster formation and synchronisation are also explained in section 2.3. Section 2.4 concludes the study.

2.2 Star Coupled HR Model

We have considered a network of 'N' HR neurons with electrical coupling in star unidirectional connection topology. The N^{th} oscillator has been chosen as the hub and oscillators 1 to $N-1$ have been arranged on the spokes of the star [13]. The equations have the form:

$$\begin{aligned} \dot{x_i} &= y_i + a{x_i}^2 - {x_i}^3 - z_i + I + g_e(x_N - x_i), \\ \dot{y_i} &= 1 - b{x_i}^2 - y_i, \\ \dot{z_i} &= r(R(x_i - x_e) - z_i), \qquad i = 1, 2, ..., N. \end{aligned} \tag{2.1}$$

The variable x_i denotes the membrane potential. y_i is the recovery variable and z_i denotes the adaptation variable. The subscript 'i' is the position of the neuron in the network. The parameters are chosen as $a = 3.0$, $b = 5.0$, $R = 4.0$, $r = 0.006$ $x_e = -1.61$ and $I = 3.1$ [14]. The coupling between the oscillators are established through the term $g_e(x_N - x_i)$ known as the electrical gap junction coupling. The

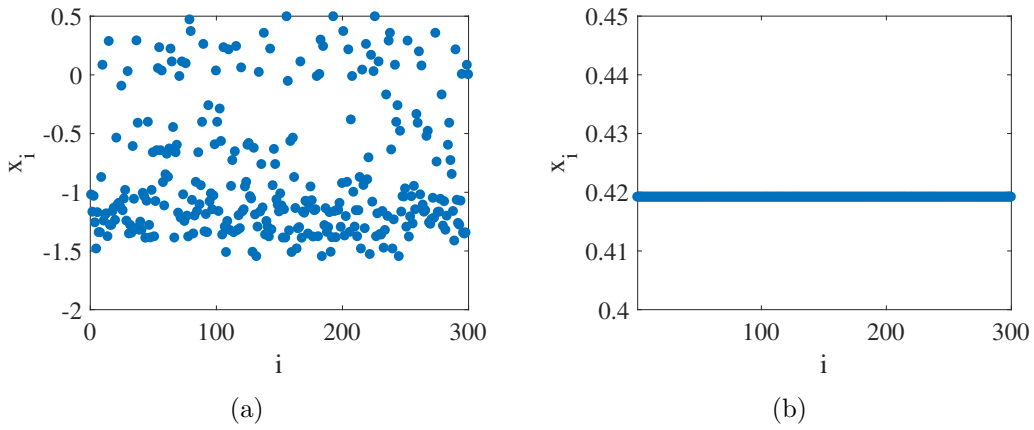

Figure 2.1: Transition from desynchronised state to complete synchrony with increase in coupling strength, where i denotes the oscillator number and x_i denotes the membrane potential of i^{th} neuron. (a) and (b) represent the dynamics of 300 HR neurons for g_e=0.1 (desynchrony) and 1.0 (complete synchrony) respectively.

parameter g_e represents the coupling strength between the oscillators. As a result of type 2 unidirectional coupling, the hub exhibits chaotic bursting irrespective of the value of g_e.

Primarily, we have analysed the collective dynamics of the system with increase in g_e using fourth order Runge-Kutta algorithm. 300 HR neurons have been used for the analysis. The parameters are identical for all neurons in the star topology. But the initial conditions for x_i, y_i and z_i are randomly chosen. For $0 < g_e < 0.85$, the oscillators show incoherent behaviour, i.e., desynchrony prevails as a result of weak coupling as indicated in Fig. 2.1(a). The chaotic systems are highly sensitive to the initial conditions and very small changes in the initial states may lead to drastic changes in the output. This is the reason for the asynchronous behaviour even with identical system parameters. When the coupling strength increases, i.e., $g_e \geq 0.85$, all neurons in the network show synchronous behaviour as illustrated in Fig. 2.1(b) with chaotic bursting time series. The star coupled HR neural network with electrical coupling shows synchronisation as the coupling strength is increased.

2.2.1 Stability of Synchronisation

The stability of synchronisation can be quantified using the master stability approach developed by Pecora and Carroll [6]. The synchronisation is stable if the master stability function is negative at each of the transverse eigenvalues. On the completely stable synchronisation manifold, the differences between neural oscillator coordinates $x_{i_\perp} = x_N - x_i$, $y_{i_\perp} = y_N - y_i$ and $z_{i_\perp} = z_N - z_i$ vanish in the limit of $t \longrightarrow \infty$ and there exists a synchronous solution $\zeta_1(t) = \zeta_2(t) = ... = \zeta_N(t)$, where $\zeta_i(t) = (x_i, y_i, z_i)$. The stability equations for perturbations transverse to the synchronisation manifold has the form:

$$\begin{aligned} \dot{x}_{i_\perp} &= y_{i_\perp} + 2axx_{i_\perp} - 3x^2x_{i_\perp} - z_{i_\perp} - g_e x_{i_\perp}, \\ \dot{y}_{i_\perp} &= -2bxx_{i_\perp} - y_{i_\perp}, \\ \dot{z}_{i_\perp} &= r(Rx_{i_\perp} - z_{i_\perp}). \end{aligned} \tag{2.2}$$

The minimal condition for the stability of synchronised state is the negativeness of the TLEs associated with Eq. (2.2) [15, 16]. Variation of two largest TLEs ($\lambda_{\perp_1}$ and $\lambda_{\perp_2}$) with increase in g_e are shown in Fig. 2.2(a). As the value of g_e is increased, the largest TLE ($\lambda_{\perp_1}$) starts to increase, reaches a peak, and then starts to decrease. The $\lambda_{\perp_1}$ crosses zero at $g_e = 0.85$ and become negative indicating a transition from desynchronised state to complete synchrony. The dynamics of the fast ion channel for weak and strong coupling has been analysed by varying the value of 'a' from 0 to 5. For weak coupling ($g_e = 0.1$), there is a desynchrony region for $2.3<a<3.3$. The largest TLE ($\lambda_{\perp_1}$) becomes positive for these 'a' values as shown in Fig. 2.2(b). From Fig. 2.2(c), it is clear that for large values of g_e (g_e =1.4), the largest TLE ($\lambda_{\perp_1}$) remains negative and the network shows synchronisation

The real part of the largest eigenvalue of the Jacobian matrix obtained by linearising Eq. (2.2) has been found to be negative, hence satisfy the criterion for stability of synchronisation.

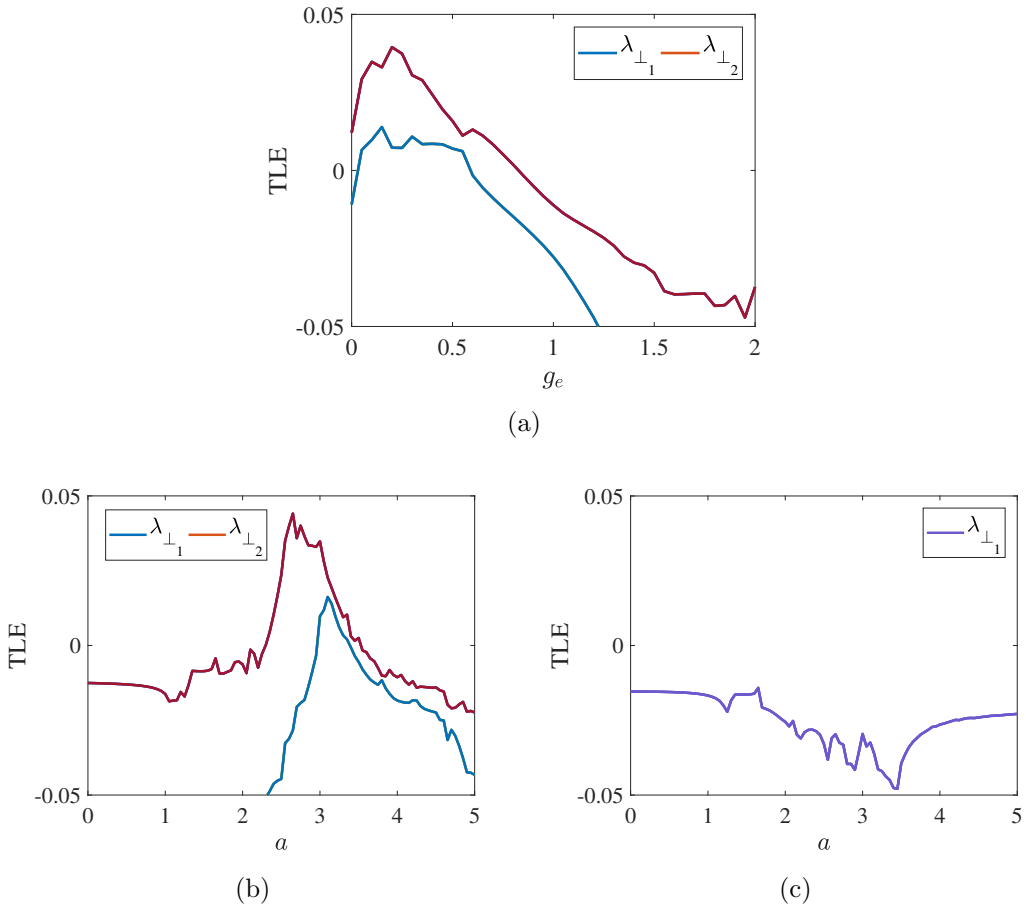

Figure 2.2: The TLEs of star coupled HR neural network. (a) g_e is plotted along x axis and TLEs along y axis. The largest TLE ($\lambda_{\perp_1}$) become negative at g_e=0.85. (b) 'a' is plotted along x axis and TLEs along y axis for $g_e = 0.1$. $\lambda_{\perp_1}$ becomes positive for 2.3<a<3.3. (c) 'a' is plotted along x axis and TLEs along y axis for $g_e = 1.4$. $\lambda_{\perp_1}$ is negative for all values of a

2.3 Analysis with Control Inputs

2.3.1 Synchronisation

We have derived the synchronisation condition for the model with control inputs using Lyapunov function method in this section. The dynamics of the system with control inputs has the following form:

$$\dot{x_i} = y_i + a{x_i}^2 - {x_i}^3 - z_i + I + g_e(x_N - x_i) + U_{(i,x)},$$

$$\dot{y_i} = 1 - b{x_i}^2 - y_i + U_{(i,y)}, \tag{2.3}$$

$$\dot{z}_i = r(R(x_i - x_e) - z_i) + U_{(i,z)}, \qquad i = 1, 2, ..., N.$$

Where $U_{(i,x)}$, $U_{(i,y)}$ and $U_{(i,z)}$ are the control inputs applied to the system. For deriving the control inputs, we have defined the error states as the deviation of each node from the hub. The synchronisation errors have been defined as: $e_{(i,x)} = x_N - x_i$, $e_{(i,y)} = y_N - y_i$ and $e_{(i,z)} = z_N - z_i$. The error dynamics has the form,

$$\begin{aligned}
\dot{e}_{(i,x)} &= e_{(i,y)} + a({x_N}^2 - x_i^2) - ({x_N}^3 - x_i^3) - e_{(i,z)} - g_e e_{(i,x)} - U_{(i,x)}, \\
\dot{e}_{(i,y)} &= -b({x_N}^2 - x_i^2) - e_{(i,y)} - U_{(i,y)}, \\
\dot{e}_{(i,z)} &= rRe_{(i,x)} - re_{(i,z)} - U_{(i,z)}, \qquad i = 1, ..., N.
\end{aligned} \tag{2.4}$$

We have considered a Lyapunov function using the difference variable [17, 18],

$$V = \frac{1}{2}\Sigma_{i=1}^{N-1}({e_{(i,x)}}^2 + {e_{(i,y)}}^2 + {e_{(i,z)}}^2).$$

Then,

$$\begin{aligned}
\dot{V} = \; & \Sigma_{i=1}^{N-1}[e_{(i,x)}e_{(i,y)} + a({x_N}^2 - x_i^2)e_{(i,x)} - ({x_N}^3 - x_i^3)e_{(i,x)} \\
& -e_{(i,z)}e_{(i,x)} - g_e{e_{(i,x)}}^2 - e_{(i,x)}U_{(i,x)} - b({x_N}^2 - x_i^2)e_{(i,y)} \\
& -{e_{(i,y)}}^2 - e_{(i,y)}U_{(i,y)} + rRe_{(i,x)}e_{(i,z)} - r{e_{(i,z)}}^2 - e_{(i,z)}U_{(i,z)}], \qquad i = 1, ..., N.
\end{aligned} \tag{2.5}$$

The controllers have been chosen to ensure that the time derivative of Lyapunov function is a negative definite. Then the errors $e_{(i,x)}$, $e_{(i,y)}$ and $e_{(i,z)}$ converge to zero as t $\to \infty$, which in turn leads to a locally asymptotically stable synchronisation manifold.

The controllers have been chosen as:

$$U_{(i,x)} = e_{(i,y)} + a({x_N}^2 - x_i^2) - ({x_N}^3 - x_i^3) - e_{(i,z)},$$

$$U_{(i,y)} = -b({x_N}^2 - x_i^2) - e_{(i,y)}, \tag{2.6}$$

$$U_{(i,z)} = rRe_{(i,x)} - re_{(i,z)}, \qquad i = 1, ..., N.$$

Then,

$$\dot{V} = -g_e \Sigma_{i=1}^{N-1} {e_{(i,x)}}^2.$$

The HR network in Eq. (2.3) has been analysed with the controllers in Eq. (2.6) (controllers are applied to the nodes). The numerical analysis has been carried out for weak coupling ($g_e = 0.1$). In the presence of controllers all neurons in the star coupled HR neural network fires in exact synchrony even with weak coupling as shown in Fig. 2.3.

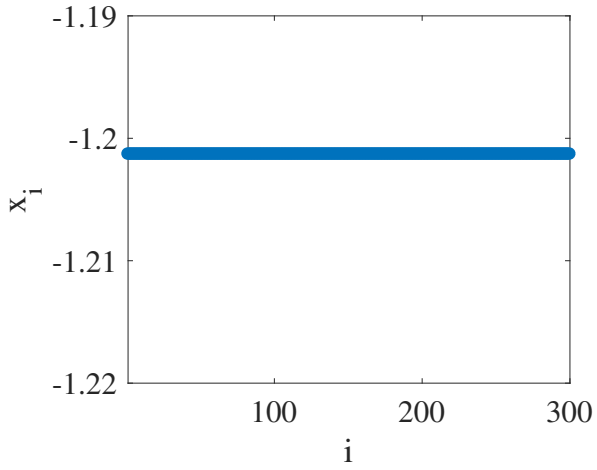

Figure 2.3: Complete synchrony for $g_e = 0.1$ in the presence of control inputs. i denotes the oscillator number and x_i denotes the membrane potential of i^{th} neuron.

2.3.2 Cluster Formation

The various control laws to produce DHM, MOS, cluster synchronisation and complete synchrony have been developed and established as the next step. Multiple numerical simulations reveal that taking the reverse component of the controllers discussed in Eq. (2.6) with a parameter mismatch in the last term $U_{(i,z)}$, i.e., replacing $re_{(i,z)}$ by $rz_N - z_i$, can provide a wide parameter space. The analysis of star coupling topology with parameter mismatch has been previously

discussed by Omelchenko *et al.* [19]. The new controllers have the form:

$$
\begin{aligned}
U_{(i,x)} &= -e_{(i,y)} - a({x_N}^2 - x_i^2) + ({x_N}^3 - x_i^3) + e_{(i,z)}, \\
U_{(i,y)} &= b({x_N}^2 - x_i^2) + e_{(i,y)}, \\
U_{(i,z)} &= -rRe_{(i,x)} + rz_N - z_i, \qquad i = 1, ..., N.
\end{aligned}
\tag{2.7}
$$

The HR network in Eq. (2.3) has been studied by applying the control inputs in Eq. (2.7). In the presence of control inputs, the hub acts as a leader which drives the system through many important dynamical states. As the network evolves, the oscillators split into different groups. There are cluster nodes, isolated nodes and floating nodes. A cluster node synchronises with other nodes and leads to the formation of a synchronised cluster. An isolated node does not synchronise with any other node and remains isolated, whereas a floating node switches between the clusters. The nonlinearity of the system tries to separate the orbits of different elements, and the coupling tends to synchronize them. As a results different clustered states are formed at specific values of g_e. Low values of g_e favour DHM, in which the nodes remain synchronous, but the hub begin to develop opposite motion as shown in Fig. 2.4(a). This is an interesting type of desynchronisation bifurcation with vast applications in real world networks [20, 21]. The driver transmits information with the nodes and drives them to synchronised state. This type of structures are found in certain neural networks i.e., the septo hippocampal region acts as the driver and connects with other neurons in the brain [19]. When g_e increases, the system shows MOS as represented in Fig. 2.4(b). A similar kind of dynamics for nonlocally coupled HR neurons is reported [7], where half of the oscillators are attracted towards a fixed point while the other half is oscillating. In our MOS, the neurons in the network show two kinds of oscillations, nearly half of the oscillators are following similar dynamics, while the other half are oscillating with a higher potential interspersed among the first group. Then the system shows a region of desynchrony as shown in Fig. 2.4(c). As g_e is increased further, stable synchronous clusters

are formed in which all neurons in one cluster behave in exact synchrony. A 6, 3 and 8 cluster states are observed with increase in g_e as shown in Figs. 2.5(a), 2.5(b) and 2.5(c) respectively. On further increasing g_e, the 8 clustered state converges to 4 clustered state which in turn converges to 2 clustered state and finally settle down to complete synchrony as denoted in Figs. 2.5(d), 2.5(e) and 2.5(f) respectively. In all clusters the hub show independent dynamics and act as the master node which drives the oscillators to synchrony via the mechanism of cluster reduction. The clustering of neurons have applications in the formation of memories, a reactivation of a specific group of neurons. In brain, an input signal produces a particular kind of pattern, i.e., some neurons become active in a specific sequence. When we recall an incident, different ensembles or clusters of nerve cells become functional and the strength of synapses control the neural activity patterns [22]. Therefore, the role of hub in forming DHM and clusters is important due to its potential applications in biological systems, especially in neural networks. The model considered here has a simple nature and we expect broad applicability for controlling synchronisation in biological systems.

2.3.3 Parameter Space

The two parameter space has been drawn to explore the rich dynamical behaviour exhibited by the system as shown in Fig. 2.6. The parameter 'a' is plotted along x axis and the 'g_e' along y axis. The value of 'a' is varied from 2.5 to 3.5 and that of 'g_e' from 0.01 to 1.4. The DHM region is denoted using red colour. The MOS is represented by blue. The yellow, black and green represents desynchrony, 6 cluster and 3 cluster states. The 8 cluster, 4 cluster and 2 cluster states are represented using cyan, brown and majenda respectively. After passing through these clusters, the system shows complete synchrony for all values of 'a' with relatively high values of g_e denoted using violet colour.

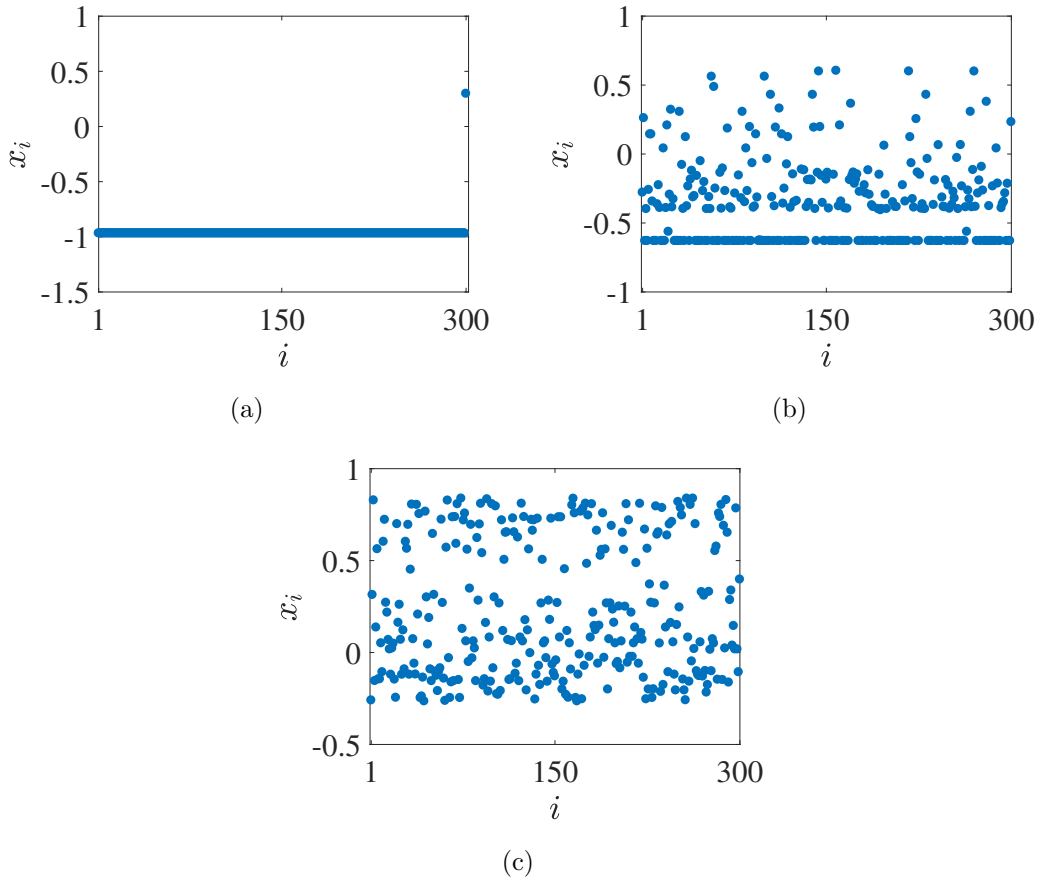

Figure 2.4: Snapshots of the variable x_i in the presence of control inputs in star coupling topology with increase in coupling strength. Oscillator number is plotted along X axis and the corresponding membrane potentials are plotted along Y axis. (a) DHM - all neurons except the hub fires in exact synchrony, ($g_e = 0.1$) (b) MOS - nearly half of the neurons fires in synchrony, while the other half oscillates with a higher potential interspersed among the first group, ($g_e = 0.5$) (c) desynchrony - all neurons show incoherent behaviour, ($g_e = 0.6$).

2.4 Results and Conclusions

We have analysed the formation of DHM, MOS, desynchrony, stable clusters and their convergence to complete synchrony in star coupled HR neural network with unidirectional electrical coupling. When the coupling strength is increased, the system exhibits synchrony. The largest TLE become negative at the point of transition from desynchrony to synchrony. The dynamics of the system by varying 'a' has also been studied in the presence of weak and strong coupling. The control inputs to synchronise the system for weak coupling has been evaluated using Lyapunov function method. On applying the control inputs, the system

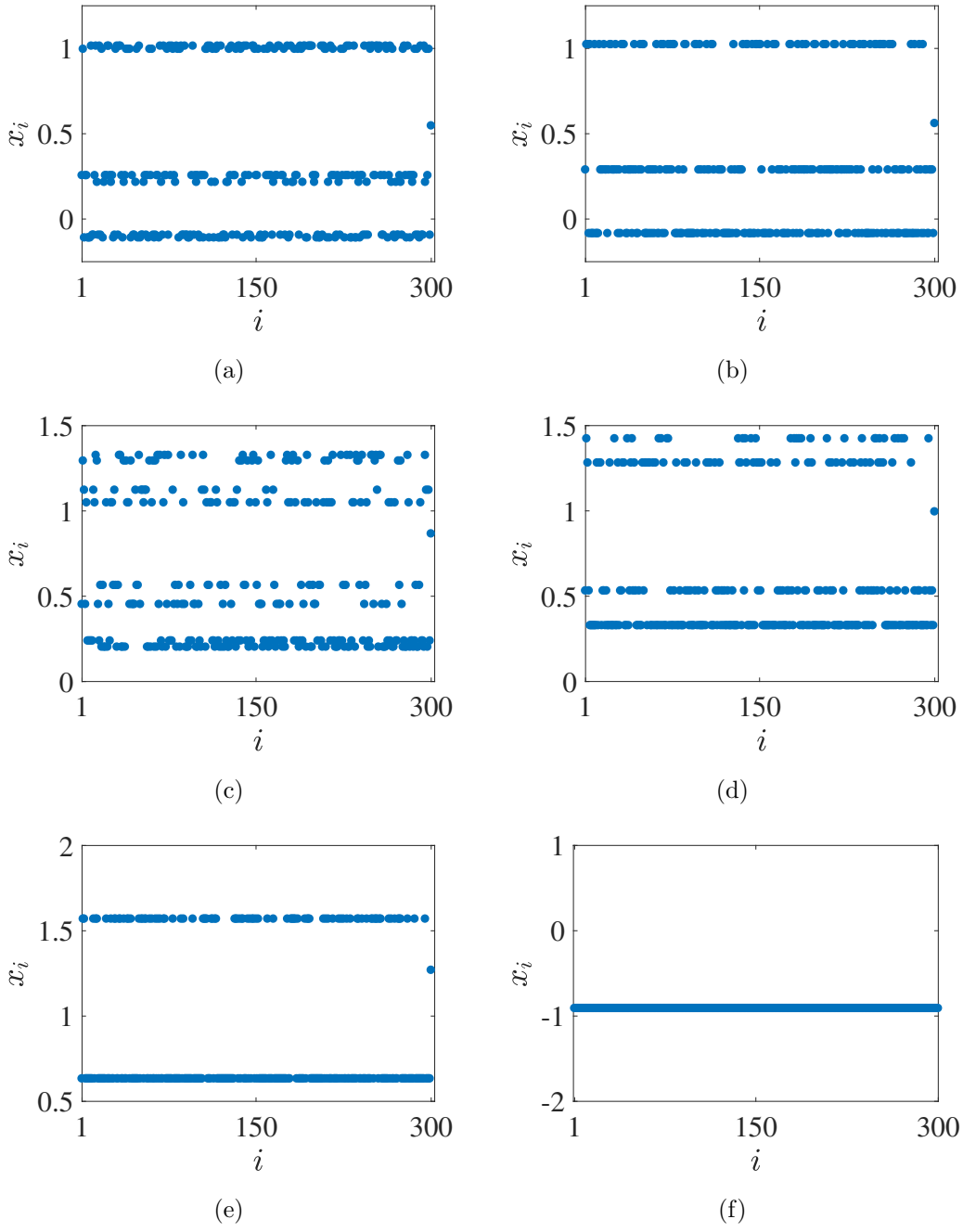

Figure 2.5: Cluster formation and synchronisation. Oscillator number is plotted along X axis and the corresponding membrane potentials are plotted along Yaxis. In Figs 2.5(a) - 2.5(e), neurons in the network except the hub arrange into six ($g_e = 0.71$), three ($g_e = 0.74$), eight ($g = 0.9$), four ($g_e = 0.95$) and two ($g_e = 1$) clusters respectively and neurons in one cluster fires in exact synchrony. In Fig. fig:Els4i all neurons including the hub show coherent behaviour ($g_e = 1.4$). In all the cases hub ($N = 300$) acts as the master node which drives the oscillators to synchrony via different states. 300 HR neurons with $a = 3$ are used for simulation.

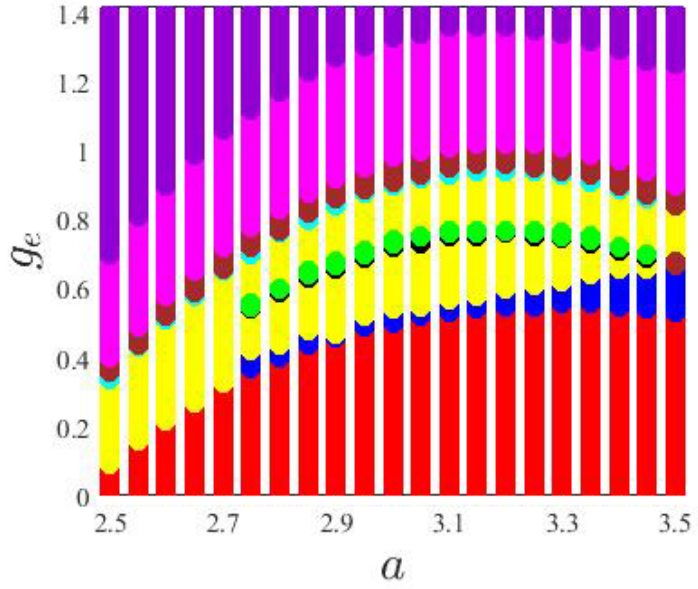

Figure 2.6: Two-parameter phase diagram in a-g_e plane for 300 star coupled HR neurons. Low values of g_e favour DHM, which is represented using red colour. The blue shows MOS and the yellow denotes desynchrony. The six cluster and three cluster states are denoted by black and green respectively. The cyan shows eight cluster state. Brown and majenda represents, four cluster and two cluster states respectively. Finally the violet colour shows complete synchronisation.

shows synchronisation even for low coupling strength. The study has been extended by applying modified controllers. For low values of g_e, the system shows DHM, which is an important type of behaviour arising as a result of spoke-hub architecture of star coupling topology. The hub in the star network acts as a driver which drives all other oscillators to synchrony. As g_e is increased, the network of oscillators shows MOS. Then a desynchrony region exists followed by a 6 clustered state. Then the 6 clustered state reduces to 3 clustered state and a desynchronous region again. With further increase in g_e, the network shows 8 cluster, 4 cluster and 2 cluster states. In all clusters, hub show independent dynamics and act as the master node which drives the nodes to synchrony via different states. The formed clusters are consistent for all initial conditions and for any number of oscillators. Finally for high values of g_e, the oscillators are completely synchronised. The parameter space for the system has also been discussed. The introduction of control inputs to the network inspire a leader to generate some interesting transitions consisting of clusters of synchronised do-

mains depending on the coupling strength. We conclude that, the star coupled HR neural network in the presence of control input shows many of the important spatiotemporal behaviours exhibited by coupled oscillator networks and provides finer insight to the route to synchrony.

Bibliography

[1] M. Foster and C. S. Sherrington. *Textbook of Physiology*, volume 3. London: Macmillan, 7 edition, 1897.

[2] Y. Maistrenko and A. Panchuk. *Chaos*, 13:990, 2003.

[3] I. Belykh and M. Hasler. *Chaos*, 21:016106, 2011.

[4] V. N. Belykh, I. V. Belykh, and E. Mosekilde. *Phys. Rev. E*, 63:036216, 2001.

[5] R. Arumugam, P. S. Dutta, and T. Banerjee. *Chaos*, 25:103121, 2015.

[6] L. M. Pecora. *Phys. Rev. E*, 58:347–360, 1998.

[7] J. Hizanidis, V. Kanas, A. Bezerianos, and T. Bountis. *Int. J. Bifurcat. Chaos*, 24(3):1450030, 2014.

[8] O. Sporns, C. J. Honey, and R. Ktter. *PLOS 1*, 0001049, 2007.

[9] S. Achard, R. Salvador, B. Whitcher, J. Suckling, and E. Bullmore. *J. of Neurosci.*, 26:63–72, 2006.

[10] H. Abdullah, N. Maddage, and D. Cvetkovic. *IEEE EMBS Conference*, 2012.

[11] F. Artoni, C. Fanciullacci, F. Bertolucci, A. Panarese, S. Makeig, S. Micera, and C. Chisari. *NeuroImage*, 159:403416, 2017.

[12] D. Cvetkovic and I. Cosic. *States of consciousness*. Springer, 2011.

[13] J. Wang and Y. Zhang. *Phys. Lett. A*, 374:1464–1468, 2010.

[14] X. Shi and Z. Wang. *Nonlinear Dyn.*, 69:2147–2153, 2012.

[15] M. Dhamala, V. K. Jirsa, and M. Ding. *Phys. Rev. Lett.*, 92:028101, 2004.

[16] C. R. Nayak and V. C. Kuriakose. *Chaos*, 18:013125, 2008.

[17] D. Hrg. *Neural Networks*, 40:73–79, 2013.

[18] L. H. Nguyen and K. S. Hong. *Applied Mathematical Modelling*, 37:2460–2468, 2013.

[19] I. Omelchenko, Y. Maistrenko, and E. Mosekilde. *Discrete Dynamics in Nature and Society*, 3:239–255, 2005.

[20] S. Jalan, A. Singh, S. Acharyya, and J. Kurths. *Phys. Rev. E*, 91:022901, 2015.

[21] R. Kalpathy and M. D. Ward. *Stat. Probability Lett.*, 87:40, 2014.

[22] D. Lu and A. Woodruff. *The brain - learning & memory*, volume 1. Queensland brain Institute, www.qbi.uq.edu.au/learning.

Chapter 3

Chemically Coupled HR Neurons in Star Network Topology

3.1 Introduction

In chemical coupling, the impulses in the presynaptic neuron stimulates the release of a chemical called neurotransmitter which binds the receptors in the postsynaptic neuron. This neurotransmitter initiates an electrical response, that can either excite or inhibit the postsynaptic cell. Unlike electrical coupling, there is a time delay of approximately $0.3 - 5.0$ milliseconds between the arrival of an impulse at the presynaptic cite and its transmission to the postsynaptic neuron. The delay is caused by the release and action of the neurotransmitter. Chemical coupling is most common in the nervous system of vertebrates [1]. Belykh and Hasler reported a theoretical investigation of cluster synchronisation of neural networks with chemical synapses for the first time [2]. Then a generally formulated model with explicit coupling thresholds for stable cluster formation using chemical synapse has been reported by Jonq *et al.* in a recent work [3]. Chimera state has also been realised in a multilayered HR neural network with electrical and chemical synapses [4]. The presence of chimera and multichimera states in an ensemble of bursting neurons connected via nearest-neighbour coupling with

chemical synapse have been reported [5].

In this chapter, we have analysed a star coupled HR neuron model with chemical coupling using unidirectional and bidirectional configuration. In unidirectional scheme, the system decomposes into a master-slave configuration in which the response system is slaved to obey the dynamics of the master, whereas in bidirectional scheme, both the subsystems are coupled to each other and the coupling term generates an adjustment of rhythms to a common scale [6]. The chapter is arranged as follows. Section 3.2 describes HR model and the synchronisation of two HR neurons coupled via chemical synapse with increase in coupling strength. The dynamics of fast ion channel for low and high coupling strength and the stability of synchronised state using TLEs have been discussed in section 3.2. In section 3.3, star coupled HR neural network with unidirectional and bidirectional connections have been described. Synchrony, desynchrony and DHM region have been discussed along with the time series analysis in this section. The parameter space has also been discussed in section 3.3. Section 3.4 concludes the study.

3.2 The Two Neuron Case

We have considered two HR neurons coupled via chemical synapse. The equations have the form:

$$
\begin{aligned}
\dot{x_1} &= y_1 + a{x_1}^2 - {x_1}^3 - z_1 + I - g_c(x_1 - V_s)\Gamma(x_2), \\
\dot{y_1} &= 1 - b{x_1}^2 - y_1, \\
\dot{z_1} &= r(R(x_1 - x_e) - z_1), \qquad (3.1) \\
\dot{x_2} &= y_2 + a{x_2}^2 - {x_2}^3 - z_2 + I - g_c(x_2 - V_s)\Gamma(x_1), \\
\dot{y_2} &= 1 - b{x_2}^2 - y_2, \\
\dot{z_2} &= r(R(x_2 - x_e) - z_2), \qquad (3.2)
\end{aligned}
$$

The variable x denotes the membrane potential. y is the recovery variable and z denotes the adaptation variable. The parameter g_c is the chemical synaptic coupling strength. V_s, the reversal potential is always greater than x_i for all neuron at all times, i.e., the synapses are excitatory. $\Gamma(x_j) = 1/[1+exp(-\lambda(x_j - \theta))]$ $(j = 1, 2)$ is an exponential function which models the synaptic junction between the neurons and θ is the threshold [7]. For each neuron to reach the threshold, we choose $\theta = -0.25$, $V_s = 2$ and $\lambda = 7.5$ [3]. The other parameters are $a = 3.0$, $b = 5.0$, $R = 4.0$, $r = 0.006$, $I = 3.1$, and $x_e = -1.61$ [8]. The system represented by Eq. (3.1) and Eq. (3.2) have been analysed using fourth order Runge-Kutta algorithm. The time series of membrane potential, recovery variable, and adaptation variable for weak coupling ($g_c < 1.5$) are shown in Fig. 3.1(a), 3.1(b) and 3.1(c) respectively. From the plots, it is clear that the two neurons show desynchronised behaviour. As the g_c is increased ($g_c > 1.5$) the trajectories merges and the neurons achieve fixed point synchronisation, i.e., after an initial period of bursting the system settle down to a stationary state [9] as shown in Fig. 3.2(a), 3.2(b) and 3.2(c).

3.2.1 Stability of Synchronisation

We have derived the dynamics transverse to the synchronisation manifold by adding and subtracting the term $g_c(x_1 - V_s)\Gamma(x_1)$ to the first equation of Eq. (3.1) and subtracting it from Eq. (3.2). We have obtained equations of the form:

$$\begin{aligned} \dot{x_2} - \dot{x_1} = \; & (y_2 - y_1) + a(x_2^2 - x_1^2) - (x_2^3 - x_1^3) - (z_2 - z_1) - g_c(x_2 - V_s)\Gamma(x_1) + \\ & g_c(x_1 - V_s)\Gamma(x_2) + g_c(x_1 - V_s)\Gamma(x_1) - g_c(x_1 - V_s)\Gamma(x_1), \\ & = (y_2 - y_1) + a(x_2^2 - x_1^2) - (x_2^3 - x_1^3) - (z_2 - z_1) - \\ & g_c\Gamma(x_1)(x_2 - x_1) + g_c(x_1 - V_s)(\Gamma(x_2) - \Gamma(x_1)), \end{aligned} \tag{3.3}$$

$$\dot{y_2} - \dot{y_1} = \; -b(x_2^2 - x_1^2) - (y_2 - y_1), \tag{3.4}$$

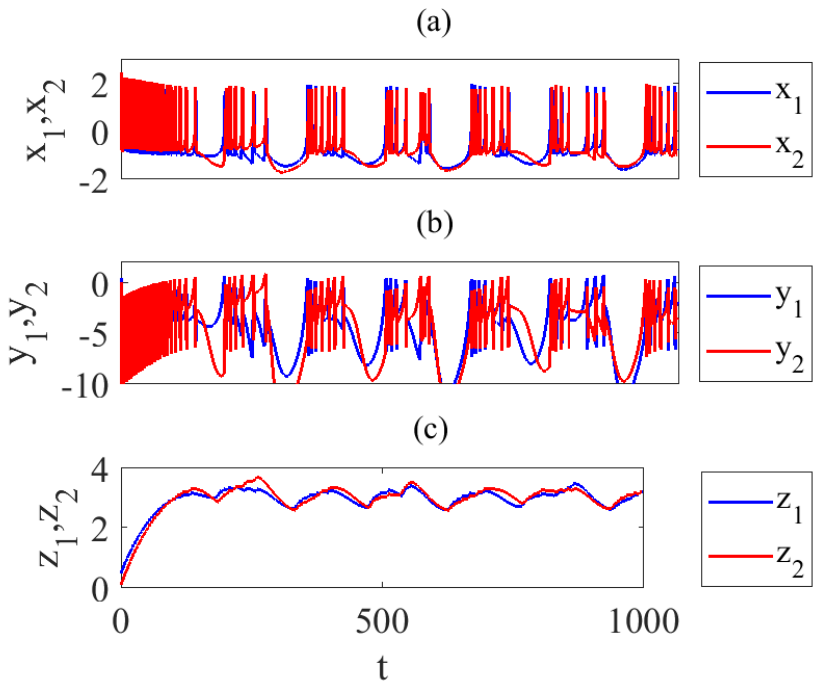

Figure 3.1: Desynchronised time series of two HR neurons with for $g_c = 1$. (a) membrane potential (b) recovery variable (c) adaptation variable.

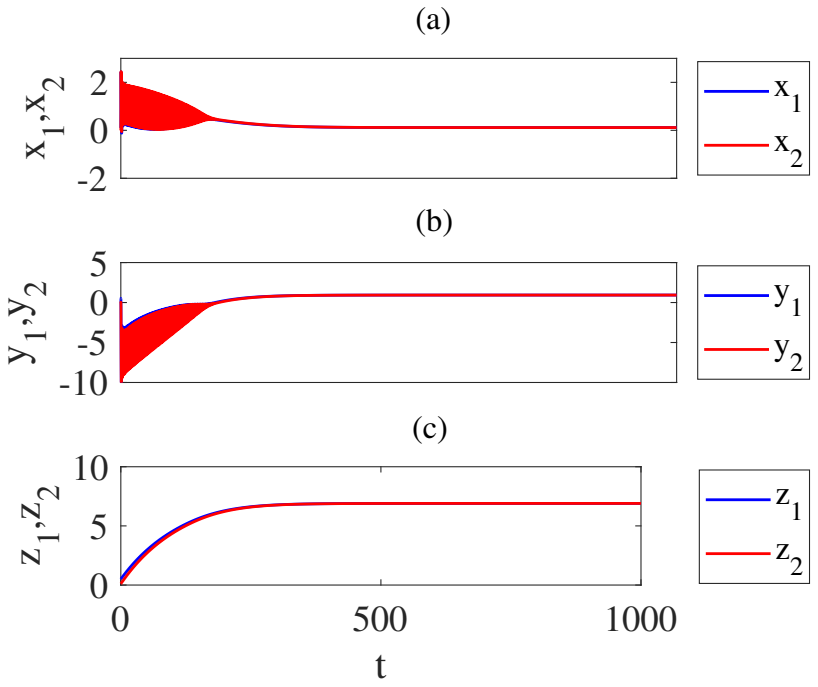

Figure 3.2: Time series of synchronous state for $g_c = 1.5$. The two time series merges as time proceeds indicating synchrony: (a) membrane potential (b) recovery variable (c) adaptation variable.

$$\dot{z_2} - \dot{z_1} = \quad r[R(x_2 - x_1) - (z_2 - z_1)]. \tag{3.5}$$

To analyse the stability of the synchronised state, we have transformed the coordinates to the transverse manifold, i.e., $x_\perp = x_2 - x_1$, $y_\perp = y_2 - y_1$, and $z_\perp = z_2 - z_1$. On the completely stable synchronisation manifold, the differences $x_\perp$, $y_\perp$, and $z_\perp$ vanish in the limit of t tends to ∞ and there exist a synchronous solution $(x_1, y_1, z_1) = (x_2, y_2, z_2) = (x, y, z)$ and we write $x_1^2 - x_2^2 = 2xx_\perp$ and $x_1^3 - x_2^3 = 3x^2x_\perp$. The dynamics transverse to the synchronisation manifold has the form:

$$\dot{x}_\perp = y_\perp + 2axx_\perp - 3x^2x_\perp - z_\perp - \Omega(x)x_\perp,$$

$$\dot{y}_\perp = -2bxx_\perp - y_\perp,$$

$$\dot{z}_\perp = r(Rx_\perp - z_\perp), \tag{3.6}$$

where,

$$\Omega(x) = g_c\Gamma(x) - g_c(x_- V_s)\Gamma_x(x).$$

$$\begin{aligned}\Omega(x) = \quad & g_c[\frac{1}{(1 + exp(-\lambda(x - \theta)))}] - \\ & g_c[(x - V_s)\frac{(\lambda(exp(-\lambda(x - \theta))))}{(1 + exp(-\lambda(x - \theta)))^2}].\end{aligned} \tag{3.7}$$

The condition for the stability of synchronisation manifold is the negativeness of the TLEs associated with Eq. (3.6). The variation of two of the largest TLEs ($\lambda_{\perp_1}$ and $\lambda_{\perp_2}$) associated with Eq. (3.6) with increase in g_c is shown in Fig. (3.3). As the coupling strength is increased, the largest TLE ($\lambda_{\perp_1}$) starts to increase, reaches a peak, and then starts to decrease. The $\lambda_{\perp_1}$ crosses zero at a coupling strength of $g_c = 1.5$ and become negative which indicates the difference $x_\perp$, $y_\perp$ and $z_\perp$ will shrink as $t \to \infty$, i.e., there is a transition from desynchronised state to complete synchrony [10]. The stability of synchronisation by varying 'a' has

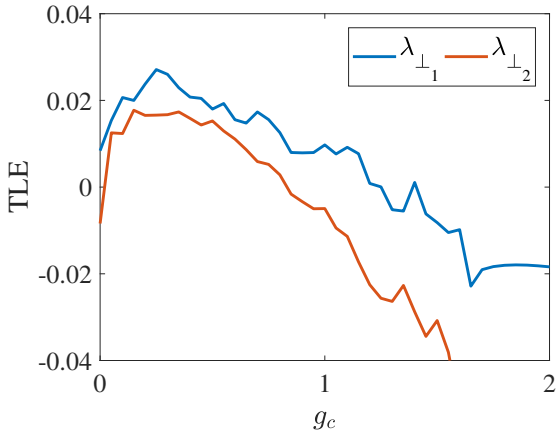

Figure 3.3: Variation of TLEs ($\lambda_{\perp_1}$ and $\lambda_{\perp_2}$) with coupling strength. The largest TLE ($\lambda_{\perp_1}$) crosses zero and become negative at a coupling strength of $g_c = 1.5$, indicating a transition from desynchrony to synchrony at this point.

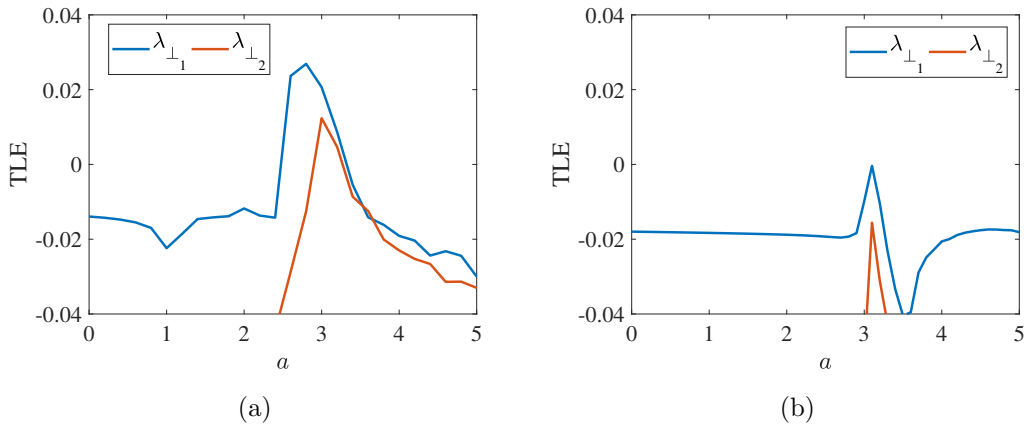

Figure 3.4: Variation of TLEs ($\lambda_{\perp_1}$ and $\lambda_{\perp_2}$) with a. (a). For low coupling strength ($g_c = 0.1$) the largest TLE ($\lambda_{\perp_1}$) becomes positive for $2.5<a<3.3$, indicating a region of desynchrony for this range of a values. (b). For high coupling strength ($g_c > 1.5$), the TLEs are negative for all values of a, i.e., the neurons are synchronised for the entire range of a.

also been analysed with weak and strong coupling. For weak coupling ($g_c = 0.1$), the largest TLE ($\lambda_{\perp_1}$) become positive for $2.5 < a < 3.3$, indicating a region of desynchrony as shown in Fig. 3.4 (a). For strong coupling ($g_c > 1.5$), the TLEs remains negative for all values of 'a' and the system remains in the synchronised state as depicted in Fig. 3.4 (b).

3.3 Star Network Topology

We have studied two different cases based on the interaction between the hub and the nodes. In the first case, we consider the unidirectional chemical coupling and in later, the effect of bidirectional chemical coupling.

3.3.1 Unidirectional Coupling

The entire network is a system of 'N' coupled differential equations. Unidirectional star topology has been chosen in which all oscillators on the spokes of the star ($i = 1$ to $N-1$) are connected to the common oscillator ($i = N$). The equations of nodes have the form:

$$\dot{x_i} = y_i + a{x_i}^2 - {x_i}^3 - z_i + I - g_c(x_i - V_s)\Gamma(x_N),$$

$$\dot{y_i} = 1 - b{x_i}^2 - y_i,$$

$$\dot{z_i} = r(R(x_i - x_e) - z_i), \qquad i = 1, 2, ..., N-1. \tag{3.8}$$

The dynamics of the hub has the form:

$$\dot{x_N} = y_N + a{x_N}^2 - {x_N}^3 - z_N + I,$$

$$\dot{y_N} = 1 - b{x_N}^2 - y_N,$$

$$\dot{z_N} = r(R(x_N - x_e) - z_N). \tag{3.9}$$

The parameters are same as in Eq. (3.1). We have analysed the system represented using Eq. (3.8) and Eq. (3.9) by varying the values of 'a' and 'g_c'. Synchrony, desynchrony and DHM are observed as shown in Figs. 3.5(a), 3.5(c) and 3.5(e) respectively. The membrane potential x_i (blue colour) and the new transformed variable, $\Delta x_i = x_N - x_i$ (red colour) are plotted against oscillator number i[11] in the left panel and the corresponding time series are shown in the right panel of Fig. 3.5. In the desynchronised state, the system possess a burst-

ing time series as shown in Fig. 3.5(b), whereas in the synchronised state, the network achieve fixed point synchronisation as depicted in Fig. 3.5(d). In DHM, the neurons show bursting time series as shown in Fig. 3.5(f). The transformed variable Δx_i has zero value for the synchronised set of oscillators, but for the desynchronised case, they are randomly distributed. In the case of DHM, the common oscillator has $\Delta x_i = 0$, while the oscillators on the spokes of the star possess different value.

3.3.2 Bidirectional Coupling

The dynamical equations of nodes in HR neural network with bidirectional chemical coupling have the form:

$$\dot{x_i} = y_i + a{x_i}^2 - {x_i}^3 - z_i + I - g_c(x_i - V_s)\Gamma(x_N),$$

$$\dot{y_i} = 1 - b{x_i}^2 - y_i,$$

$$\dot{z_i} = r(R(x_i - x_e) - z_i), \qquad i = 1, 2, ..., N-1. \tag{3.10}$$

The dynamics of the hub has the form:

$$\dot{x_N} = y_N + a{x_N}^2 - {x_N}^3 - z_N + I - g_c(x_N - V_s)\Sigma_{i=1}^{N-1} C_{N,i}\Gamma(x_i),$$

$$\dot{y_N} = 1 - b{x_N}^2 - y_N,$$

$$\dot{z_N} = r(R(x_N - x_e) - z_N). \tag{3.11}$$

In bidirectional coupling scheme, all oscillators on the spokes of the star are connected to the common oscillator and vice versa. $C = (c_{Ni})$ is the $N \times N$ connectivity matrix: $c_{Ni} = 1$ if the N^{th} neuron receives synaptic input from neuron i; otherwise $c_{Ni} = 0$. The dynamics of chemically coupled HR neurons in bidirectional coupling topology has also been analysed. The membrane potential x_i (blue colour) and the new transformed variable, $\Delta x_i = x_N - x_i$ (red colour) are plotted against oscillator number i. Desynchronised, synchronised and DHM

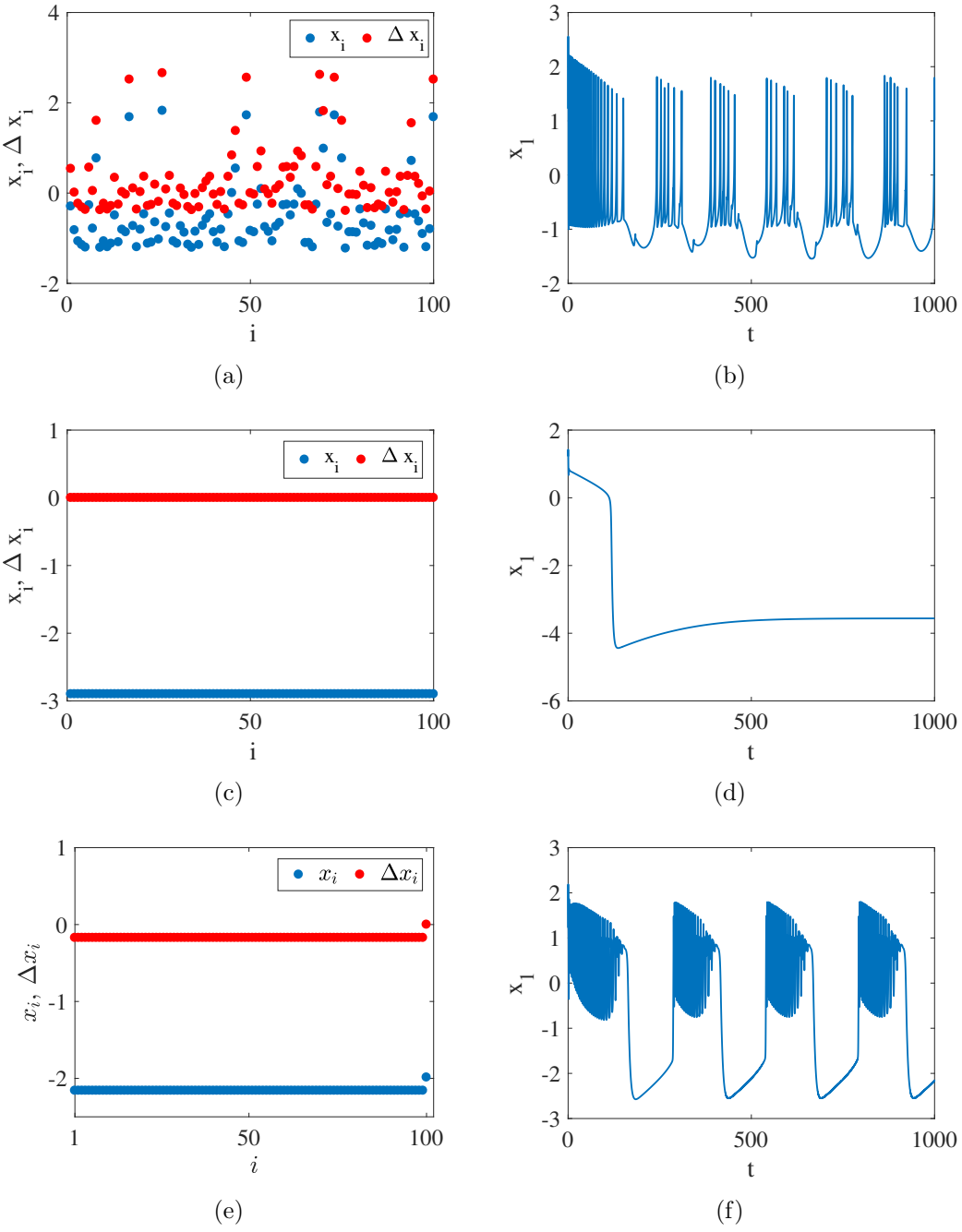

Figure 3.5: Star coupled HR neurons in unidirectional configuration in terms of the variables x_i (blue colour) and the transformed variables $\Delta x_i = x_N - x_i$ (red colour): (a) desynchronised state ($a = 3$ and $g_c = 0.1$), (c) synchronised state ($a = 1$ and $g_c = 0.01$) and (e) DHM ($a = 2.5$ and $g_c = 3$). The figures in the right panel are the corresponding time series. The number of oscillators used is 100.

regions are obtained by varying the values of 'a' and 'g_c' as shown in Fig. 3.6(a), 3.6(c) and 3.6(e) respectively. The corresponding time series are shown in the right panel of Fig. 3.6. In the desynchronised state, the system possess a bursting time series as shown in Fig. 3.6(b). In the synchronised state, the network achieve fixed point synchronisation as depicted in Fig. 3.6(d). Unlike unidirectional coupling, in DHM the system collapses into the stationary state as shown in Fig. 3.6(f). The transformed variable Δx_i has zero value for the synchronised set of oscillators. In the desynchrony, they are scattered. In the case of DHM, the common oscillator has $\Delta x_i = 0$, while the oscillators on the spokes of the star possess different values.

3.3.3 Parameter Space

To figure out the effect of the coupling strength 'g_c' and the activation-inactivation variable of fast ion channel 'a' on the dynamics of the unidirectionally and bidirectionally connected star network, we have plotted the parameter space for every possible value of 'g_c' and 'a' as shown in Figs. 3.7(a) and 3.7(b) respectively. 'g_c' is varied from 0 to 5 and 'a' from 0 to 3. In both types of couplings, we observe synchrony, desynchrony and DHM, represented using blue, red, and white regions respectively. From the figure, it is clear that in unidirectional coupling synchrony and DHM are the most observed regions, whereas in bidirectional coupling, the DHM spreads most of the parameter space but synchronised and desynchronised states prevail in a small region. The results are consistent for networks with more number of oscillators.

3.4 Results and Conclusions

We have studied the patterns like synchrony, desynchrony and DHM in a network of HR neurons with chemical synapse in unidirectional and bidirectional star topology. Synchronisation of two chemically coupled HR neuron with increase in coupling strength has been discussed and the TLEs are plotted to observe the

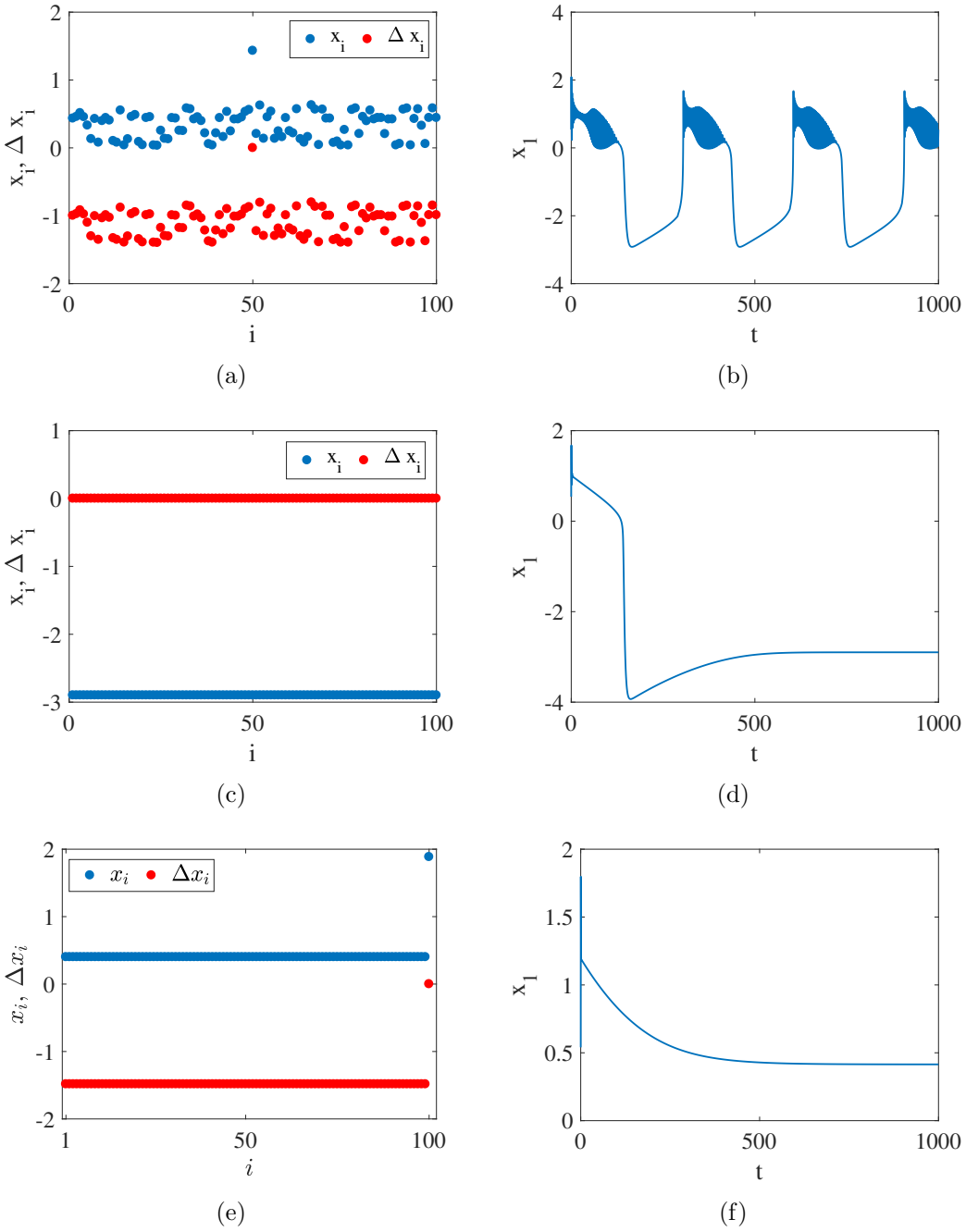

Figure 3.6: Star coupled HR neurons in bidirectional configuration in terms of the variables x_i (blue colour) and the transformed variables $\Delta x_i = x_j - x_i$ (red colour): (a) desynchrony ($a = 2$ and $g_c = 0.1$), (c) synchrony ($a = 1$ and $g_c = 0.1$) and (e) DHM ($a = 1$ and $g_c = 0.2$). The figures in the right panel are the corresponding time series. The number of oscillators used is 100.

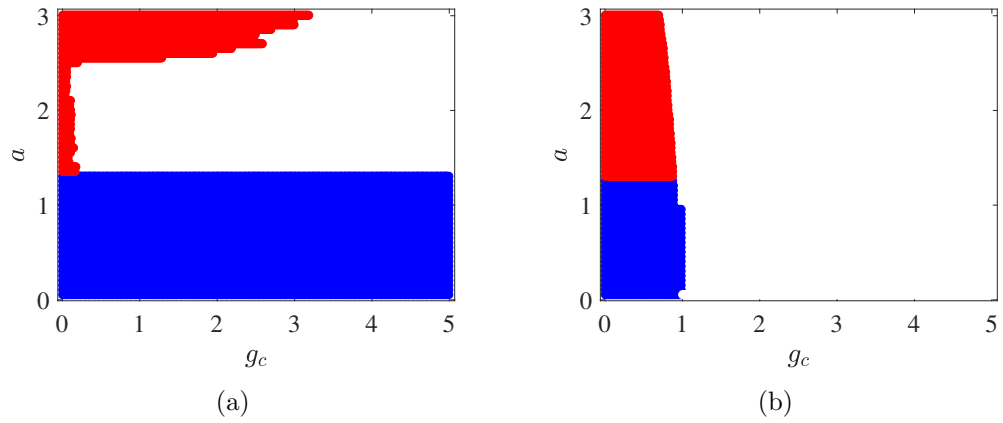

Figure 3.7: Two parameter (g_c, a) phase diagram for star coupled network of HR neurons. (a) unidirectional coupling. (b) bidirectional coupling. Synchrony, desynchrony and DHM are indicated using blue, red and white colours respectively. 100 oscillators are used for numerical calculation.

point of transition from desynchrony to synchrony. The system has been analysed by varying the parameter describing the dynamics of the fast ion channel in the presence of weak and strong coupling with the aid of TLEs. For strong coupling ($g_c > 1.5$), the TLEs remains negative for all values of 'a' and the system remains in the synchronised state. For for weak coupling, there is a region $2.5 < a < 3.3$, where the TLEs become positive and the system exhibits desynchrony. The study has been extended by connecting the neurons in unidirectional and bidirectional star topology. In both cases, the observed states are desynchrony, synchrony and DHM. The time series analysis corresponding to each state has been carried out. In the case of unidirectional coupling, the desynchronised state possess a bursting time series and in the synchronised state the network achieve fixed point synchronisation. In DHM, the neurons exhibit bursting dynamics. Similar analysis with bidirectionally coupled oscillators have shown that in synchrony, the oscillators possess a bursting time series and in desynchrony the network achieve fixed point synchronisation. In DHM, the system collapses into the stationary state. The parameter space confirms that synchrony and DHM are the most observed states in unidirectional coupling, whereas in bidirectional coupling, DHM is the most observed state. The coupled nonlinear systems exhibit some interesting dynamics compared to uncoupled system. One of the important phenomenon

is the complete suppression of oscillations (AD) which depends on the synaptic coupling strength. In bidirectional coupling, AD is the most observed temporal dynamics (in synchrony and DHM) because, the dynamics of both nodes and hub get influenced by each other and lead to the formation of a stable state. The hub acts as a leader in forming DHM and is important due to its applications in biological systems.

Bibliography

[1] M. Foster and C. S. Sherrington. *Textbook of Physiology*, volume 3. London: Macmillan, 7 edition, 1897.

[2] I. Belykh and M. Hasler. *Chaos*, 21:016106, 2011.

[3] J. Jonq and L. Yu-Hao. *Chaos*, 24:013110, 2014.

[4] S. Majhi, M. Perc, and D. Ghosh. *Chaos*, 27:073109, 2017.

[5] B. K. Bera and D. Ghosh. *Phys. Rev. E*, 93:052223, 2016.

[6] S. Boccaletti. *The Synchronized Dynamics of Complex Systems*, volume 6. Elsevier, 2008.

[7] D. Somers and N. Kopell. *Biol. Cybern*, 68:393, 1993.

[8] X. Shi and Z. Wang. *Nonlinear Dyn.*, 69:2147–2153, 2012.

[9] N. Buric, K. Todorovic, and N. Vasovic. *Phys. Lett. E*, 78:036211, 2008.

[10] R. N. Chitra and N. Gupte. *AIP Conference Proceedings*, 1339:172–180, 2011.

[11] B. K. Bera, D. Ghosh, and M. Lakshmanan. *Phys. Rev. E*, 93:012205, 2016.

Chapter 4

HR Neuron Model with Memristors

4.1 Introduction

In 1971 Chua [1] postulated a basic two-terminal electronic circuit element called 'memristor' (memory resistor), which can mimic the key characteristics of synapses and neurons. Unlike other electronic memories such as those made from CMOS devices, memristors are capable of remembering their state even after losing power and they consume less energy. Diffusive memristors can realistically mimic the transport of Ca^{2+} ions through synapses, and they are the suitable candidates for compact neuromorphic implementation [2, 3]. The memristor based neural network analysis, which combines the storage capability of the memristor and the memory pattern of the human brain is widely investigated. Wen *et al.* introduced the circuit model of memristor based neural network in a recent work [4]. The exponential synchronisation of coupled memristive neural networks via pinning control has been proposed by Guan *et al.* [5].

The synchronisation of nonlinear systems when coupled through memristors is an active research area. It has widespread applications in secure communication, neuromorphic circuits and biological systems [6]. The four dimensional version of

HR neuron model with field effects has been studied in this chapter. Memristors are used to realise the relations between the magnetic flux of the electromagnetic field and the membrane potential. The dynamics of single system with memristor has been discussed in section 4.2. Two coupled system with electrical, chemical and field couplings have been studied in section 4.3. Section 4.4 concludes the study.

4.2 HR Model with Field Effects

The repeated exchange of charged ions across the membrane of neurons induce some fluctuations in the concentration of ions. Hence a time varying electromagnetic field is created across the membrane to regulate the membrane potential of neurons. The variable ϕ is used to describe the magnetic flux of the electromagnetic field [7]. The improved HR model with field effects has the form:

$$\begin{aligned}
\dot{x} &= y + ax^2 - x^3 - z + I - k_1\rho(\phi)x, \\
\dot{y} &= 1 - bx^2 - y, \\
\dot{z} &= r(R(x - x_e) - z), \\
\dot{\phi} &= k_2 x - k_3\phi,
\end{aligned} \tag{4.1}$$

where x represents the membrane potential of the neuron. y and z are called recovery variable and adaptation variable respectively [8]. The term $k_1\rho(\phi)x$ denotes the induced current through electromagnetic induction, where k_1 represents the modulation intensity of induced current on the membrane potential. The term k_2x represents the change in magnetic flux induced by membrane potential of the cell and $k_3\phi$ denotes the leakage of the magnetic flux.

4.2.1 Memristors

Memristors are used to realise the coupling between the magnetic flux and the membrane potential as indicated by the term '$k_1\rho(\phi)x$' in Eq. (4.1). The connection between induced current, magnetic flux and memristor can be understood using Faraday's law of electromagnetic induction.

$$i = \frac{dq(\phi)}{dt} = \frac{dq(\phi)}{d\phi}\frac{d\phi}{dt} = \rho(\phi)x.$$

Here ϕ represents the magnetic flux across the memristor. Two types of memristors have been used for the analysis as given below [9].

$$\rho(\phi) = \alpha + 3\beta\phi^2 \tag{4.2}$$

$$\rho(\phi) = \alpha\phi^2 + \beta\phi + \gamma \tag{4.3}$$

α, β and γ are memristor parameters.

4.2.2 Dynamics of Single System

Case 1:

We have analysed Eq. (4.1) with memristor of the form: $\rho(\phi) = \alpha + 3\beta\phi^2$, by changing the strength of modulation intensity (k_1). The parameters used are $a = 3.0, b = 5.0, R = 4.0, r = 0.006, x_e = -1.61$, $I = 3.1, k_2 = 0.9, k_3 = 0.5, \alpha = 0.4$ and $\beta = 0.02$ [7]. The bifurcation diagrams of Inter Spike Interval (ISI) and local maxima of membrane potential with increase in k_1 are shown in Fig. 4.1. The $(k_1 - ISI)$ bifurcation diagram for constant (I=3.1) and periodic stimulus are shown in Figs. 4.1(a) and 4.1(b) respectively, whereas Figs. 4.1(c) and 4.1(d) represents the corresponding bifurcations in the $(k_1 - x_{max})$ plane. The constant and periodic stimulus have the forms $I = 3.1$ and $I = 2sin(0.05t)$ respectively. From the plots it is clear that, for low modulation intensity, the system shows chaotic bursting. For optimum values, the dynamics is bursting and periodic

spiking. For high values, the system settle down to a quiescent state.

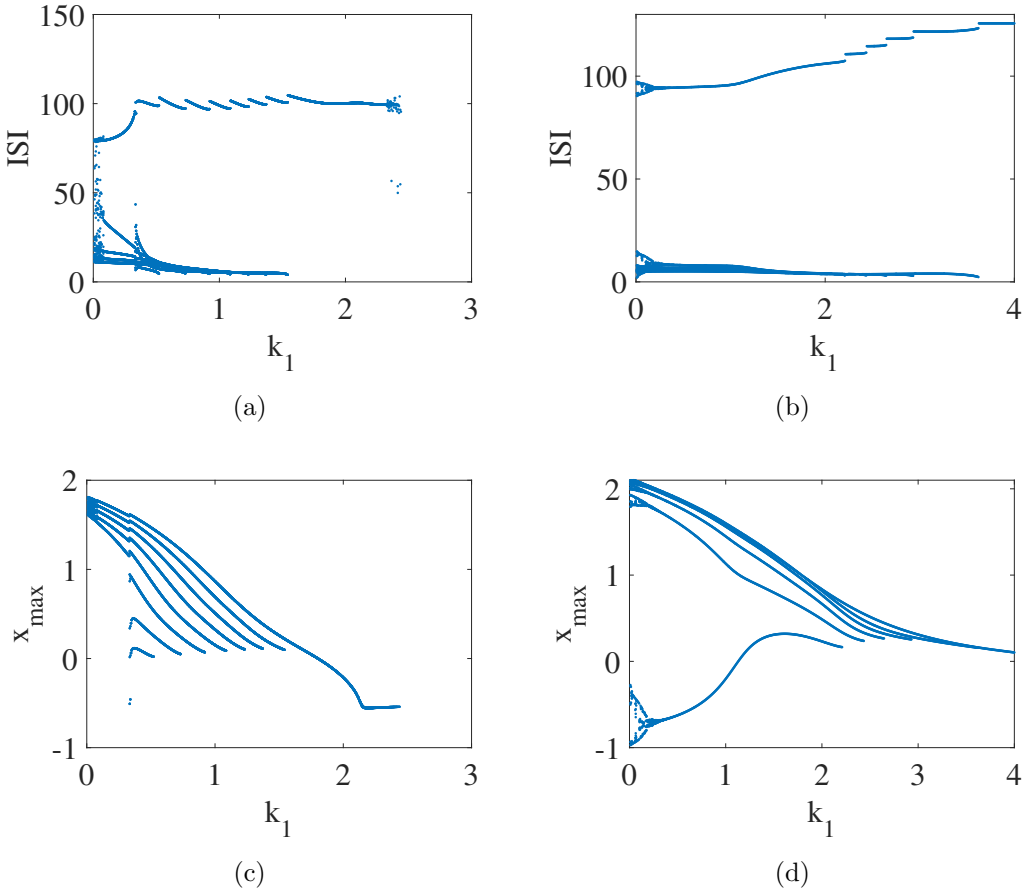

Figure 4.1: Bifurcation diagrams of (a) and (b) ISI of membrane potentials for constant stimulus and periodic stimulus and (c) and (d) local maxima of membrane potential (x) for constant stimulus and periodic stimulus respectively

Case 2:

The system in Eq. (4.1) has been studied with memristor in Eq. (4.3). The memristor parameters are $\alpha = 0.4, \beta = 0.02, \gamma = 0.1$. The system has been analysed by changing the strength of modulation intensity of the field (k_1). The ($k_1 - ISI$) and ($k_1 - x_{max}$) bifurcation diagrams for constant stimulus (I=3.1) are shown in Figs. 4.2(a) and 4.2(c) respectively. As the value of k_1 is increased the system passes through chaotic bursting, periodic bursting (with 3 and 2 spikes per burst) and periodic spiking. For high values of k_1 the system settle down to a quiescent state. The bifurcation analysis by applying a periodic stimulus

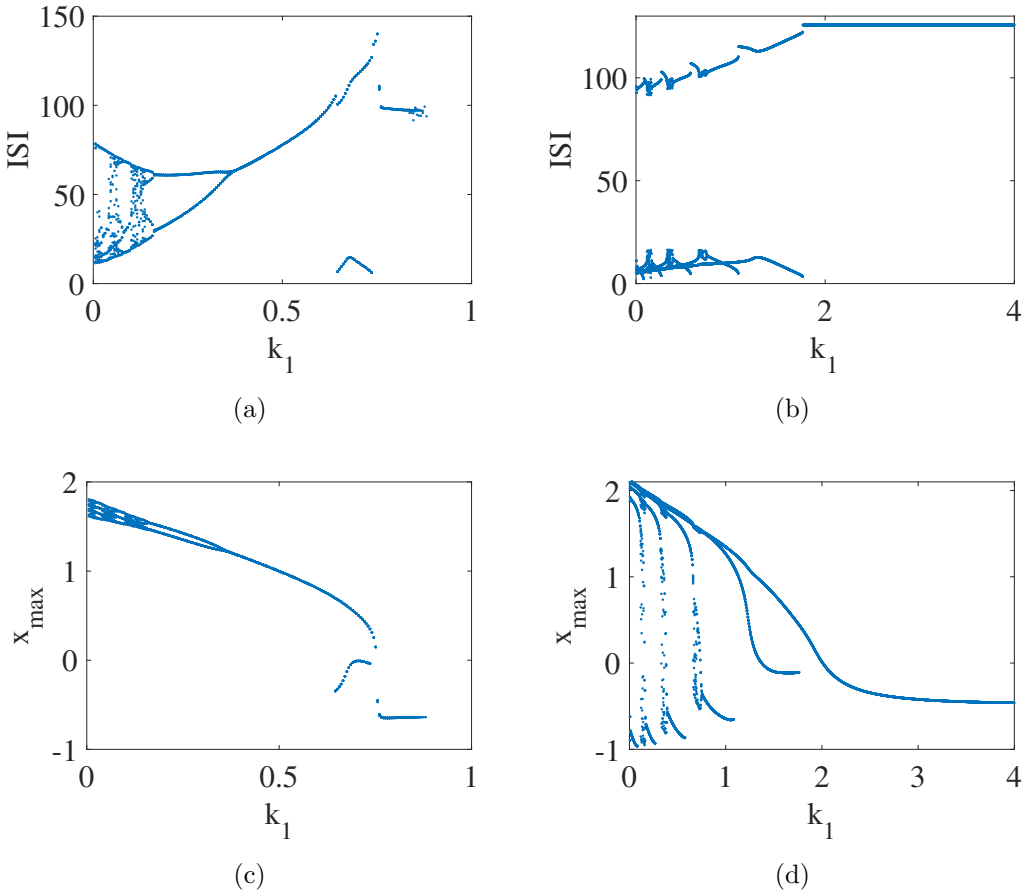

Figure 4.2: The bifurcation diagrams are drawn by applying various external stimuli. (a) and (b) ISI of membrane potentials for constant stimulus and periodic stimulus. The corresponding bifurcations of membrane potential (x) are shown in (c) and (d) respectively

of the form $Asin(\omega t)$, where A=2.0 an $\omega = 0.05$, are shown in Figs. 4.2(b) and 4.2(d).

4.3 Two Coupled System

4.3.1 HR Model with Electrical and Field Couplings

The model in Eq. (4.1) with electrical and field couplings has the form:

$$\dot{x_i} = y_i + a{x_i}^2 - {x_i}^3 - z_i + I - k_1\rho(\phi_i)x_i - g_e(x_i - x_j),$$

$$\dot{y_i} = 1 - b{x_i}^2 - y_i,$$

$$\dot{z}_i = r(R(x_i - x_e) - z_i),$$

$$\dot{\phi}_i = k_2 x_i - k_3 \phi_i + D(\phi_i - \sum_{\substack{j=1 \\ i \neq j}}^{2} \frac{W}{|i-j|}\phi_j), \quad i, j = 1, 2; i \neq j. \tag{4.4}$$

Where 'g_e' and 'D' denote the electrical coupling strength and the field interaction respectively. The weight factor 'W' describes the intensity of the field associated with distance between neurons. The change in dynamics by changing the intensity of field coupling and weight can be performed. Here, the field coupling parameters $D = 0.0001$ and $W = 1$ have been taken for numerical analysis [10].

Case 1: $\rho(\phi_i) = \alpha + 3\beta\phi_i^2$

We have analysed the dynamics of the coupled system in Eq. (4.4) by varying the strength of modulation intensity for weak ($g_e = 0.1$) and strong ($g_e = 1.5$) electrical coupling. Memristor in Eq. (4.2) has been used for the analysis with $\alpha = 0.4$ and $\beta = 0.02$. In weakly coupled case, the neurons show anti-phase oscillations for low values of modulation intensity as shown in Fig 4.3(a). For high values, the system exhibits synchronised firing as depicted in Fig. 4.3(b). For strong electrical coupling, the system always remains in the synchronised state irrespective of the value of k_1. Fig. 4.3(c) shows the time series of membrane potential for strong coupling with 5 spikes per burst for $k_1 = 0.2$. The dynamics transverse to the synchronisation manifold has been studied to analyse the point of transition from desynchrony to synchrony. The coordinates in the transverse manifold are defined as, $x_\perp = x_2 - x_1$, $y_\perp = y_2 - y_1$, $z_\perp = z_2 - z_1$ and $\phi_\perp = \phi_2 - \phi_1$. In the synchronised state, the differences $x_\perp$, $y_\perp$, $z_\perp$ and $\phi_\perp$ approaches zero as t tends to ∞ and the solution becomes $(x_1, y_1, z_1, \phi_1) = (x_2, y_2, z_2, \phi_2) = (x, y, z, \phi)$ [11]. The dynamics transverse to the synchronisation manifold has the form:

$$\dot{x}_\perp = y_\perp + 2axx_\perp - 3x^2 x_\perp - z_\perp - k_1\alpha x_\perp - 3\beta k_1 \phi^2 x_\perp - 2g_e x_\perp,$$

$$\dot{y}_\perp = -2bxx_\perp - y_\perp,$$

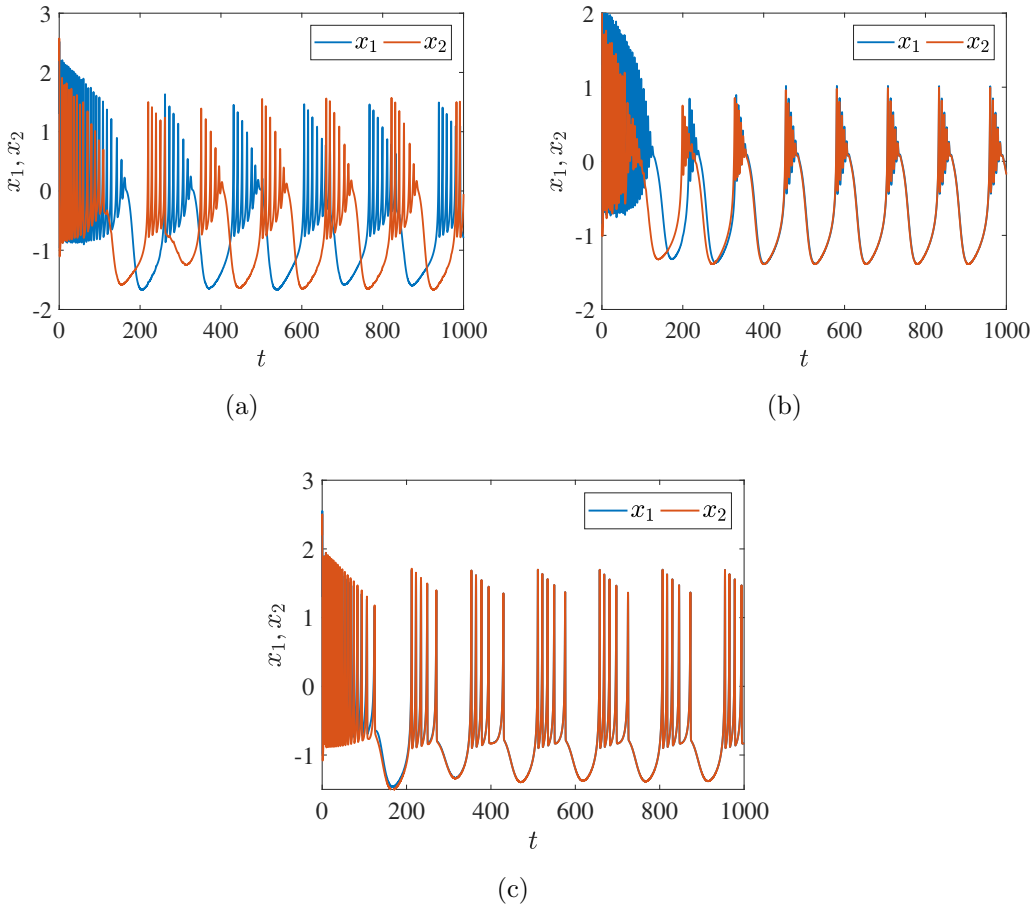

Figure 4.3: The time series of membrane potential with electrical synapse. (a) anti-phase oscillations for $g_e = 0.1$ and $k_1 = 0.2$. (b) Synchronisation for $g_e = 0.1$ and $k_1 = 0.9$. (c) Synchronised bursting with 5 spikes per burst for $g_e = 1.5$ and $k_1 = 0.2$.

$$\dot{z}_\perp = r(Rx_\perp - z_\perp),$$

$$\dot{\phi_\perp} = k_2 x_\perp - k3\phi_\perp + 2D\phi_\perp. \tag{4.5}$$

The TLEs associated with Eq. (4.5) becomes negative at the point of complete synchronisation. We have plotted the TLEs by varying the strength of modulation intensity of the field, for weak and strong coupling. Fig. 4.4(a) shows that, for weak coupling, the largest TLE becomes negative at $k_1 = 0.9$, i.e., the neurons show complete synchronisation. From Fig. 4.4(b), it is evident that, with strong coupling, the $\lambda_{\perp_1}$ remains negative irrespective of the value of k_1 and the system shows synchronisation.

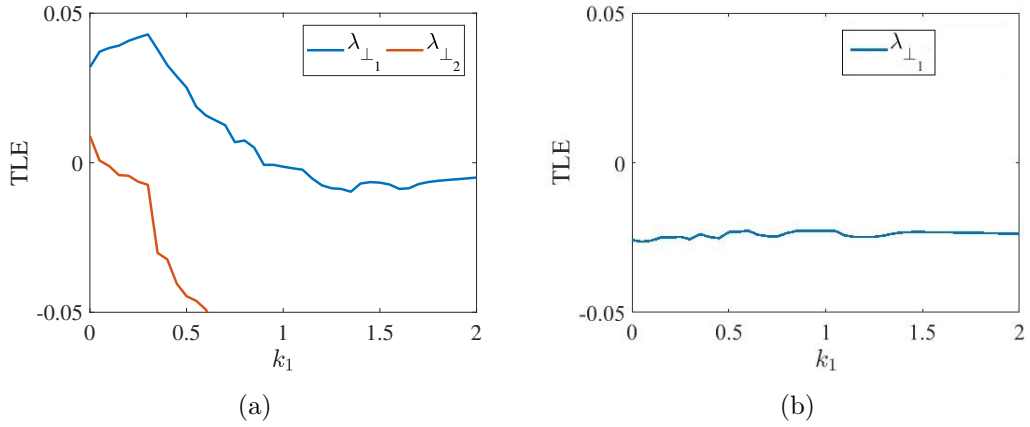

Figure 4.4: Variation of TLEs ($\lambda_{\perp_1}$ and $\lambda_{\perp_2}$) with k_1. The neurons are coupled via electrical synapse. (a) For weak coupling the largest TLE ($\lambda_{\perp_1}$) crosses zero and become negative at $k_1 = 0.9$, indicating a transition from desynchrony to synchrony at this point. (b) For strong coupling ($\lambda_{\perp_1}$) remains negative through out the range which indicates that the system shows synchronisation.

Case 2: $\rho(\phi_i) = \alpha\phi_i^2 + \beta\phi_i + \gamma$

The system in Eq. (4.4) with memristor of the form in Eq. (4.3) has been analysed in this section. A peculiar dynamical state arises when the parameters have been chosen as $\alpha = 0.02, \beta = 0, \gamma = 0, k_1 = 0.9, I = 1.4$ and $g_e = 0.01$, in which one neuron remains in the firing state while the other shows death state, as shown in Fig. 4.5(e). On decreasing α, the two neurons show anti-phase oscillations. The two simplest patterns observed in brain are in-phase and anti-phase oscillations. In in-phase pattern, the neurons fire simultaneously and helps to integrate separated functions performed in different regions. The functional magnetic resonance imaging (fMRI) studies reveal that, spontaneous blood oxygen level-dependent signal during resting state varies slowly with a small frequency in a highly organised anti-phase pattern[12]. During attentional tasks different functional regions of brain also show two opposite type of responses [13]. The anti-phase oscillatory state enables brain to memorise many object representations in visual working memory without making confusion [14]. In both cases, the communication can be in the form of spikes or bursts. Compared to spikes, bursts increase the reliability of communication between neurons and have a stronger effect on their targets than single spikes. Figs. 4.5(a) - 4.5(d)

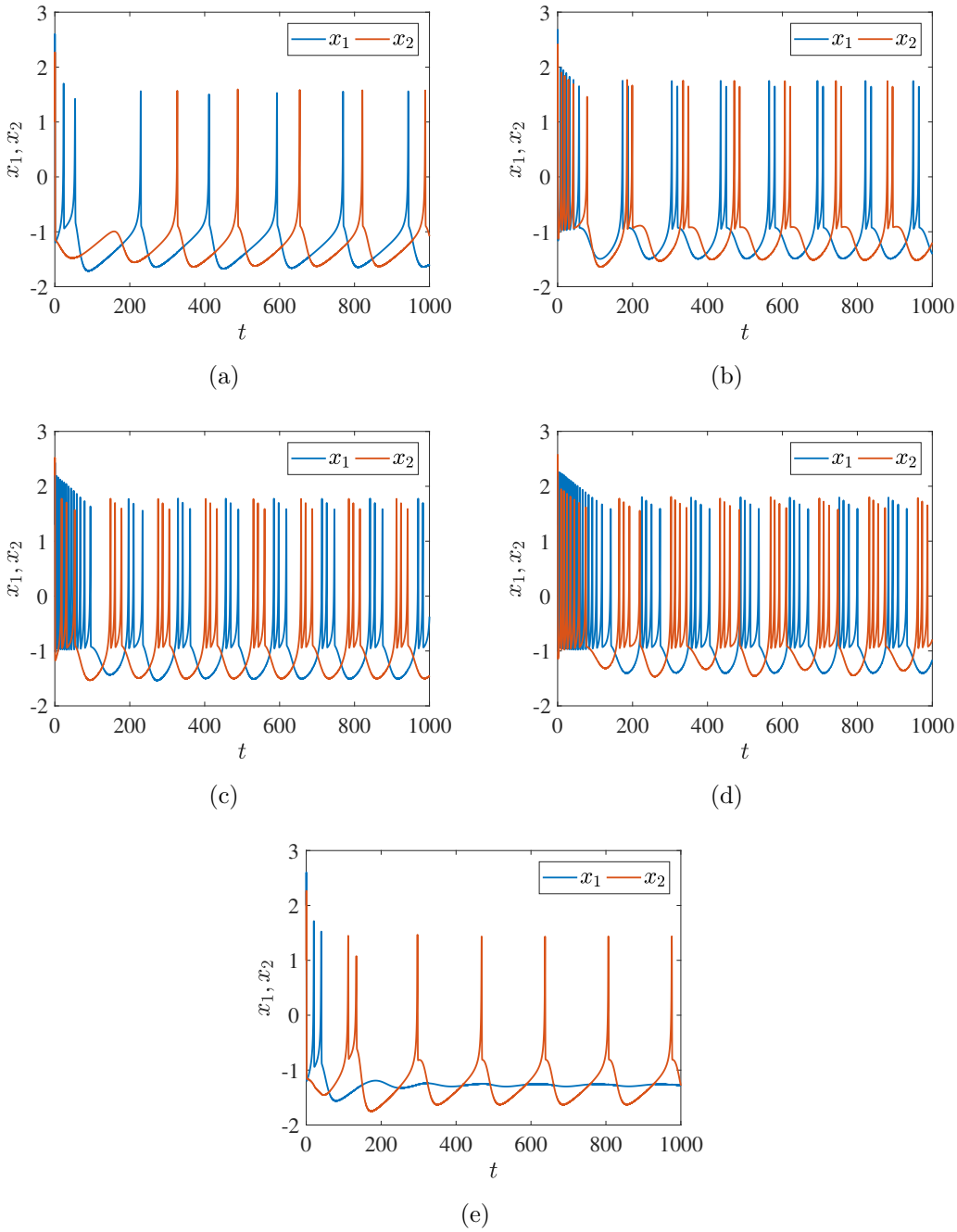

Figure 4.5: Anti-phase oscillations by varying I for $\alpha = 0.002$(a) tonic spiking ($I = 1.4$) Bursting oscillations with (b) 2 spikes per burst ($I = 1.8$) (c) 3 spikes per burst ($I = 2.4$) (d) 4 spikes per burst ($I = 2.9$) (e) one neuron shows AD and while the other exhibits tonic spiking for $\alpha = 0.02$ and $I = 1.4$.

show the anti-phase oscillations with tonic spiking, bursting with 2, 3, and 4 spikes per burst observed for different values of the external stimuli.

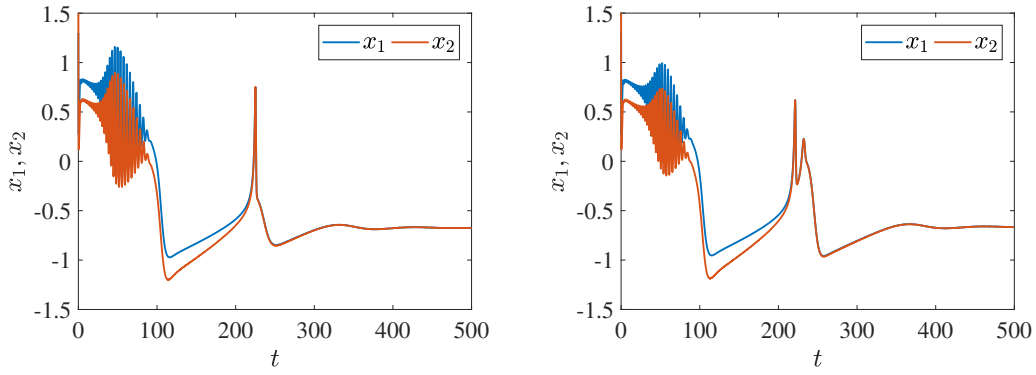

Figure 4.6: The time series of membrane potential (a) near death rare spike for $\alpha = 5, \beta = 3, \gamma = 0.1, k_1 = 0.1, I = 3.1$, and $g_e = 1$ (b) An additional small peak along with near death rare spike for $\gamma = 0.5$.

Near Death Experience (NDE)

An important dynamical state called NDE have been observed when both neurons are subjected to the same magnetic flux variations, i.e., the ϕ_1 and ϕ_2 in Eq. (4.4) are replaced by ϕ. During NDE rare spikes are observed before the neuron goes to the death state. Experimentally, it is confirmed that, a few seconds before death people experience an abrupt change in brain activities characterised by the emergence of synchronised spikes called near death rare spikes [15]. Experimental studies in rats also confirmed the presence of NDE [16]. Borjigin *et al.* have reported a transient surge of synchronised gamma oscillations in the electroencephalogram of rats, which occur immediately after the cardiac arrest. The activity of different regions of brains get synchronised at the time of NDE [16]. Synchronised near death rare spikes have been observed for the parameter set $\alpha = 5.0, \beta = 3.0, \gamma = 0.1, k_1 = 0.1, I = 3.1$, and $g_e = 1.0$ as shown in Fig. 4.6(a). As the value of γ is increased to 0.5, an additional small spike emerges close to near death spike as depicted in Fig. 4.6(b). The dynamics transverse to the synchronisation manifold has the form:

$$\dot{x}_\perp = y_\perp + 2axx_\perp - 3x^2x_\perp - z_\perp - k_1\alpha\phi^2x_\perp - \beta k_1\phi x_\perp - k_1\gamma x_\perp - 2g_e x_\perp,$$

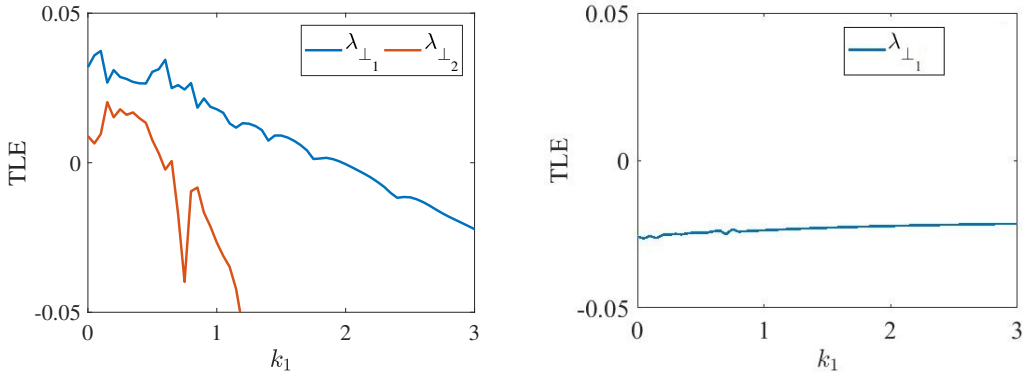

Figure 4.7: Variation of TLEs ($\lambda_{\perp_1}$ and $\lambda_{\perp_2}$) with k_1. (a) For weak coupling the largest TLE ($\lambda_{\perp_1}$) crosses zero and become negative at of $k_1 = 2.2$, indicating a transition from desynchrony to synchrony at this point. (b) For strong coupling ($\lambda_{\perp_1}$) remains negative through out the range which indicates that the system shows synchronisation.

$$\dot{y}_\perp = -2bxx_\perp - y_\perp,$$

$$\dot{z}_\perp = r(Rx_\perp - z_\perp),$$

$$\dot{\phi_\perp} = k_2 x_\perp - k3\phi_\perp + 2D\phi_\perp. \tag{4.6}$$

To analyse the regions of synchrony and desynchrony, the TLEs associated with Eq. (4.6) have been plotted by varying the strength of modulation intensity of the field for weak and strong synaptic coupling ($\alpha = 0.4, \beta = 0.02$, and $\gamma = 0.1$). For weak coupling, $\lambda_{\perp_1}$ become negative at $k_1 = 2.2$ as shown in Fig. 4.7(a) and in the case of strong coupling, $\lambda_{\perp_1}$ remains negative always as shown in Fig. 4.7(b).

4.3.2 HR Model with Chemical and Field Couplings

The dynamics of HR neurons in the presence of chemical and field couplings have the form:

$$\dot{x_i} = y_i + a{x_i}^2 - {x_i}^3 - z_i + I - k_1\rho(\phi_i)x_i - g_c(x_i - V_s)\Gamma(x_j),$$

$$\dot{y_i} = 1 - b{x_i}^2 - y_i,$$

$$\dot{z}_i = r(R(x_i - x_e) - z_i),$$

$$\dot{\phi}_i = k_2 x_i - k_3 \phi_i + D(\phi_i - \sum_{\substack{j=1 \\ i \neq j}}^{2} \frac{W}{|i-j|}\phi_j), \quad i,j = 1,2; i \neq j. \tag{4.7}$$

Here g_c denotes the coupling strength of chemical synaptic junction. V_s is the reversal potential and it is always greater than x_i for all neuron at all times for excitatory synapses. $\Gamma(x_j) = 1/[1 + exp(-\lambda(x_j - \theta))]$ is an exponential function which models the synaptic junction and θ is the threshold [17]. For each neuron to reach the threshold, we have chosen $\theta = -0.25$, $V_s = 2$ and $\lambda = 7.5$ [18].

Case 1: $\rho(\phi_i) = \alpha + 3\beta\phi_i^2$

We have analysed the synchronisation transitions of HR model in Eq. (4.7) with memristor in Eq. (4.2). The dynamics transverse to the synchronisation manifold [19] has the form:

$$\dot{x}_\perp = y_\perp + 2axx_\perp - 3x^2x_\perp - z_\perp - k_1\alpha x_\perp - 3\beta k_1\phi^2 x_\perp - \Omega(x)x_\perp,$$

$$\dot{y}_\perp = -2bxx_\perp - y_\perp,$$

$$\dot{z}_\perp = r(Rx_\perp - z_\perp),$$

$$\dot{\phi} = k_2 x_\perp - k_3\phi_\perp + 2D\phi_\perp, \tag{4.8}$$

where,

$$\Omega(x) = g_c\Gamma(x) - g_c(x\_V_s)\Gamma_x(x),$$

$$\begin{aligned} \Omega(x) = \quad & g_c[\frac{1}{(1 + exp(-\lambda(x-\theta)))}] - \\ & g_c[(x - V_s)\frac{(\lambda(exp(-\lambda(x-\theta))))}{(1 + exp(-\lambda(x-\theta)))^2}]. \end{aligned} \tag{4.9}$$

The TLEs associated with Eq. (4.8) for weak and strong coupling are shown in Fig. 4.8. In the case of weak coupling, $\lambda_{\perp_1}$ become negative at $k_1 = 0.5$ as shown in Fig. 4.8(a), and in the case of strong coupling, $\lambda_{\perp_1}$ remains negative

as depicted in Fig. 4.8(b). With strong coupling the chemically coupled HR neurons show synchronisation. The dynamics in the synchronised state is AD as shown in Fig. 4.9. This behaviour is essential to stabilise the system. AD in neural network is very important to understand the temporal activity emerging in the olfactory bulb [20].

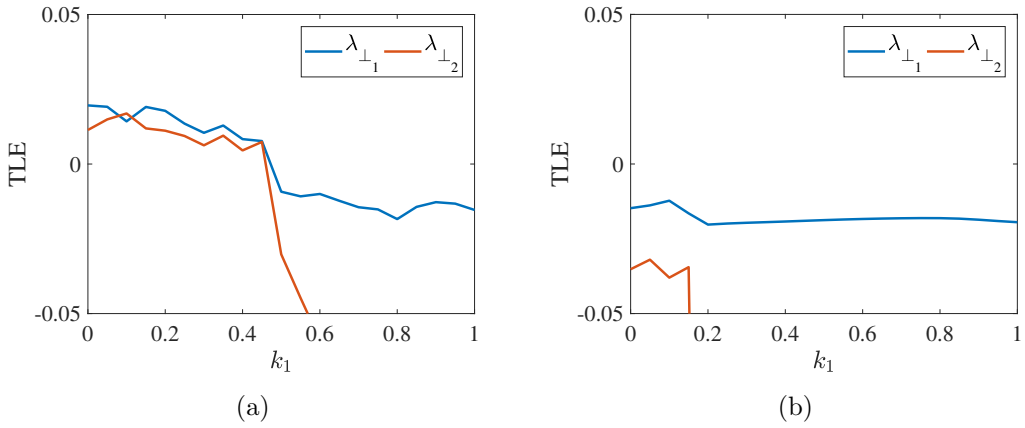

Figure 4.8: Variation of TLEs ($\lambda_{\perp_1}$ and $\lambda_{\perp_2}$) with k_1. Chemical synaptic coupling is considered. (a) For weak coupling ($g_c = 0.1$) the largest TLE ($\lambda_{\perp_1}$) crosses zero and become negative at of $k_1 = 0.5$. (b) For strong coupling ($g_c = 1.5$), $\lambda_{\perp_1}$ remains negative through out the range which indicates that the system shows synchronisation.

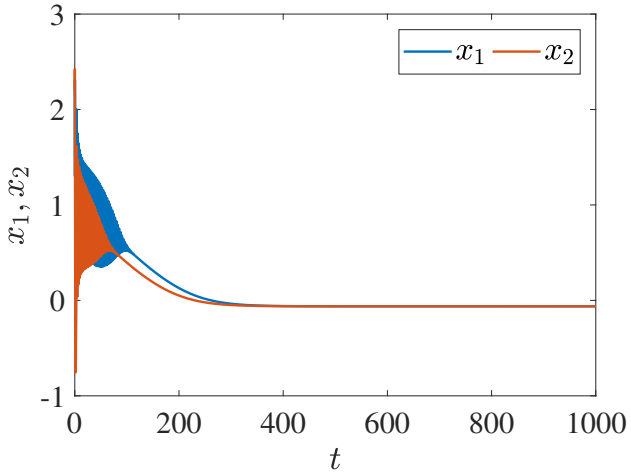

Figure 4.9: Synchronisation of chemically coupled HR neurons with strong coupling. The dynamics in the synchronised state is AD.

Case 2: $\rho(\phi_i) = \alpha\phi_i^2 + \beta\phi_i + \gamma$

We have analysed the dynamics of the system in Eq. (4.7) with memristor of the form in Eq. (4.3). The dynamics transverse to the synchronisation manifold has the form:

$$\begin{aligned}
\dot{x}_\perp &= y_\perp + 2axx_\perp - 3x^2x_\perp - z_\perp - k_1\alpha\phi^2x_\perp - \beta k_1\phi x_\perp - k_1\gamma x_\perp - \Omega(x)x_\perp, \\
\dot{y}_\perp &= -2bxx_\perp - y_\perp, \\
\dot{z}_\perp &= r(Rx_\perp - z_\perp), \\
\dot{\phi} &= k_2x_\perp - k3\phi_\perp + 2D\phi_\perp.
\end{aligned} \tag{4.10}$$

$\Omega(x)$ has the same form as that in Eq. (4.9). The TLEs associated with Eq. (4.10) for weak and strong coupling are shown in Figs. 4.10(a) and 4.10(b) respectively. In the case of weak coupling, $\lambda_{\perp_1}$ become negative at $k_1 = 2.1$, whereas $\lambda_{\perp_1}$ always remains negative for strong coupling. The dynamics in the synchronised state is AD as shown in Fig. 4.9.

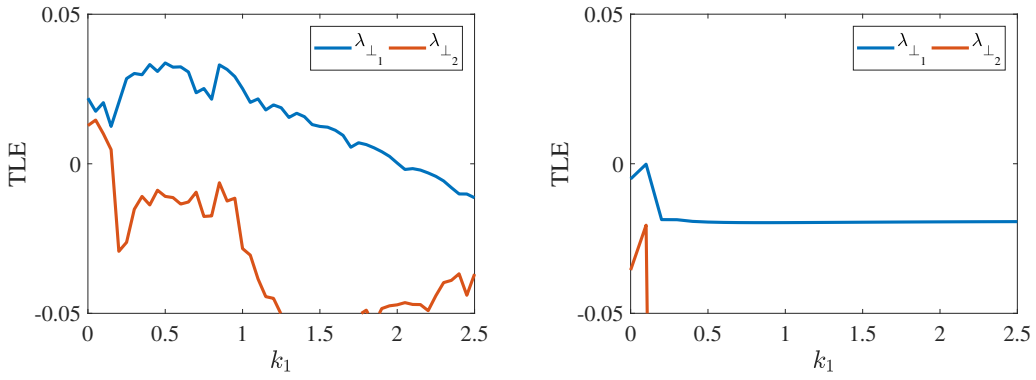

Figure 4.10: Variation of TLEs ($\lambda_{\perp_1}$ and $\lambda_{\perp_2}$) with k_1. (a) For weak coupling the largest TLE ($\lambda_{\perp_1}$) crosses zero and become negative at of $k_1 = 2.1$. (b) For strong coupling ($\lambda_{\perp_1}$) remains negative through out the range.

4.4 Results and Conclusions

We have analysed the dynamics and synchronisation of HR neurons with field effects. Memristors are used to describe the interaction of the field and the membrane potential of neurons. The bifurcation diagrams confirm that HR neurons with memristors show chaotic bursting, periodic bursting, periodic spiking and quiescent state with the increase in strength of modulation intensity of the field. The study has been extended to a two coupled system of HR neurons with memristors. The numerical studies has been performed for both weak and strong coupling. In the presence of memristors of the form, $\rho(\phi) = \alpha + 3\beta\phi^2$, the HR neurons with weak electrical coupling ($g_e = 0.1$) show anti-phase oscillations for low values of k_1 and synchronised firing with increasing k_1. With strong coupling the system always remains in the synchronised state. The analysis of HR model with electrical synapse in the presence of improved memristor with an additional linear dependence in ϕ, i.e., $\rho(\phi) = \alpha\phi^2 + \beta\phi + \gamma$, show many of the important dynamical states like synchrony, desynchrony, AD, anti-phase oscillations, coexistence of resting and spiking state and NDE. Motivated by fMRI studies of brain [12], we have performed a detailed analysis on the anti-phase oscillations with tonic spiking and bursting (with 2, 3, and 4 spikes per burst) with increase in I. When coupled via chemical synapse, the system shows oscillation quenching in the form of AD in the synchronised state. In all types of coupling, the TLEs have been plotted to observe the point of transition from desynchrony to synchrony.

Bibliography

[1] L.O. Chua. *IEEE Trans. Circuit Theory*, pages 507–519, 1971.

[2] Z. Wang. *Nature Materials*, 16:101–108, 2017.

[3] D. B. Strukov, G. S. Snider, D. R. Stewart, and R. S. Williams. *Nature*, 453:80, 2008.

[4] S. Wen, Z. Zeng, and T. Huang. *Neurocomputing*, 97:233, 2012.

[5] W. Guan, S. Yi, and Y. Quan. *Chin. Phys. B*, 22:050504, 2013.

[6] A. Abdurahman, H. Jiang, and Z. Teng. *Neural Networks*, 69:20–28, 2015.

[7] Y. Xu, H. Ying, Y. Jia, J. Ma, and T. Hayat. *Scientific Reports*, 7:43452, 2017.

[8] M. Storace, D. Linaro, and E. de Lange. *Chaos*, 18:033128, 2008.

[9] S. K. Thottil and R. P. Ignatius. *Nonlinear Dyn.*, 87:1879–1899, 2017.

[10] Y. Xu, Y. Jia, J. Ma, T. Hayat, and A. Alsaedi. *Scientific Reports*, 8:1349, 2018.

[11] M. Dhamala, V. K. Jirsa, and M. Ding. *Phys. Rev. Lett.*, 92:028101, 2004.

[12] M. D. Fox, A. Z. Snyder, J. L. Vincent, M. Corbetta, D. C. Van Essen, and M. E. Raichle. *Proc. Natl. Acad. Sci. U.S.A.*, 102:9673, 2005.

[13] R. Cabeza and L. Nyberg. *J. Cogn. Neurosci.*, 12:1–47, 2000.

[14] P. Tseng, Y. T. Chang, C. F. Chang, W. K. Liang, and C. H. Juan. *Scientific Reports*, 6:32138, 2016.

[15] I. Klotz. *Chin. Phys. B*, 24:118401.

[16] J. Borjigin, U. Lee, T. Liu, D. Pal, S. Huff, D. Klarr, J. Sloboda, J. Hernandez, M. M. Wang, and G. A. Mashour. *PNAS*, 110:144432–144437, 2013.

[17] D. Somers and N. Kopell. *Biol. Cybern*, 68:393, 1993.

[18] J. Jonq and L. Yu-Hao. *Chaos*, 24:013110, 2014.

[19] K. Usha and P. A. Subha. *Int. J. Mod. Phys. C*, 29:1850023, 2018.

[20] L. H. A. Monteiro, A. P. Filho, J. G. Chaui-Berlinck, and J. R. C. Piqueira. *J. of Bio. Sys.*, 15:49–61, 2007.

Chapter 5

Chaos Control via Energy Feedback in the Modified HR Neuron Model

5.1 Introduction

The calculation of metabolic energy required to maintain the signalling activity in neurons is an active research area [1]. Neuron models are used to analyse the connection between energy demands and firing modes [2]. The energy function associated with the dynamical system can be derived using the generalised Hamiltonian approach [3]. Using this formalism Sarasola *et al.* have derived the energy function associated with Lorenz, Rossler and Chua systems [1]. Moujahid *et al.* have reported the energy consumption during the synchronisation process in electrically coupled HR neurons [4]. The consumption of energy in transmitting nerve impulse using Hodgkin-Huxley model has also been reported [5].

It is also important to investigate the energy utilisation of neurons subjected to different kinds of external stimuli during information encoding. Biological experiments confirm that the electrical activities of neurons change with external

stimuli [6–8]. The periodic external stimuli influences the bursting modes and neuronal activities [9]. In addition, computational models have been developed to study the effect of noise. The statistical features of Gaussian white noise seem to be appropriate to mimic the complex behaviour shown by a neuron under the influence of other neurons and the environment. Zambrano *et al.* have analysed the synchronisation of uncoupled FHN neurons with common noise both experimentally and numerically [10]. Noise-induced resonances in the HR model has also been studied [11]. Wang *et al.* have reported that the forced HR neurons with white Gaussian noise leads to firing modes like multi-modal firing, intrinsic oscillation and bi-modal firing [12]. Lindner *et al.* have studied the dynamics of mathematical models of excitable systems in the presence of white Gaussian noise [13]. The energy aspects of memristor based neuron models have significant importance. The electrical activities in the cardiac tissues exposed to electromagnetic radiation can be described using memristor models. This provides significant clues about the mechanism of heart disorders induced by electromagnetic radiation [14]. The synchronisation of coupled memristive neural network has been proposed by Guan *et al.* [15]. Recently Ma *et al.* have discussed the RCL-shunted junction circuit with memristor [16]. The control of dynamical systems with negative feedback in energy has been reported recently [17].

In this chapter, chaos control via energy feedback in HR neuron model with memristor has been discussed. Section 5.2 describes the model. The Hamilton energy of the system has been derived in section 5.3 and the energy change in the presence of different external stimuli has been discussed. In section 5.4, the control of chaotic trajectories by applying a negative feedback have been analysed. The synchronous dynamics of electrically and chemically coupled neurons with field effects are discussed in section 5.5. Section 5.6 concludes the study.

5.2 Bifurcations

The dynamical equations of modified HR model with memristor have the form:

$$\dot{x} = y + ax^2 - x^3 - z + I - k_1\rho(\phi)x,$$

$$\dot{y} = 1 - bx^2 - y,$$

$$\dot{z} = r(R(x - x_e) - z),$$

$$\dot{\phi} = k_2 x - k_3\phi, \tag{5.1}$$

where $\rho(\phi) = \alpha\phi^2 + \beta\phi + \gamma$. x, y and z are the membrane potential, recovery variable and adaptation variable respectively. The parameters used are $a = 3.0$, $b = 5.0$, $R = 4.0$, $r = 0.006$, $I = 3.1$, and $x_e = -1.61$ [18].

We have analysed the dynamics of the system in Eq. (5.1) by varying the external current I. The memristor parameters are taken as $\beta = 1.0, \gamma = 1.0, k_2 = 0.9$ and $k_3 = 0.5$. The value of k_1 is fixed at 0.1 and by increasing the value of α the inter spike interval bifurcation (ISI) diagrams have been plotted. Figs. 5.1(a), 5.1(c) and 5.1(e) show the distribution of ISI for $\alpha = 0.1, 0.4$ and 0.8 respectively. It is found that as the value of α is increased, the system eventually transforms to its normal response state. The study has been extended by fixing $\alpha = 0.1$ and by varying k_1. Figs. 5.1(b), 5.1(d) and 5.1(f) represent the I verses ISI for $k_1 = 0.8, 0.4$ and 0.1 respectively. From the plots it is clear that, for constant α, a decrease in k_1 is needed for normal firing. The response of a neuron to external signals can be enhanced by selecting the memristor parameters appropriately [19].

5.3 Hamilton Energy

The Hamilton energy of the system has been derived in this section. The differential equation of an autonomous dynamical system is of the form: $\dot{x} = f(x)$.

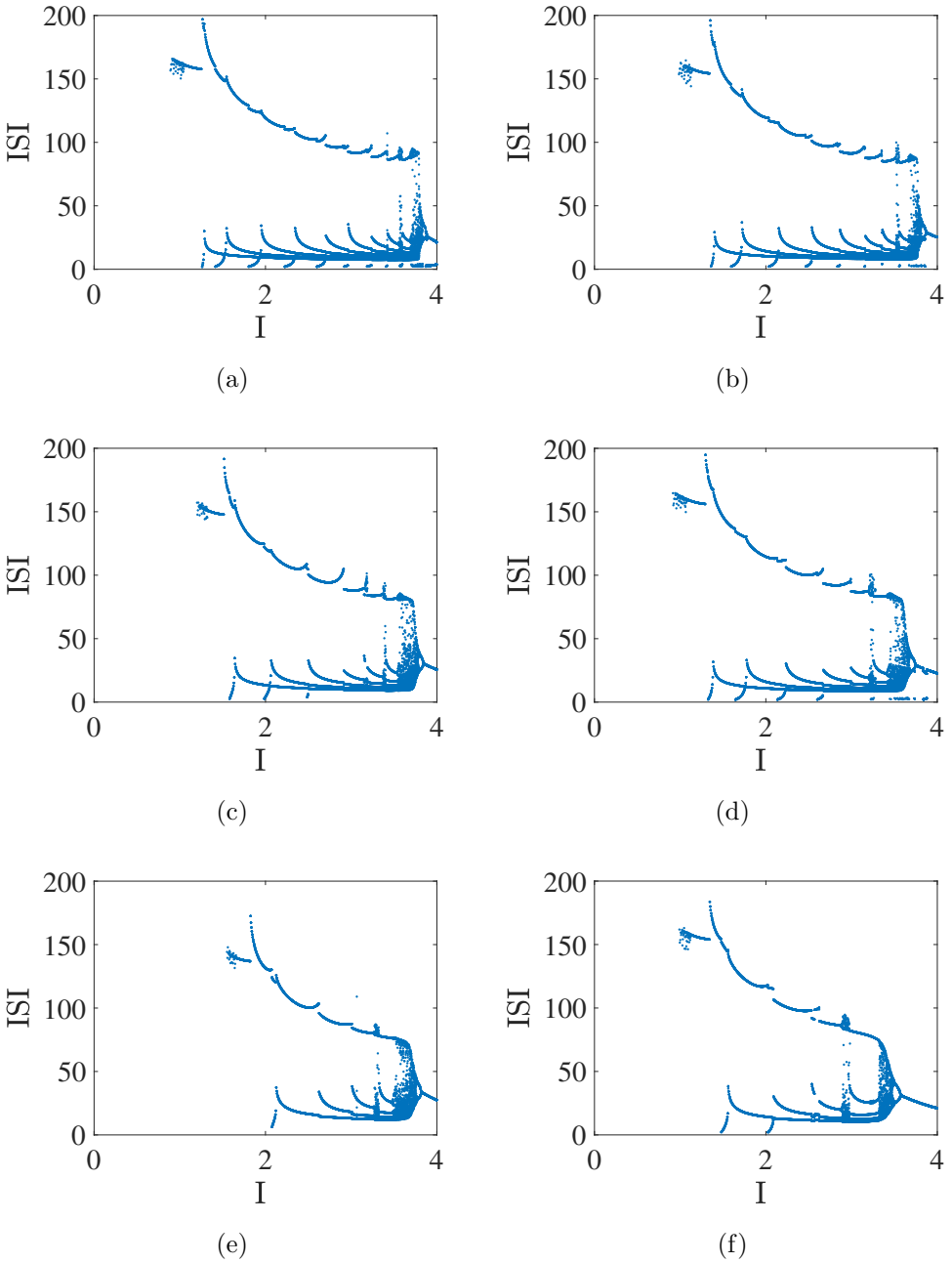

Figure 5.1: ISI bifurcation diagram of HR neuron with memristor. Figs. 5.1(a), 5.1(c), and 5.1(e) shows I verses ISI for $k_1 = 0.1$ and $\alpha = 0.1, 0.4$, and 0.8. Figs. 5.1(b), 5.1(d), and 5.1(f) are drawn for $\alpha = 0.1$, $k_1 = 0.8, 0.4$, and 0.1. The parameters β and γ are set as 1.0.

According to Helmholtz's theorem the velocity vector field $f(x)$ can be written as,

$$f(x) = f_c(x) + f_d(x), \tag{5.2}$$

where f_c component of the vector field is conservative. It does not contribute to the energy change along any trajectory of the system and satisfies the following equation,

$$\nabla H^T f_c(x) = 0. \tag{5.3}$$

The dissipation of energy due to the f_d part obeys the relation:

$$\nabla H^T f_d(x) = \dot{H}. \tag{5.4}$$

Where $H(x)$ is the Hamilton energy function. The conservative and dissipative part of HR model in Eq. (5.1) can be expressed in the form:

$$\begin{bmatrix} \dot{x} \\ \dot{y} \\ \dot{z} \\ \dot{\phi} \end{bmatrix} = f_c(x, y, z, \phi) + f_d(x, y, z, \phi)$$

where

$$f_c(x, y, z, \phi) = \begin{bmatrix} y - z + I - \phi \\ 1 - bx^2 \\ rR(x - x_e) \\ k_2 x \end{bmatrix}$$

and

$$f_d(x,y,z,\phi) = \begin{bmatrix} ax^2 - x^3 - k_1\rho(\phi)x + \phi \\ -y \\ -rz \\ -k_3\phi \end{bmatrix}$$

Then, according to Eq. (5.3), the Hamilton energy associated with the system will satisfy the following partial differential equation:

$$(y - z + I - \phi)\frac{\partial H}{\partial x} + (1 - bx^2)\frac{\partial H}{\partial y} + rR(x - x_e)\frac{\partial H}{\partial z} + k_2 x\frac{\partial H}{\partial \phi} = 0. \quad (5.5)$$

A general solution for Eq. (5.5) is of the form:

$$H = \frac{2}{3}bx^3 - 2x + rR(x - x_e)^2 + (y - z + I - \phi)^2 + k_2x^2. \quad (5.6)$$

The rate of change of Hamilton energy function has been obtained as:

$$\begin{aligned} \dot{H} = \; & 2bx^2\dot{x} - 2\dot{x} + 2rR(x - x_e)\dot{x} \\ & +2(y - z + I - \phi)(\dot{y} - \dot{z} - \dot{\phi}) + 2k_2x\dot{x}. \end{aligned} \quad (5.7)$$

Substituting the values of $\dot{x}, \dot{y}, \dot{z}$ and $\dot{\phi}$ from Eq. (5.1), $\dot{H}$ becomes:

$$\begin{aligned} \dot{H} = \; & 2bx^2(y + ax^2 - x^3 - z + I - k_1\rho(\phi)x) \\ & -2(y + ax^2 - x^3 - z + I - k_1\rho(\phi)x) \\ & +2rR(x - x_e)(y + ax^2 - x^3 - z + I - k_1\rho(\phi)x) \\ & +2(y - z + I - \phi)(1 - bx^2 - y - rR(x - x_e) + rz - k_2x + k_3\phi \\ & +2k_2x(y + ax^2 - x^3 - z + I - k_1\rho(\phi)x), \end{aligned} \quad (5.8)$$

rearranging Eq. (5.8), $\dot{H}$ has the form:

$$\begin{aligned}\dot{H} = \; & 2bx^2(y - z + I_{ext} - \phi) + 2bx^2(ax^2 - x^3 - k_1\rho(\phi)x + \phi) \\ & -2(y - z + I_{ext} - \phi) - 2(ax^2 - x^3 - k_1\rho(\phi)x + \phi) \\ & +2rR(x - x_e)(y - z + I - \phi) \\ & +2rR(x - x_e)(ax^2 - x^3 - k_1\rho(\phi)x + \phi) \\ & +2(y - z + I_{ext} - \phi)(1 - bx^2 - y - rR(x - x_e) + rz - k_2x + k_3\phi) \\ & +2k_2x(y - z + I - \phi) + 2k_2x(ax^2 - x^3 - k_1\rho(\phi)x + \phi), \end{aligned} \tag{5.9}$$

simplifying and rearranging Eq. (5.9), the expression for $\dot{H}$ takes the form:

$$\begin{aligned}\dot{H} = \; & 2(ax^2 - x^3 - k_1\rho(\phi)x + \phi)(bx^2 - 1 + rR(x - x_e) + k_2x) \\ & +2(y - z + I - \phi)(-y + rz + k_3\phi), \end{aligned} \tag{5.10}$$

and hence obeys the relation in Eq. (5.4).

The average energy of the system is evaluated using the expression,

$$< H >= \int_{t_0}^{t_0+T} H(x, y, z, \phi)dt/T. \tag{5.11}$$

Where T is the energy calculation period (1000 time units) and t_0 is the starting time to calculate the average energy. Fig. 5.2 shows the variations in average energy with constant stimulus (I). The parameters used are $k_1 = 0.1, k_2 = 0.9$, and $k_3 = 0.5, \alpha = 0.4, \beta = 0.02$ and $\gamma = 0.1$ [9]. From the plot it is clear that, when the strength of external stimulus is increased, the average energy is decreased. The rate of change of Hamilton energy in the resting and bursting state of membrane potential has been analysed by applying various external stimuli.

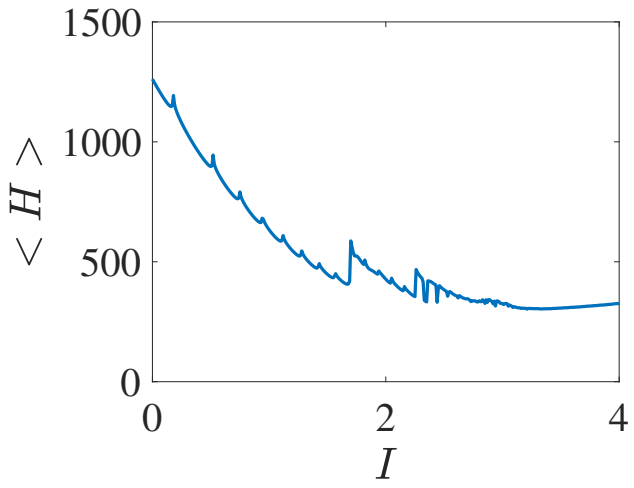

Figure 5.2: The variations in average energy of HR neuron with memristor for different values of constant external stimulus.

5.3.1 Constant External Stimulus

A constant external stimulus (I) has been applied to the system. The strength of the stimulus has been changed from 2.0 to 3.0 at $t = 1000$ and then switched to 1.0 at $t = 1500$ as depicted in Fig. 5.3(a). The corresponding variations in energy utilisation and membrane potential are shown in Figs. 5.3(b) and 5.3(c) respectively. From the plots, it is clear that as the external stimulus is varied the bursting mode of neuron change and for generating the action potential energy is consumed. The energy demand is maximum during the repolarisation period of the spike and minimum during the refractory period between two spikes. The energy utilisation approaches zero when the membrane potential is close to the quiescent state.

5.3.2 Periodic External Stimulus

The effect of periodic stimulus in neural activity has been analysed by applying an input of the form $I = I_1 + Asin(0.05t)$, where $I_1 = 3.1$ and 'A' represents the amplitude. The membrane potential and energy utilisation during the electrical activities are plotted. The amplitude of periodic stimulus has been changed from 0.1 to 1.0 at $t = 1000$ and then switched to 2.0 at $t = 1500$ as shown

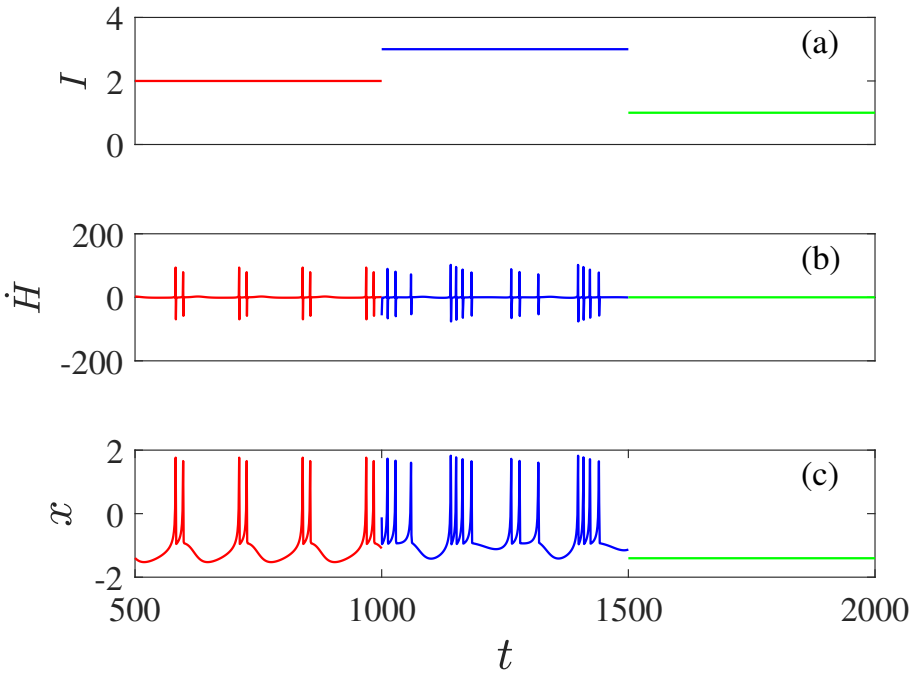

Figure 5.3: (a) Variation of external current (b) rate of change of energy function and (c) time evolution of membrane potential of neuron. The external current I is changed from 2.0 to 3.0 at t = 1000 time units and switched to 1.0 at t = 1500 time units.

in Fig. 5.4(a). In the case of periodic input, A acts as control parameter for generating different types of electrical responses. As amplitude is increased, the number of spikes per burst in membrane potential is also increased as shown in Fig. 5.4(c). The transition in bursting mode induce some transition in Hamilton energy. In the case of state with less number of spikes per burst, the Hamilton energy consumed also become smaller as depicted in Fig. 5.4(b).

5.3.3 White Gaussian Noise

The influence of noise in the firing pattern is discussed in Fig. 5.5. The white Gaussian noise is added through the electrical potential of the membrane, i.e., the effective current imposed to the neuron contains a random term [20]. The noise is of the form $I = I_1 + \zeta\xi(t)$, with parameters $\langle\xi(t)\rangle = 0$, $\langle\xi(t)\ \xi^T(t+\tau)\rangle = \delta(\tau)$ and ζ defines the noise intensity. The value of I_1 is fixed as 3.1 and ζ is changed from 0.01 to 0.1 at $t = 1000$ and then switched to 1.0 at $t = 1500$ as shown in Fig.

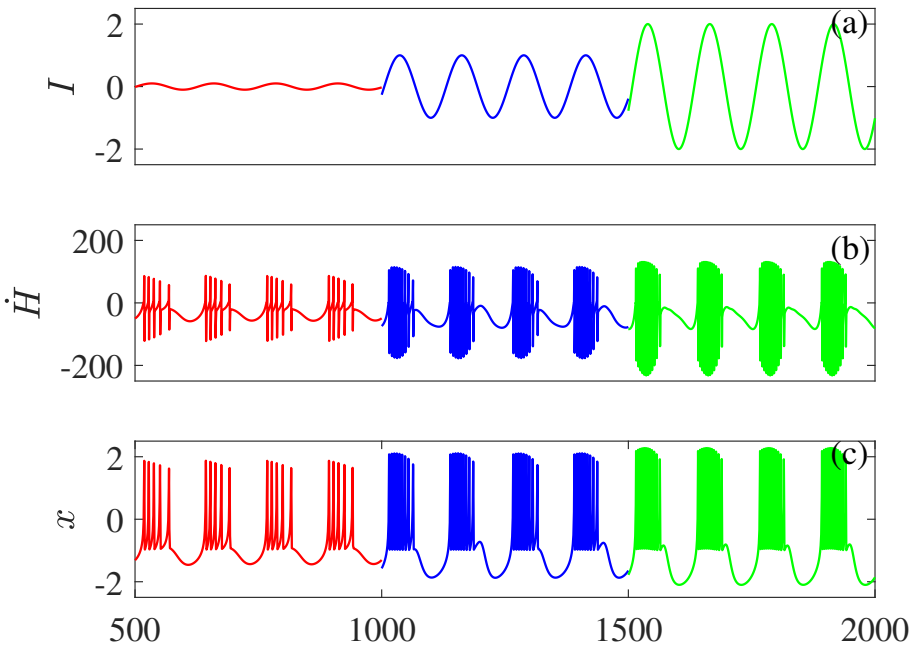

Figure 5.4: (a) Variation of periodic input (b) rate of change of energy function and (c) time evolution of membrane potential of neuron. The external periodic forcing has the form $I = I_1 + Asin(0.05t)$. I_1 is fixed at 3.1 and A is changed from 0.1 to 1.0 at $t = 1000$ and then switched to 2.0 at $t = 1500$.

5.5(a). The corresponding variations in membrane potential are shown in Fig. 5.5(c). From the plot it is clear that the bursting mode changes with the increase in noise intensity. The energy utilisation in the presence of noise is depicted in Fig. 5.5(b). It is confirmed that noisy stimulus can trigger complex discharge in energy utilisation and the effect of noise is more evident in the refractory period of the action potential. Bifurcation diagram in $(A - x_{max})$ and $(A - ISI)$ plane for periodic stimulus is shown in Figs. 5.6(a) and 5.6(b) respectively. The amplitude of periodic forcing is varied as $0 \leq A \leq 4$. The plots show that, an alternate sequence bursting states occur with increase in A. The bifurcations in the presence of noisy external stimulus are shown in Figs. 5.6(c) and 5.6(d). The noise intensity is varied in the range $0 \leq \zeta \leq 1$. It is found that an increase in ζ produces complex rhythm and the electrical discharge of the nerve cell becomes more complex leading to chaos.

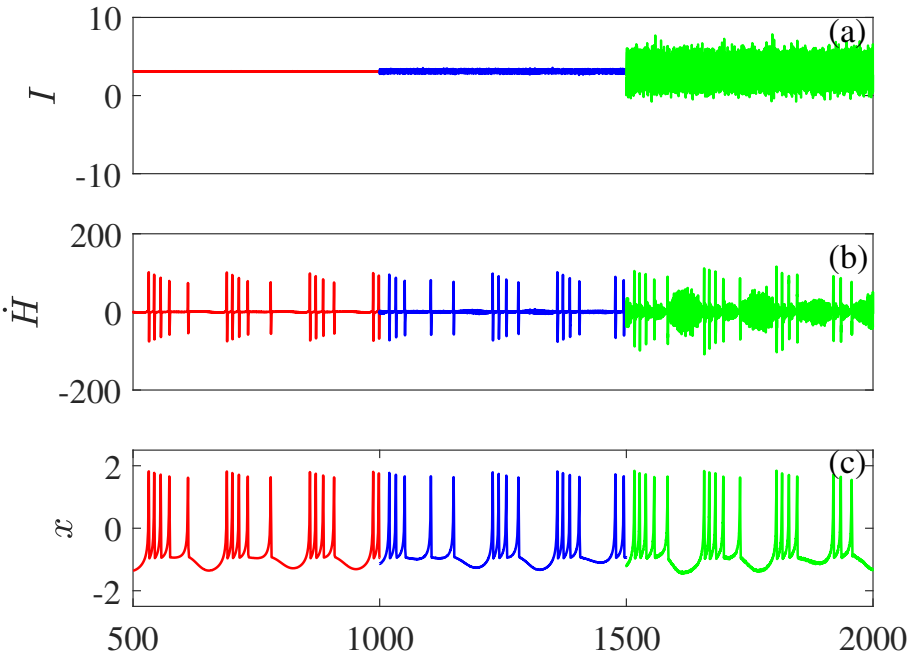

Figure 5.5: (a) External noise variations (b) rate of change of energy function and (c) time evolution of membrane potential of neuron. The noise applied is $I = I_1 + \zeta\xi(t)$. $I_1 = 3.1$, ζ is changed from 0.01 to 0.1 at $t = 1000$ and then switched to 1.0 at $t = 1500$

5.4 Energy Feedback

The Hamilton energy of the system depends on all system parameters, and hence the changes made to energy function causes significant change in the phase space of the dynamical system [17]. Guo *et al.* [21] reported that, energy modulation can be used to control chaotic Lorenz system. In this section, the energy feedback and phase space dynamics of HR model with memristor have been studied. The negative energy feedback is realised as follows:

$$\begin{aligned} \dot{H} = \; & 2(ax^2 - x^3 - k_1\rho(\phi)x + \phi)(bx^2 - 1 + rR(x - x_e) + k_2x) \\ & +2(y - z + I_{ext} - \phi)(-y + rz + k_3\phi) - k_4H, \end{aligned} \tag{5.12}$$

where k_4 is the feedback gain. The phase space dynamics by varying k_4 has been plotted.

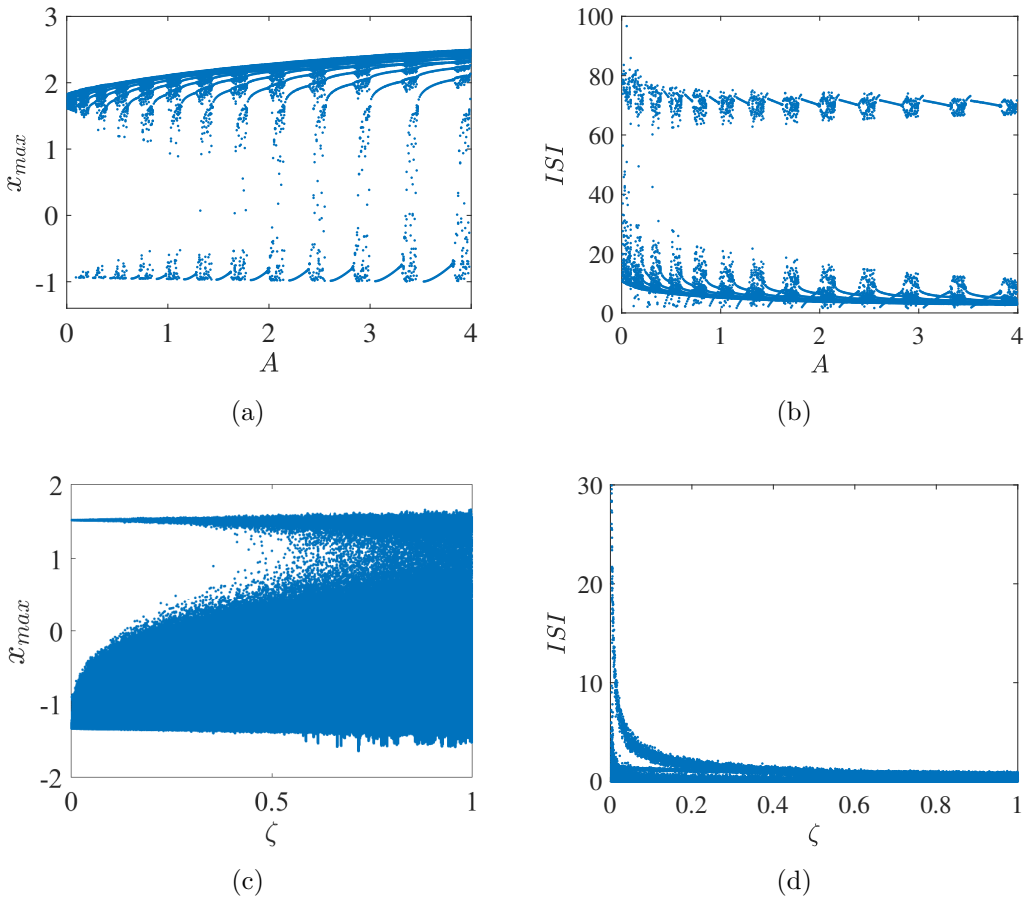

Figure 5.6: The bifurcation diagrams. (a), (b) local maxima of membrane potential and ISI by varying the amplitude of periodic forcing. (c), (d) local maxima of membrane potential and ISI by varying the intensity of external noise.

Case 1. Constant External Stimulus

The formation of attractors in the presence of constant external stimulus ($I = 3.1$) is illustrated in Fig. 5.7. The phase space for $k_4 = 0.0$, $k_4 = 1.0$, $k_4 = 5.0$ and $k_4 = 10.0$ are shown in Figs. 5.7(a), 5.7(b), 5.7(c) and 5.7(d) respectively. As the feedback gain is increased, the number of dense orbits in the attractor is reduced and the chaotic trajectories are controlled. The results are further confirmed by plotting the Largest Lyapunov exponent (LLE). The variation of LLE with k_4 is shown in Fig. 5.8. It is found that the LLE is decreased below zero with increase in k_4 and ensure the stabilisation of chaotic trajectories.

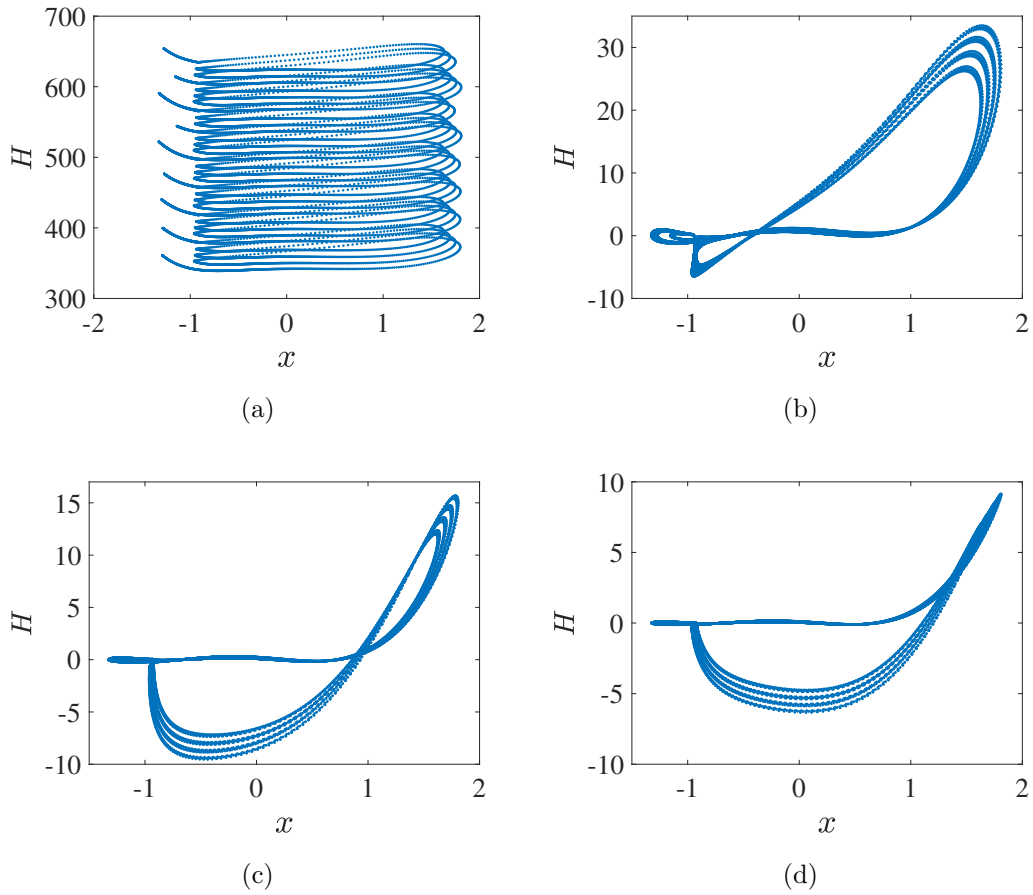

Figure 5.7: Phase space of dynamics for $I = 3.1$. The energy feedback obeys Eq. (5.12). (a) $k_4 = 0$, (b) $k_4 = 1.0$, (c) $k_4 = 5.0$, (d) $k_4 = 10.0$.

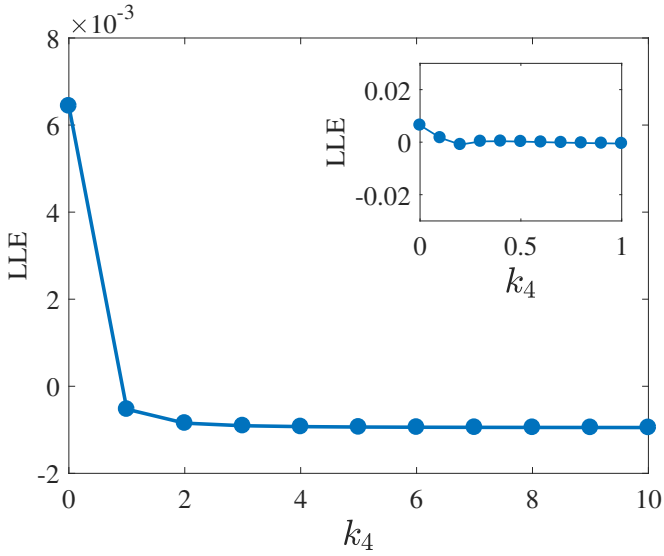

Figure 5.8: Transition of LLE for different feedback gain in energy function in the presence of constant external current. The inserted figure is the enlarged version.

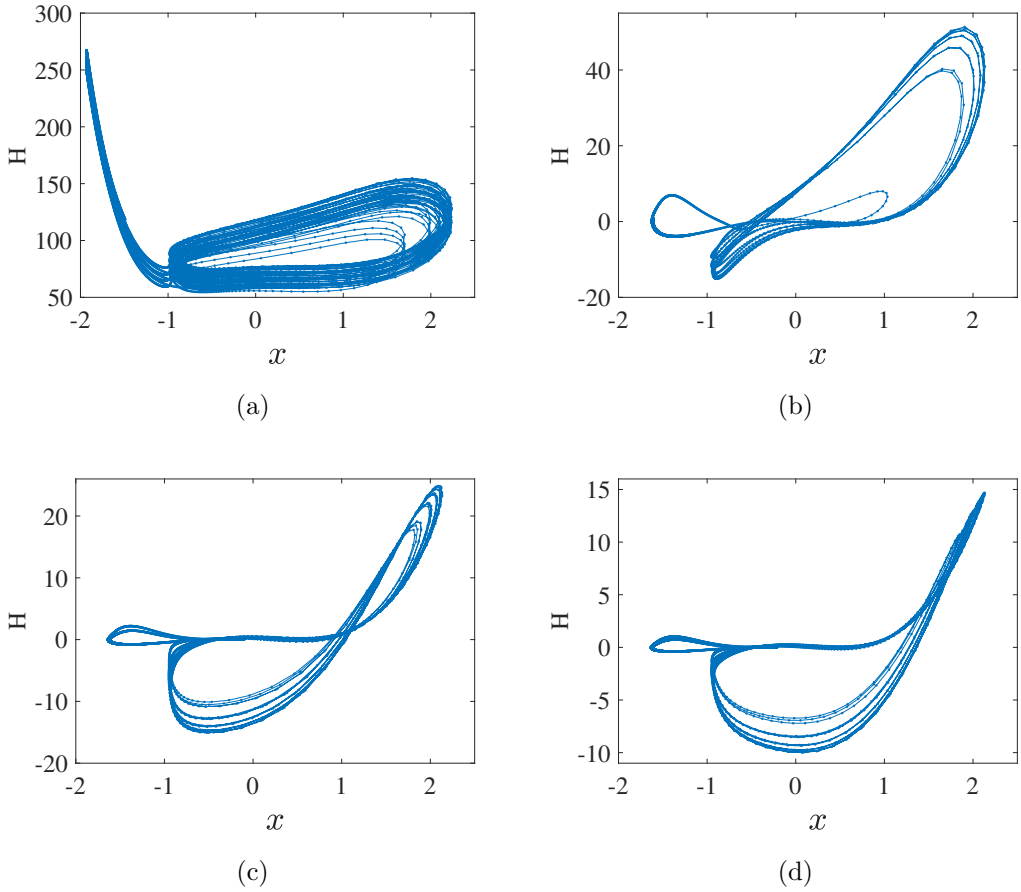

Figure 5.9: Phase space of dynamics for periodic external forcing $I = I_1 + Asin(0.05t)$, where $I_1 = 3.1$ and $A = 2.0$. The energy feedback is according to Eq. (5.12). (a) $k_4 = 0$, (b) $k_4 = 1.0$, (c) $k_4 = 5.0$, (d) $k_4 = 10.0$.

Case 2. Periodic External Stimulus

The phase space dynamics in the presence periodic stimulus, $I = I_1 + 2sin(0.05t)$ with feedback gains, $k_4 = 0$, $k_4 = 1.0$, $k_4 = 5.0$ and $k_4 = 10.0$ are shown in Figs. 5.9(a), 5.9(b), 5.9(c) and 5.9(d) respectively. The plots show that, as the feedback gain k_4 is increased the Hamilton energy function which is composed of the variables and bifurcation parameters control the time evolution of the system and the chaotic trajectories are stabilised. The variation of LLE is shown in Fig. 5.10. The maximum value of LLE is nearly equal to 0.005, greater than compared to the one obtained for constant external stimulus.

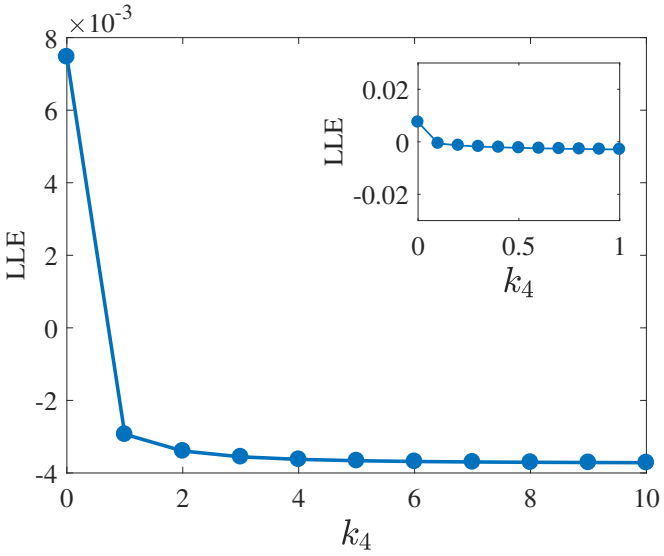

Figure 5.10: Transition of LLE with k_4. Periodic variations are applied in the external current. The inserted figure is the enlarged version.

Case 3. White Gaussian Noise

The phase portrait of the system with energy feedback in the presence of external noise $I = I_1 + \zeta\xi(t)$ has also been studied with $I_1 = 3.1$ and $\zeta = 1$. As the feedback gain k_4 is increased, the noisy trajectories are controlled. Figs. 5.11(a), 5.11(b), 5.11(c) and 5.11(d) represent the mechanism of control for $k_4 = 0$, $k_4 = 1.0$, $k_4 = 5.0$, and $k_4 = 10.0$ respectively. The LLE for noisy external forcing has the largest value compared to the previous cases as shown in Fig. 5.12. The increased LE indicates sensitivity to initial conditions.

5.5 Energy Aspects of Synchronous Dynamics

The dynamical equations of two coupled HR neurons with field effects have the form:

$$\dot{x_i} = y_i + a{x_i}^2 - {x_i}^3 - z_i + I - k_1\rho(\phi_i)x_i - g_{(e/c)}\sum_{\substack{j=1\\ i\neq j}}^{2} C_{(i,j)}\delta(x_i, x_j),$$

$$\dot{y_i} = 1 - b{x_i}^2 - y_i,$$

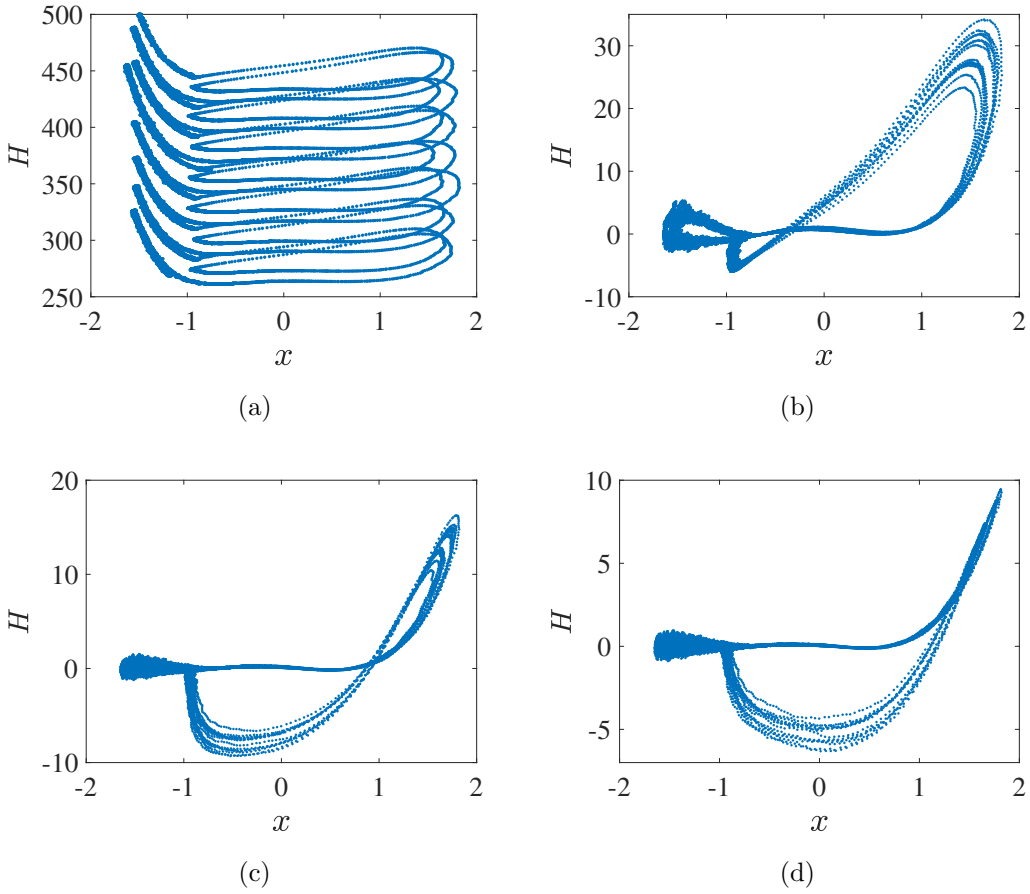

Figure 5.11: Phase space in the presence of white Gaussian noise, $(I = 2 + \xi(t))$. The energy feedback obeys Eq. (5.12). (a) $k_4 = 0$, (b) $k_4 = 1.0$, (c) $k_4 = 5.0$, (d) $k_4 = 10.0$.

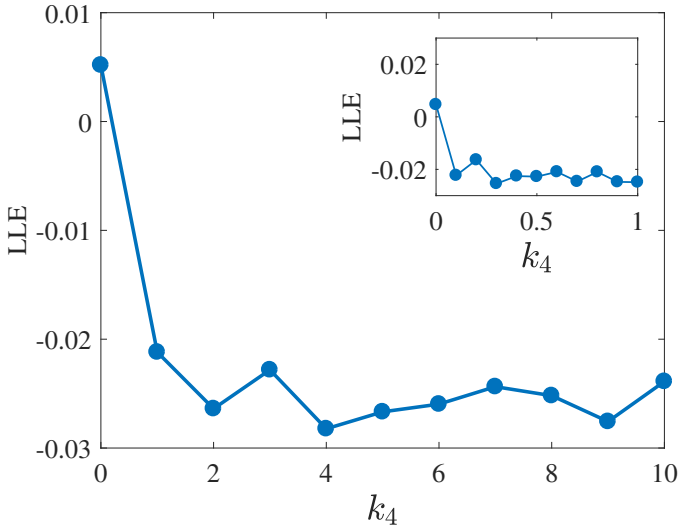

Figure 5.12: Variations of LLE with k_4. White Gaussian noise is added as the external stimuli. The inserted figure is the enlarged version.

$$\dot{z}_i = r(R(x_i - x_e) - z_i),$$

$$\dot{\phi}_i = k_2 x_i - k_3 \phi_i + D(\phi_i - \sum_{\substack{j=1 \\ i \neq j}}^{2} \frac{W}{|i-j|} \phi_j), \tag{5.13}$$

where

$$\rho(\phi_i) = \alpha \phi_i^2 + \beta \phi_i + \gamma, \quad i, j = 1, 2.$$

The parameter $g_{(e/c)}$ is the electrical/ chemical coupling strength of synaptic junction. D describes the field coupling strength.

5.5.1 Electrical and Field Couplings

For an electrically coupled system the coupling term in Eq. (5.13) is of the form $\delta(x_i, x_j) = (x_i - x_j)$, where $i, j = 1, 2; i \neq j$. We have evaluated the effect of modulation intensity of electromagnetic field in regulating the average energy of neurons in the synchronised state. The energy of neurons are averaged on its respective manifold at various values of the coupling strength. Fig. 5.13(a) shows the average energy variations for $k_1 = 0.1$. The plot verifies that with increase in coupling strength, the average energy changes in a waving pattern and it stabilises at the point of synchronisation. The membrane potential of both neurons are equal in the synchronised state and this leads to the vanishing of coupling term. As a result the energy in the synchronised state returns to its initial uncoupled value. Our results with memristor is in accordance with the results obtained for HR model without memristor [22]. The variation in average energy for an increased value of k_1 ($k_1 = 0.5$) is shown in Fig. 5.13(b). From the plot it is clear that, as the value of k_1 is increased, the onset of synchronisation occurs at a low value of g_e. The results imply that, an autonomous chaotic system with linear feedback coupling will move to its natural oscillatory regime in the synchronised state by gaining or dissipating energy. If the system continues in the same state, the change in total average energy will be zero due to the repeating nature of trajectories with arbitrarily close energy values.

The transition to the synchronised state is further confirmed by plotting the

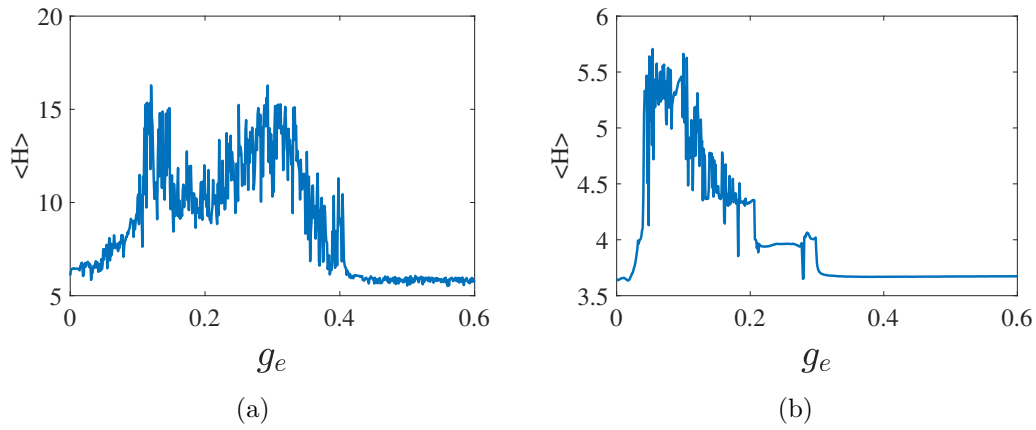

Figure 5.13: Average energy of electrically coupled HR model by varying the coupling strength. (a) $k_1 = 0.1$. (b) $k_1 = 0.5$.

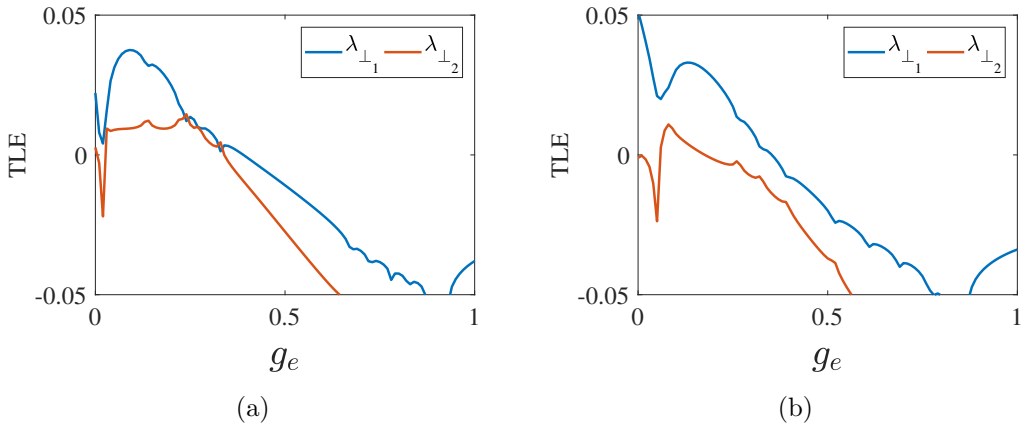

Figure 5.14: TLEs of electrically coupled HR model by varying the coupling strength. (a) $k_1 = 0.1$. (b) $k_1 = 0.5$.

TLEs [23]. Fig. 5.14(a) shows the variations of two of the largest TLEs with g_e for $k_1 = 0.1$. With increase in g_e, the largest TLE ($\lambda_{\perp_1}$) also starts to increase, reaches a maximum, and then starts to decrease. $\lambda_{\perp_1}$ crosses zero at $g_e = 0.41$ indicating a transition from desynchronized state to synchrony at this point. Fig. 5.14(b) shows the variations in TLEs for $k_1 = 0.5$. Here $\lambda_{\perp_1}$ crosses zero at a low value of g_e ($g_e = 0.37$). The results are consistent with the average energy changes shown in Fig. 5.13.

5.5.2 Chemical and Field Couplings

When the neurons are coupled via chemical synapse the coupling term in Eq. (5.13) is of the form $\delta(x_i, x_j) = (x_i - V_s)/[1 + exp(-\lambda(x_j - \theta))]$. The parameters g_c and D are the chemical and the field coupling strengths respectively. V_s, the reversal potential is always greater than x for all neuron at all times. For each neuron to reach the threshold, we choose $\theta = -0.25$, $V_s = 2$ and $\lambda = 7.5$ [24]. The change in average energy with g_c for $k_1 = 0.1$ is shown in Fig. 5.15(a). From the plot it is clear that, the fluctuating nature of average energy disappears at the point of synchronisation. This occurs at $g_c = 1.55$. After that the system shows an interesting behaviour, i.e., average energy linearly increases with increase in g_c. To unravel the reason for increase in average energy after $g_c = 1.55$, we have examined the time series of the system in the linearly increasing regime of average energy. The results are shown in the inset plot of Fig. 5.15(a). The $'X'$ axis represents time and $'Y'$ axis denotes the membrane potential. The plot verifies that, even though both neurons are synchronised ($g_c \geq 1.55$), their membrane potential is in the AD state. The green, red, black and blue lines show the AD state which has been obtained for $g_c = 1.55, 1.7, 1.8$ and 2 respectively. As the value of g_c is increased the value of membrane potential at which AD takes place also increases. Thus in chemical synaptic coupling, where the interaction terms do not go to zero, permits a change in average energy in the synchronised state. We have further analysed the effect of k_1 in regulating average energy. Fig. 5.15(b) shows the average energy variations for $k_1 = 0.2$. For $0 < g_c \leq 0.55$, average energy shows some fluctuations and this region corresponds to the desynchronised state. After that, average energy remains constant for $0.55 < g_c \leq 1.484$ and linearly increases for $1.484 < g_c \leq 2.0$.

The time evolution of membrane potential corresponds to these two cases are shown in the inset plot of Fig. 5.15(b). The periodically oscillating (red) time series is for the constant average energy regime, i.e., in the synchronised state there occurs a transition to stable orbit and the total average energy change is zero due to the repeating nature of trajectories. The black line in the inset plot is

the time evolution of membrane potential corresponding to the linearly increasing regime of average energy. The AD occurs at different points for different values of g_c leading to a net average energy change.

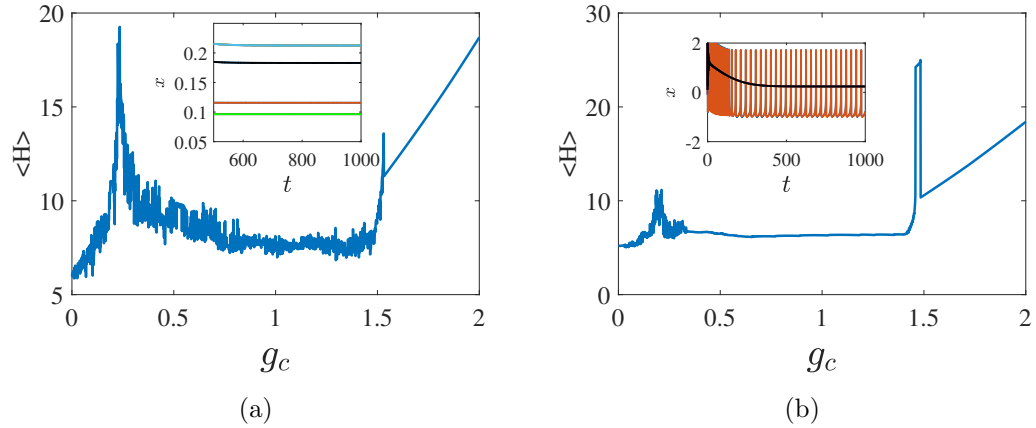

Figure 5.15: Average energy of chemically coupled HR model by varying g_c for (a) $k_1 = 0.1$. The green, red, black and blue lines in the inset plot shows the AD state obtained for $g_c = 1.55, 1.7, 1.8$ and 2 respectively. (b) $k_1 = 0.2$. the inset plot represents the time series of membrane potential corresponding to periodically oscillating (red) and AD (black) states.

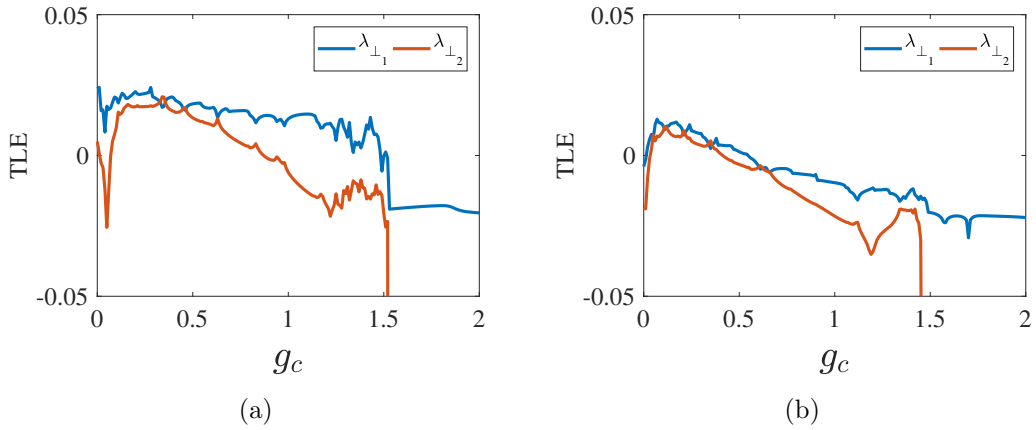

Figure 5.16: TLEs of chemically coupled HR model by varying the coupling strength. (a) $k_1 = 0.1$. (b) $k_1 = 0.2$.

The transitions to the synchronised state are verified by plotting the TLEs. Fig. 5.16(a) depicts the variations of two of the largest TLEs with chemical coupling strength for $k_1 = 0.1$. The largest TLE crosses zero at $g_c = 1.55$ corresponds to the synchronised state. For $k_1 = 0.2$, this transition occur at a low value of g_c ($g_c = 0.55$) as shown in Fig. 5.16(b).

Thus, it can be concluded that, an extra amount of energy is needed when a coupled system is forced to oscillate in different regions of the phase space, where the average energy change is not zero. The extra demand of energy required for the collective dynamics is provided by the coupling mechanism [25]. In central nervous system, some specialised structures are located at the postsynaptic sites for producing ATP molecules to balance the energy demands [26].

5.6 Results and Conclusions

The energy aspects, feedback and synchronous dynamics of HR neuron model with memristor has been analysed in this chapter. The bifurcation analysis of single system by increasing the value of I suggest that, response of the system in the presence of external stimuli can be improved by properly modulating the electromagnetic induction. Based on Helmholtz theorem the rate of change of Hamilton energy of HR model with memristor has been derived. It is found that the average Hamilton energy decreases with increase in external constant stimulus. The time evolution of membrane potential and the rate of change of energy function for different external stimuli have been analysed. In the case of constant external stimulus, the electrical mode of neuron changes with the external forcing and energy is consumed for generating each action potential. In the presence of periodic stimulus, the firing mode changes with the change in amplitude of external forcing. The energy consumption of bursting state with less number of spikes per burst is found to be low compared to burst with more number of spikes. The analysis of the system by applying Gaussian white noise reveals that, bursting mode changes with increase in noise intensity. The bifurcation analysis corresponding to periodic and noisy inputs have been drawn. The bifurcation diagram in the presence of noise has revealed that, as the noise intensity is increased, the system shows complex chaotic dynamics. The dependence of Hamilton energy function on system parameters has been used to control and stabilise chaotic trajectories by giving a negative energy feedback. The suppres-

sion of chaotic trajectories and the stabilisation of phase space of the system for periodic input and noise have been discussed. As the feedback gain in the energy function is increased, the initially positive LLE become negative which in turn ensure the stabilisation of chaotic trajectories.

In the case of electrically coupled neurons, as g_e is increased, the average energy changes in a fluttering pattern and it stabilises at the point of synchronisation. The energy in the synchronised state returns to its initial uncoupled value due to the vanishing of coupling term in the synchronised state. The study has been repeated by increasing k_1 and found that for an increased value of k_1 the onset of synchronisation occurs at a low value of g_e. The average energy variations exhibit three important regions when the neurons are coupled via chemical synapse. The fluctuating region indicates desynchrony. In the region where the average energy remains constant, the system shows synchronisation with periodically oscillating dynamics. The total average energy change in this state is zero due to the repeating nature of trajectories. In the linearly increasing regime, the dynamics is AD. As the value of g_c is increased, the value of membrane potential at which the system stabilises is also increased and leads to a net average energy change. Thus we conclude that, if two neurons are coupled and forced to oscillate, their phase space may contain different oscillatory regimes. As a result, the change in average energy of the system will not be zero and an additional amount of energy is used to sustain the synchronised state. The proposed method will be useful to study the energy aspects of other coupled chaotic and hyperchaotic systems.

Bibliography

[1] C. Sarasola, F. J. Torrealdea, A. d'Anjou, A. Moujahid, and M. Grana. *Phys. Rev. E*, 69:011606, 2004.

[2] F. J. Torrealdea, C. Sarasola, and A. d'Anjou. *Chaos, Solitons & Fractals*, 40:60–68, 2009.

[3] H. Sira-Ramirez and C. Cruz-Hernandez. *Int. J. Bifurcation Chaos Appl. Sci. Eng.*, 11:1381, 2001.

[4] A. Moujahid, A. d'Anjou, F.J. Torrealdea, and F. Torrealdea. *Chaos, Solitons & Fractals*, 44:929–933, 2011.

[5] A. Moujahid, A. d'Anjou, F.J. Torrealdea, and F. Torrealdea. *Phys. Rev. E*, 83:031912, 2011.

[6] Ji.Quan-Bao, Z. Yi, Y. Zhuo-Qin, and M. Xiang-Ying. *Chin. Phys. Lett.*, 32:050501, 2015.

[7] H. Gu. *Chaos*, 23:023126, 2013.

[8] A. N. Pisarchik, R. Jaimes-Reategui, and M. A. Garcia-Vellisca. *Chaos*, 28: 033605, 2018.

[9] Y. Xu, H. Ying, Y. Jia, J. Ma, and T. Hayat. *Scientific Reports*, 7:43452, 2017.

[10] S. Zambrano, I. P. Marino, J. M. Seoane, M. A. F. Sanjuan, S. Euzzor, A. Geltrude, R. Meucci, and F. T. Arecchi. *New J. Phys.*, 12:053040, 2010.

[11] J. P. Baltanas and J. M. Casado. *Phys. Rev. E*, 65:041915, 2002.

[12] Y. Wang, Z. D. Wang, and W. Wang. *J. Phys. Soc. Jpn.*, 69(1):276–283, 2000.

[13] B. Lindner, J. Garcia-Ojalvo, A. Neimand, and L. Schimansky-Geiere. *Phys. Rep.*, 392:321, 2004.

[14] F. Q. Wu, C. N. Wang, Y. Xu, and J. Ma. *Scientific Reports*, 6:28, 2016.

[15] W. Guan, S. Yi, and Y. Quan. *Chin. Phys. B*, 22:050504, 2013.

[16] J. Ma, P. Zhou, B. Ahmad, G. Ren, and C. Wang. *PLOS ONE*, 0191120: 1–21, 2018.

[17] J. Ma, F. Wu, W. Jin, P. Zhou, and T. Hayat. *Chaos*, 27:053108, 2017.

[18] J. Jonq and L. Yu-Hao. *Chaos*, 24:013110, 2014.

[19] F. Xu, J. Zhang, T. Fang, S. Huang, and M. Wang. *Nonlinear Dyn.*, 92(3): 13951402, 2018.

[20] S. R. D. Djeundam, R. Yamapi, T. C. Kofane, and M. A. Aziz-Alaoui. *Chaos*, 23:033125, 2013.

[21] S. L. Guo, J. Ma, and A. Alsaedi. *Pramana*, 90(39), 2018.

[22] F. J. Torrealdea, A. d'Anjou, M. Grana, and C. Sarasola. *Phys. Rev. E*, 74: 011905, 2006.

[23] K. Usha, P. A. Subha, and C. R. Nayak. *Chaos, Solitons & Fractals*, 108: 25–31, 2018.

[24] D. Somers and N. Kopell. *Biol. Cybern*, 68:393, 1993.

[25] K. Wu, C. Aoki, A. Elste, A. Rogalski-Wilk, and P. Siekevitz. *Proc. Natl. Acad. Sci. U.S.A.*, 13273:94, 1997.

[26] P. Siekevitz. *Science*, 306:410, 2004.

Chapter 6

Collective Dynamics and Energy Aspects of Star Coupled HR Neurons

6.1 Introduction

The collective dynamics of neural network has great influence in the propagation of information from one region to the other and their collective behaviours are greatly influenced by the energy demands. Properties of individual neurons, network topology and the coupling strength will influence the collective dynamics [1]. Synchronisation is one of the important collective response shown by neural networks. Based on the nature of coupling the network shows different types of synchronisation such as chaotic bursting, regular bursting and fixed point synchronisation. Signalling in synchrony is the chief mechanism for impulse transmission. The evaluation of the metabolic energy needed to maintain the signalling activity is of practical interest [2]. The energy variations corresponding to each dynamical state may be different and the system consumes energy to change from one state to the other.

The collective dynamics and energy aspects of coupled HR neurons with field

effects have been discussed in this chapter. Section 6.2 describes the dynamics of HR neurons with electrical, chemical and field couplings. The dependence of electrical mode of neuron on field coupling strength has also been discussed in section 6.2. In section 6.3, the variations in average energy of electrically and chemically coupled neurons with field effects have been explained. Section 6.4 concludes the study.

6.2 Collective Dynamics

The dynamical equations of star coupled HR neurons with field effects have the form:

$$\dot{x_i} = y_i + a{x_i}^2 - {x_i}^3 - z_i + I - k_1\rho(\phi_i)x_i - g_{(e/c)}\sum_{\substack{j=1\\ i\neq j}}^{N} C_{(i,j)}\delta(x_i, x_j),$$

$$\dot{y_i} = 1 - b{x_i}^2 - y_i,$$

$$\dot{z_i} = r(R(x_i - x_e) - z_i),$$

$$\dot{\phi_i} = k_2 x_i - k_3\phi_i + D(\phi_i - \sum_{\substack{j=1\\ i\neq j}}^{N} \frac{W}{|i-j|}\phi_j), i = 1, 2, ..., N. \tag{6.1}$$

Where x_i, y_i and z_i respectively denote the membrane potential, recovery variable and adaptation variable of the i^{th} neuron. The coupling topology used is star bidirectional where oscillators on the spokes of the star (nodes) are connected to the common oscillator (hub) and vice versa [3]. 'i' is the node position of the neuron in the network and $g_{e/c}$ denotes the electrical/chemical synaptic coupling strength between the neurons. The N^{th} neuron is taken as the hub and other neurons (1 to $N-1$) are arranged on the spokes of the star. $C = (C_{i,j})$ is the $N \times N$ connectivity matrix: $C_{i,j} = 1$ if the ith neuron receives synaptic input from neuron j; otherwise $C_{i,j} = 0$. A memristor with memductance $\rho(\phi_i) = \alpha\phi_i^2 + \beta\phi_i + \gamma$ is used to couple the magnetic flux of the field with membrane potential of the neuron; where ϕ_i is the magnetic flux across the memristor,

α, β and γ are parameters [4]. The term $k_1\rho(\phi)x_i$ denotes the induced current through electromagnetic induction, where k_1 is the modulation intensity of electromagnetic field. The term k_2x_i represents the change in magnetic flux induced by membrane potential of the cell and $k_3\phi_i$ denotes the leakage of magnetic flux. D is the field coupling strength [5]. The parameters are $a = 3.0, b = 5.0, R = 4.0, r = 0.006, x_e = -1.61, \alpha = 0.4, \beta = 0.02, \gamma = 0.1, k_2 = 0.9, k_3 = 0.5, W = 1$, and $D = 0.0001$ [5, 6].

6.2.1 Star Network with Electrical and Field Couplings

In a star network of HR neurons with electrical synapse, the coupling term in Eq. (6.1) has the form:

$$\delta(x_i, x_j) = (x_i - x_j). \tag{6.2}$$

The star network is composed of 100 neurons whose initial values are randomly selected. The transient period for numerical calculation is about 1000 time units with time step $h = 0.01$. By modulating the values of k_1 and g_e, the system show different types of synchronisations as shown in Fig. 6.1. For $k_1 = 0.1$ and $g_e = 0.95$, the dynamics is bursting synchronisation as shown in Fig. 6.1 (a). Fig. 6.1(b) shows AD behaviour obtained for $k_1 = 0.9$ and $g_e = 0.1$. For intermediate values of k_1 and g_e ($k_1 = 0.5$ and $g_e = 0.6$), the system shows periodic spiking behaviour in the synchronised state as depicted in Fig. 6.1(c).

The two parameter space diagram ($k_1 - g_e$) is plotted in Fig. 6.2. The system passes through two main states for k_1 and g_e in the range $0 < k_1 \leq 1$ and $0 \leq g_e \leq 1$. The desynchronised and synchronised regions are denoted using blue and red colours respectively. The plot verifies that for high values of k_1 or g_e the system shows synchronisation.

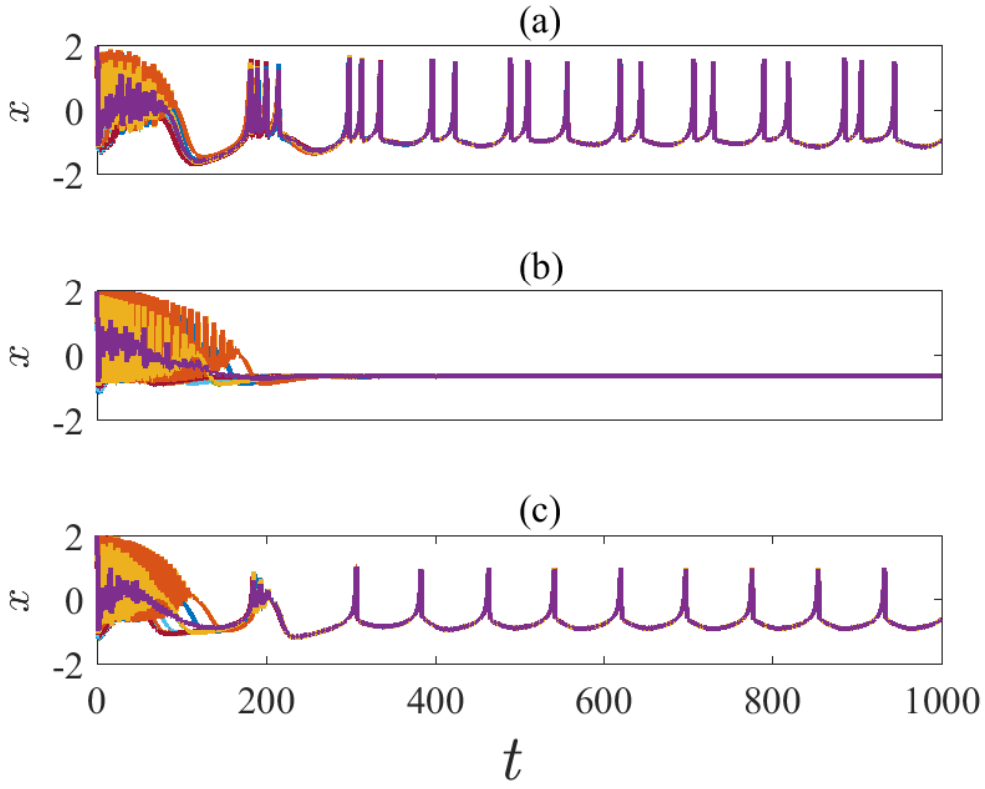

Figure 6.1: Different kinds of synchronisation obtained for star coupled HR neurons with electrical coupling and field effects. (a) Bursting state ($k_1 = 0.1$ and $g_e = 0.95$). (b) AD ($k_1 = 0.9$ and $g_e = 0.1$). (c) Periodic oscillations ($k_1 = 0.5$ and $g_e = 0.6$).

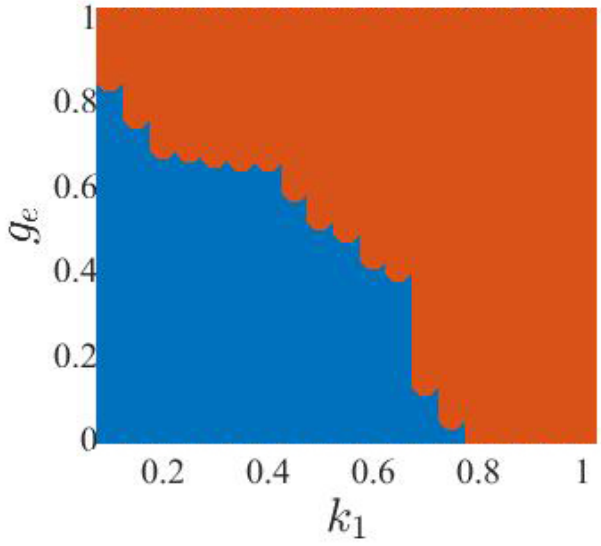

Figure 6.2: Parameter space for star coupled HR neurons with electrical coupling and field effects. k_1 is plotted along X axis and g_e along Y axis. The blue and red regions denote desynchronised and synchronised states respectively.

6.2.2 Star Network with Chemical and Field Couplings

For chemical synaptic coupling, the coupling term in Eq. (6.1) has the form:

$$\delta(x_i, x_j) = (x_i - V_s)\Gamma(x_j) = (x_i - V_s)/[1 + exp(-\lambda(x_j - \theta))]. \tag{6.3}$$

The exponential function models the synaptic junction between the neurons and θ is the threshold. For each neuron to reach the threshold, we choose $\theta = -0.25$, $V_s = 2$ and $\lambda = 7.5$ [1]. We have analysed the dynamics of chemically coupled HR neurons with field effects. The collective dynamics of the system is illustrated in Fig. 6.3. The oscillator numbers are plotted along X axis and the corresponding membrane potentials are plotted along Y axis. For low values of k_1 and g_c ($k_1 = g_c = 0.1$) the system shows desynchronised state as shown in Fig. 6.3(a). For $k_1 = 1$ and $g_c = 0.3$, all neurons are in the synchronised state as depicted in Fig 6.3(b). For high values of k_1 and g_c ($k_1 = g_c = 1.0$) the dynamics is DHM and is shown in Fig. 6.3(c). Fig. 6.4 shows the time evolution of membrane potential in each state. The dynamics of the hub and nodes are denoted using red and blue colours respectively. In the desynchronised state the neurons show bursting dynamics as depicted in Fig. 6.4(a). The time series corresponding to the synchronised state is shown in Fig. 6.4(b). It is found that, as the strength of modulation intensity (k_1) is increased, AD behaviour is induced in the system. In the DHM state, the hub and the nodes stabilise at different points. It can be considered as an oscillation quenching in the form of oscillation death (OD) where the system settles down to multiple equilibria as depicted in Fig. 6.4(c).

We have plotted the parameter space in the (k_1, g_c) plane and is shown in Fig. 6.5. The values of k_1 and g_c are varied from 0 to 1.0. The desynchronised, synchronised and DHM states are denoted using blue, red and white colours respectively. From the figure it is clear that, desynchronised and DHM regions spread most of the parameter space and synchronised state prevails in a small region. The results are consistent for networks with more or less number of oscillators.

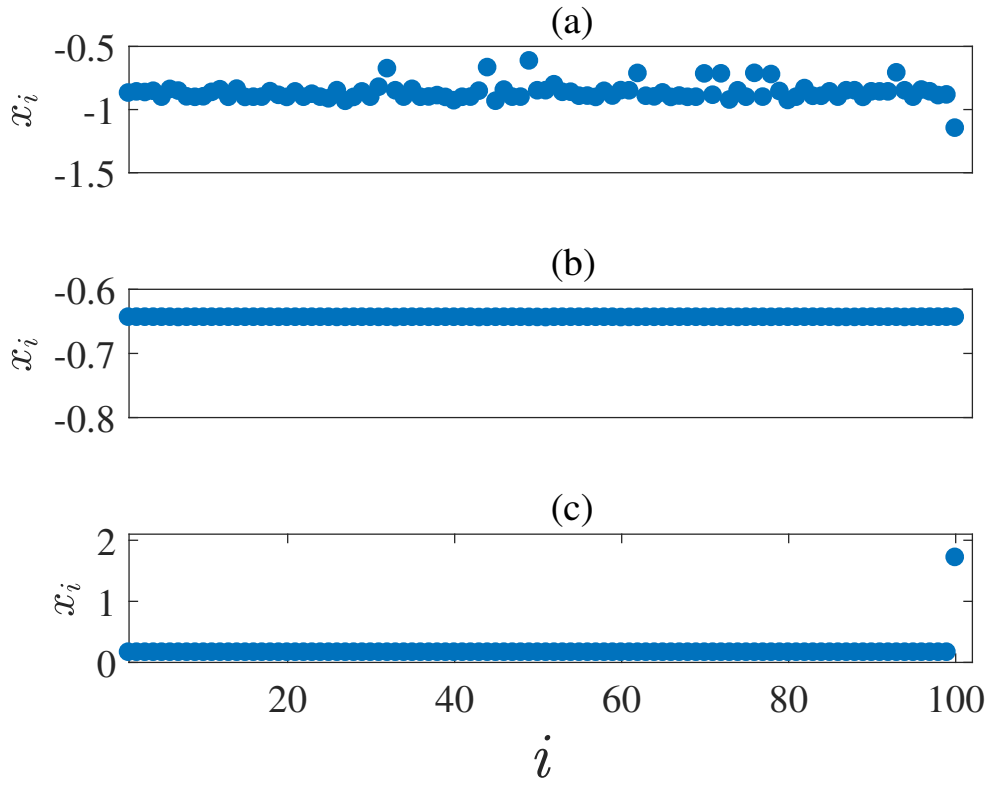

Figure 6.3: The collective dynamics of star coupled HR neurons with chemical coupling and field effects. Oscillator number is plotted along X axis and the corresponding membrane potentials are plotted along Y axis. (a) Desynchronised state ($k_1 = g_c = 0.1$). (b) Synchronised state ($k_1 = 1$ and $g_c = 0.3$). (c) DHM ($k_1 = g_c = 1.0$).

6.2.3 Field Coupling

We have further analysed the effect of field coupling strength (D) in regulating the electrical modes of the network and the results are shown in Fig. 6.6. The synaptic coupling strength $g_{(e/c)}$ is taken as zero and the field coupling strength is varied. Time is plotted along X axis and membrane potential along Y axis. For $D = 0.0001$, bursting oscillations with 3 spikes per burst is obtained as shown in 6.6 (a). As D is increased ($D = 0.005$), the dynamics changes to bursting with 2 spikes per burst as depicted in Fig. 6.6 (b). Fig. 6.6 (c) shows the tonic spiking behavior for $D = 0.01$.

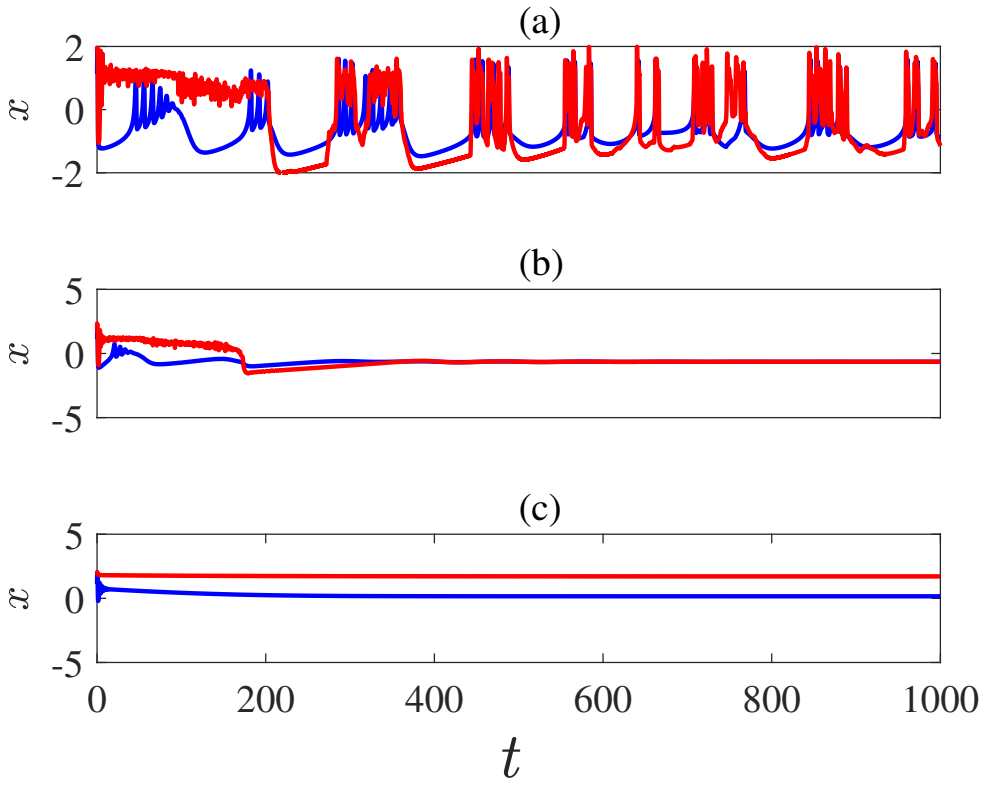

Figure 6.4: The time series of membrane potential of star coupled HR neurons with chemical coupling and field effects. The dynamics of the hub and nodes are denoted using red and blue colours respectively. (a) Bursting state ($k_1 = g_c = 0.1$). (b) AD ($k_1 = 1$ and $g_c = 0.3$). (c) OD ($k_1 = g_c = 1.0$).

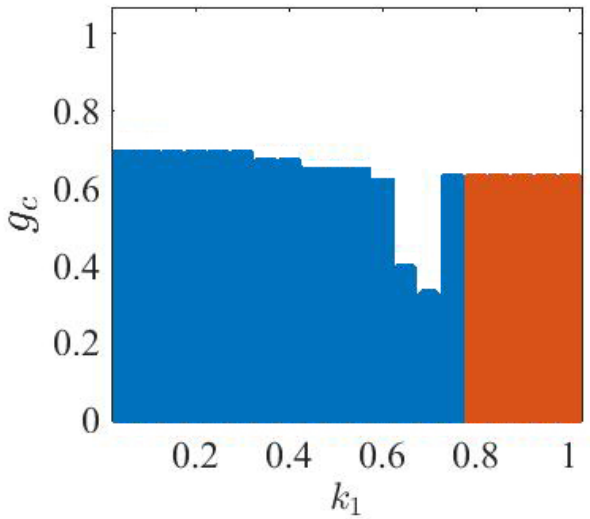

Figure 6.5: Parameter space. k_1 is plotted along X axis and g_c along Y axis. The blue, red and white regions denote desynchronised, synchronised and DHM states respectively.

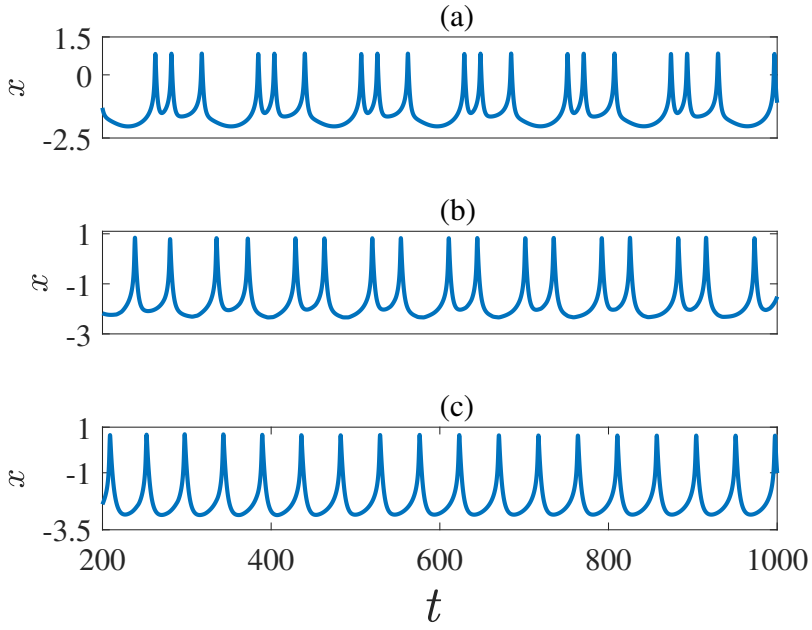

Figure 6.6: Time series for membrane potential of neuron are calculated by applying different field coupling strengths. The synaptic coupling $g_{(e/c)}$ is taken as 0. (a) bursting oscillations with 3 spikes per burst for $D = 0.0001$ (b) bursting with 2 spikes per burst for $D = 0.005$. (c) tonic spiking behavior for $D = 0.01$.

6.3 Energy Aspects of N Coupled System

The energy aspects of a neural network have been analysed by assigning an energy function to a single neuron and the energy variations in the synchronisation process with other neurons have been calculated [7]. The energy function for HR neuron with memristor has been derived in Chapter 5. The energy function H and its derivative $\dot{H}$ are obtained as,

$$H = \frac{2}{3}bx^3 - 2x + rR(x - x_e)^2 + (y - z + I - \phi)^2 + k_2x^2, \tag{6.4}$$

$$\begin{aligned}\dot{H} = \; & 2(ax^2 - x^3 - k_1\rho(\phi)x + \phi)(bx^2 - 1 + rR(x - x_e) + k_2x) \\ & +2(y - z + I - \phi)(-y + rz + k_3\phi).\end{aligned} \tag{6.5}$$

We have analysed the variations in average energy of star coupled HR neurons using the following expression:

$$< H >= \int_{t_0}^{t_0+T} H(x, y, z, \phi)dt/T. \tag{6.6}$$

T is the energy calculation period (1000 time units) and t_0 is the starting time to calculate the average energy.

Case 1: Star Network with Electrical and Field Couplings

Fig. 6.7 illustrates the variations in average energy with g_e for electrically coupled star network with field effects. The red and blue colours indicates the energy variations of the hub and nodes respectively. As the value of g_e is increased the average energy also increases in a fluctuating manner and reaches a peak. With further increase in g_e, the average energy begins to fall. The energy values are stabilised in their initial uncoupled level at $g_e = 0.82$. This is due to the vanishing of coupling term in the synchronised state, which is a peculiarity of linear feedback coupling. The parameter space in Fig. 6.2 also confirms the transition to the synchronised state.

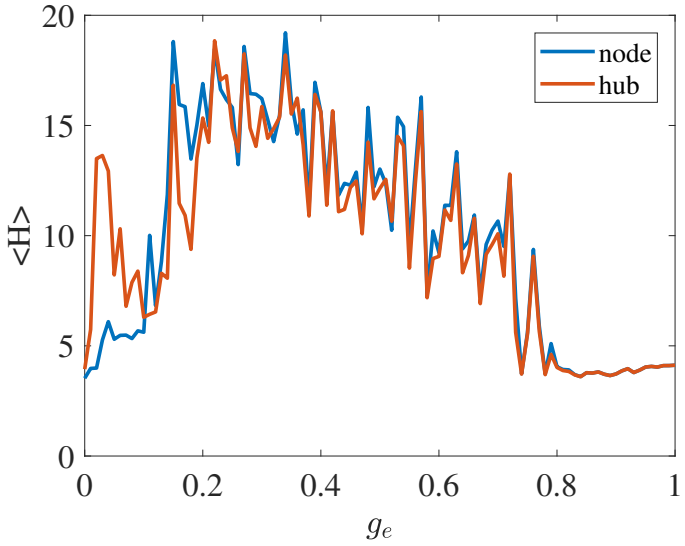

Figure 6.7: Average energy of electrically coupled neurons. The coupling strength g_e is varied by keeping $k_1 = 0.1$ and $D = 0.0001$.

Case 2: Star Network with Chemical and Field Couplings

The average energy of the neuron in the star network with chemical coupling, by varying the coupling strength g_c is shown in Fig. 6.8. The energy of the neurons in the network is averaged on their respective manifold. The red curve indicates the energy variations of the hub, whereas the blue curve denotes the energy fluctuations of the nodes. Even though the neurons follow different temporal dynamics, their average energy function shows the same behaviour. As the coupling strength is increased by keeping k_1 a constant ($k_1 = 0.1$), the average energy of the neuron starts to increase in a waving pattern and reaches a maximum. The fluctuating nature disappears at $g_c = 0.72$. From the parameter space in Fig. 6.5, it is evident that this g_c value corresponds to the transition from the desynchronised state to DHM. As g_c is increased further, the average energy increases linearly. The hub shows rapid increase, whereas the nodes exhibit very small variations. For better visibility, the linearly increasing regime of node is depicted in the inset plot of Fig. 6.8. The time evolution of the nodes and the hub in the DHM region are depicted in Fig. 6.9 (a) and (b) respectively. It is found that at $g_c = 0.72$, the dynamics of the system changes from chaotic bursting to AD. The blue, red, yellow, violet and green lines are the AD states obtained for $g_c = 0.8, 0.85, 0.9, 0.95$ and 1 respectively. From the plot it is clear that, as the value of g_c is increased, the membrane potential at which AD occur also increases. The magnitude of membrane potential is high for the hub compared to that of the node for the same coupling strength. Thus in chemically coupled oscillators, the interaction terms do not go to zero in the synchronised state and permit a change in the total average energy. According to Ref. [8], the coupling mechanism supplies the extra energy needed for the collective dynamics.

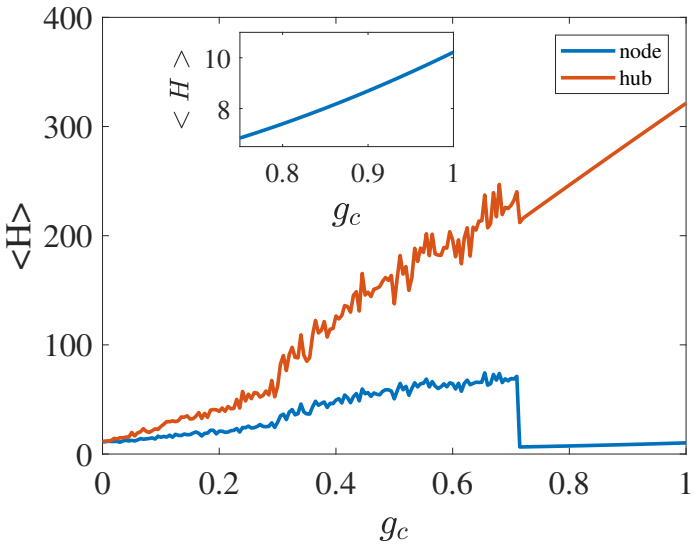

Figure 6.8: Average energy of chemically coupled neurons. The coupling strength g_c is varied by keeping $k_1 = 0.1$ and $D = 0.0001$. The linearly increasing regime of node is depicted in the inset plot.

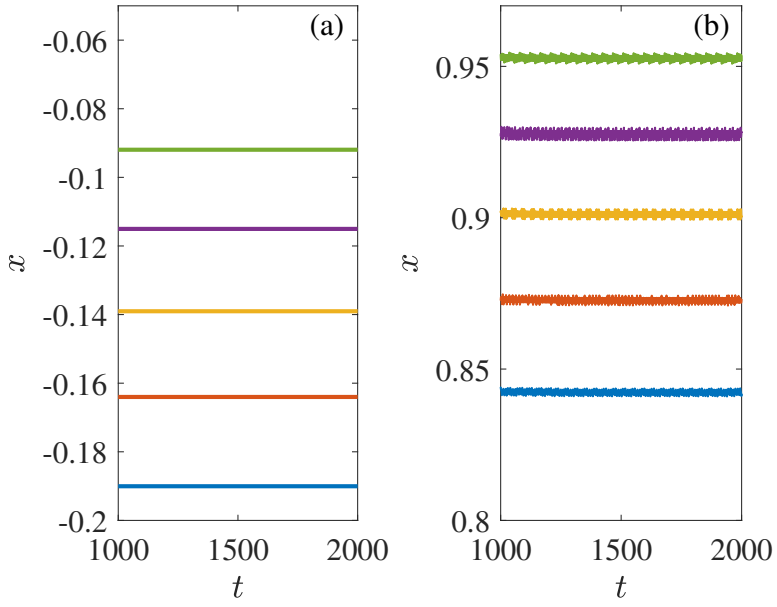

Figure 6.9: Time series of chemically coupled oscillators in the DHM state for $k_1 = 0.1$. (a) nodes (b) hub. The blue, red, yellow, violet and green lines are the AD state obtained for $g_c = 0.75, 0.8, 0.85, 0.9, 0.95$ and 1 respectively.

6.4 Results and Conclusions

We have analysed star coupled network of HR neurons with memristor. The collective dynamics and the energy aspects are studied with electrical, chemical and

field couplings. An electrically coupled star network with field effects has been analysed. The system shows chaotic bursting, AD and periodic spiking behaviour in the synchronised state depending on the values of synaptic coupling strength and modulation intensity of the field. In the case of a chemically coupled system with field effects, desynchronised, synchronised and DHM states have been observed. In the desynchronised state, the system possesses a bursting time series and in the synchronised state the network achieve fixed point synchronisation. In DHM, the nodes and hub stabilise at different points, denoting oscillation death. The system shows tonic spiking and bursting oscillations with two and three spikes per burst by varying the field coupling with zero synaptic coupling strength. The average energy variations of electrically and chemically coupled system have also been analysed. In electrically coupled star network, the average energy returns to its initial uncoupled value due to the vanishing of coupling term in the synchronised state. In the case of chemically coupled system, the average energy increases with coupling strength in a waving manner and reaches a maximum. At the point of synchronisation, the fluctuations disappear and the energy increase linearly. The system shows AD in this regime. Our approach can be extended to analyse the energy aspects of different oscillatory regimes of nonidentical oscillators. These results find application in neural networks with different coupling topologies.

Bibliography

[1] J. Jonq and L. Yu-Hao. *Chaos*, 24:013110, 2014.

[2] A. Moujahid, A. d'Anjou, F.J. Torrealdea, and F. Torrealdea. *Chaos, Solitons and Fractals*, 44:929–933, 2011.

[3] K. Usha and P. A. Subha. *Int. J. Mod. Phys. C*, 29:1850023, 2018.

[4] S. K.Thottil and R. P. Ignatius. *Nonlinear Dyn.*, 87:1879–1899, 2017.

[5] Y. Xu, Y. Jia, J. Ma, T. Hayat, and A. Alsaedi. *Scientific Reports*, 8:1349, 2018.

[6] Y. Xu, H. Ying, Y. Jia, J. Ma, and T. Hayat. *Scientific Reports*, 7:43452, 2017.

[7] F. J. Torrealdea, A. d'Anjou, M. Grana, and C. Sarasola. *Phys. Rev. E*, 74: 011905, 2006.

[8] C. Sarasola, F. J. Torrealdea, A. d'Anjou, A. Moujahid, and M. Grana. *Phys. Rev. E*, 69:011606, 2004.

Chapter 7

Summary and Future Prospects

7.1 Summary

This thesis presents a theoretical study of the collective responses and energy aspects of HR neuron model with electrical, chemical and field couplings.

- The star coupled HR neural network with unidirectional connections modelled using electrical coupling has been analysed. In strongly coupled case, the system exhibits synchrony. The largest TLE becomes negative at the point of transition from desynchrony to synchrony. The system has been analysed by varying the parameter describing the dynamics of the fast ion channel. The controllers to synchronise the system for weak coupling have been derived using Lyapunov function method. On applying the controllers, the system shows synchronisation even with weak coupling. The study has been extended by applying modified controllers. Interesting behaviours like DHM, MOS, desynchrony and multi-cluster states are formed before settling to complete synchrony in the presence of modified controllers. In all clusters, the common oscillator (hub) in the star network shows independent dynamics and acts as the master node which drives the nodes to synchrony via different states. The parameter space for the system has also been discussed.

- The study has been extended to HR neurons interacting via chemical synapse in unidirectional and bidirectional star topology. A two coupled system has been studied for synchronisation by varying the coupling strength and the parameter describing the dynamics of the fast ion channel. The TLEs are plotted to observe the point of transition from desynchrony to synchrony. The synchronised, desynchronised and DHM regions are observed when the neurons are connected in unidirectional and bidirectional coupling configurations. A detailed analysis of the time evolution of membrane potential corresponding to each region is presented. The annihilation of synchronised region and the expansion of DHM region in bidirectional coupling have been discussed using parameter space.

- The modified HR model with field effects have also been studied using memristors. The bifurcation analysis has been carried out by varying the modulation intensity of induced current on the membrane potential. The two coupled system with electrical, chemical and field couplings has been studied. Important dynamical behaviours such as synchrony, desynchrony, AD, anti-phase oscillations, coexistence of resting and spiking state and near death rare spikes are observed. In all cases the TLEs are plotted to observe the point of transition from desynchrony to synchrony.

- Chaos control via energy feedback in the modified HR neuron model with different external stimuli have been analysed. The Hamilton energy of the system has been derived. It is found that, the average Hamilton energy decreases with increase in external stimulus. The time evolution of membrane potential and the rate of change of energy function have been analysed. The dependence of Hamilton energy function on system parameters is used to control and stabilise chaotic trajectories by giving a negative energy feedback. The suppression of chaotic trajectories and the stabilisation of phase space of the system for periodic input and noise are discussed. As the feedback gain in the energy function is increased,

the initially positive LLE becomes negative which in turn ensures the stabilisation of chaotic trajectories.

- The energy aspects of two HR neurons with synaptic coupling and field effects have also been analysed. When the neurons are coupled via electrical synapse with field effects, the average energy fluctuates and stabilises at the point of synchronisation. In the case of a two coupled system with chemical synapse and field effects, the average energy variations show three important regimes with increase in coupling strength. A fluctuating regime corresponding to desynchrony, a stable region indicating synchrony and a linearly increasing regime corresponding to the AD state have been observed.

- The study has been extended to a star network of HR neurons with electrical, chemical and field couplings. The collective behaviour and the energy aspects have been discussed. The electrically coupled network with field effects shows desynchronised and synchronised regions, whereas in the presence of chemical coupling and field effects, the system exhibits desynchrony, synchrony and DHM region. The parameter space has been plotted to explain the transition from desynchronised to synchronised state and DHM region. The time evolution of membrane potential in the absence of synaptic coupling reveals that the field coupling regulates the electrical modes of the system. The energy aspects of the network with synaptic coupling and field effects have been analysed. In electrically coupled star network with field effects, the average energy increases with coupling strength and reaches a maximum. In the synchronised state, the energy returns to its initial uncoupled value. The average energy variations of chemically coupled system with field effects have also been analysed. It is found that in DHM region, both hub and nodes stabilise at different points. With increase in coupling strength, the membrane potential value at which stabilisation oc-

cur also increases. For the same coupling strength, the magnitude of the membrane potential is high for the hub compared to the nodes. Therefore, the hub shows rapid increase in average energy in this region, whereas the nodes exhibit very small variations.

7.2 Future Prospects

- The common oscillator in star network acts as a leader. In neural networks, the leader may be a neuron, which initiate certain biological activities or regulate the communication between other nerve cells in the network. The study can be extended to neural networks with different coupling topologies and multilayered systems. Metabolic network, gene regulation network and protein interaction network can be analysed in multilayer topology.

- Our approach of energy can be extended to analyse the energy aspects of different oscillatory regimes of nonidentical oscillators. The study of energy consumption in other networks and multilayered systems are also under consideration.

Appendix

1. Program for Two Coupled HR Model

```
function [t, x1, y1, z1,u1,x2,y2,z2,u2] = test2(a,r, b, ~)
t=2000;
%  x0 = [1.3;0.3;0.3;0.5];
[t, X] = ode45(@f, [0, t], x0);
x1 = X(:, 1);
y1 = X(:, 2);
z1 = X(:, 3);
u1=X(:,4);
x2=X(:,5);
y2=X(:,6);
z2=X(:,7);
u2=X(:,8);
% Plot of the solution
% display(X)

plot(t,x1,t,x2,'Linewidth',1.5);
xlabel('$t$','interpreter','latex','FontSize', 21,
'Fontname','Times New Roman');
ylabel('$x_1,x_2$','interpreter','latex','FontSize', 21,
```

```
 'Fontname','Times New Roman');
lgd=legend('$x_1$','$x_2$');
legend('Orientation','horizontal')
lgd.FontSize = 20;
set(lgd,'Interpreter','latex');
set(gca,'fontsize',19);
set(gca,'YDir','normal')
set(gca,'xtick',[0 500 1000 ])

    function xdot = f(t, x)

        a=3;
        b=5;
        R=4;
        r=0.006;
        e=-1.61;
        I=3.1;
        k1=2.2;
        k2=0.9;
        k3=0.5;
        alpha=.4;
        beta=.02;
        gamma=0.1;
        g=.1;
        D=0.0001;
        W=1;
        xdot=[x(2)+(a*x(1)*x(1))-(x(1)*x(1)*x(1))-x(3)+I
```

```
              -(k1*x(1)*((alpha*x(4)*x(4))+ (beta*x(4))+gamma))-g*(x(1)-x(5));...
               1-(b*x(1)*x(1))-x(2); ...
               r*(R*(x(1)-e)-x(3));...
               k2*x(1)-k3*x(4)+(D*(x(4)-(W*x(4))));...
               x(6)+(a*x(5)*x(5))-(x(5)*x(5)*x(5))-x(7)+I
               -(k1*x(5)*((alpha*x(4)*x(4))+(beta*x(4))+gamma))-g*(x(5)-x(1));...
               1-(b*x(5)*x(5))-x(6); ...
               r*(R*(x(5)-e)-x(7));...
               k2*x(5)-k3*x(8)+(D*(x(8)-(W*x(4))))];

    end

end
```

2. Lyapunov Exponent of HR Model

```
function f=HR_ext(t,X)
 a=3;b=5;r=0.006;R=4;e=-1.61;
 I=3.1;
%   global R;
x=X(1); y=X(2); z=X(3);

Y= [X(4), X(7), X(10);
    X(5), X(8), X(11);
    X(6), X(9), X(12)];
% Y=[X(4);X(5);X(6)];

f=zeros(9,1);
```

```
%HR model
f(1)=y+a*x*x-x*x*x-z+I;
f(2)=1-b*x*x-y;
f(3)=r*(R*(x-e)-z);

%Linearized system

 Jac=[2*a*x-3*x*x, 1,     -1;
         -2*b*x,    -1,    0;
           r*R,     0, -r];

%Variational equation
 Jac*Y;
trace(Jac);
f(4:12)=Jac*Y;

%Output data must be a column vector



%% Lyapunov Continue
 function[R,Lexp]=lyapunov(n,rhs_ext_fcn,fcn_integrator,tstart,
 stept,tend,ystart,ioutp);
  function [Texp,Lexp]=lyapunov(n,rhs_ext_fcn,fcn_integrator,tstart,
  stept,tend,ystart,ioutp);
 size(ystart);
n1=n; n2=n1*(n1+1);
```

```
%  Number of steps
%     global R;
nit = round((tend-tstart)/stept);

% Memory allocation

y=zeros(n2,1); cum=zeros(n1,1); y0=y;
gsc=cum; znorm=cum;

% Initial values

y(1:n)=ystart(:);

for i=1:n1 y((n1+1)*i)=1.0; end;

t=tstart;

% Main loop

for ITERLYAP=1:nit
%j=0;
% Solutuion of extended ODE system
% for I=.1:.1:.5
  [T,Y] = feval(fcn_integrator,rhs_ext_fcn,[t t+stept],y);
  %j=j+1;
 % I1(j)=I;
  t=t+stept;
```

```
  y=Y(size(Y,1),:);

  for i=1:n1
      for j=1:n1
          y0(n1*i+j)=y(n1*j+i);
      end;
  end;
%  end
% end


%       construct new orthonormal basis by gram-schmidt
%

  znorm(1)=0.0;
  for j=1:n1 znorm(1)=znorm(1)+y0(n1*j+1)^2; end;

  znorm(1)=sqrt(znorm(1));

  for j=1:n1 y0(n1*j+1)=y0(n1*j+1)/znorm(1); end;

  for j=2:n1
      for k=1:(j-1)
          gsc(k)=0.0;
          for l=1:n1 gsc(k)=gsc(k)+y0(n1*l+j)*y0(n1*l+k); end;
      end;
```

```
      for k=1:n1
          for l=1:(j-1)
              y0(n1*k+j)=y0(n1*k+j)-gsc(l)*y0(n1*k+l);
          end;
      end;

      znorm(j)=0.0;
      for k=1:n1 znorm(j)=znorm(j)+y0(n1*k+j)^2; end;
      znorm(j)=sqrt(znorm(j));

      for k=1:n1 y0(n1*k+j)=y0(n1*k+j)/znorm(j); end;
  end;

%
%       update running vector magnitudes
%

  for k=1:n1   cum(k)=cum(k)+log(znorm(k)); end;



%
%       normalize exponent
%
l=[];
  for k=1:n1
      lp(k)=cum(k)/(t-tstart);
      L=[l,lp];
```

```
  end;

%Output modification

  if ITERLYAP==1
     Lexp=lp;
     Texp=t;
  else
     Lexp=[Lexp; lp];
     Texp=[Texp; t];
  end;
%
% %
%
%   if (mod(ITERLYAP,ioutp)==0)
%      fprintf('t=%6.4f',t);
%      for k=1:n1 fprintf(' %10.6f',lp(k)); end;
%      fprintf('\n');
%   end;

  for i=1:n1
      for j=1:n1
          y(n1*j+i)=y0(n1*i+j);
      end;
  end;

    end;
```

```
%% Lyapunov Continue

%%%%single HR system
clear all;
close all;
clc;clf;

[T,Res]=lyapunov(3,@HR_ext,@ode45,0,1,100,[0 0.1 0 ],200);

plot(T,Res);

title('Dynamics of Lyapunov exponents');
xlabel('Time'); ylabel('Lyapunov exponents');

%%%%%%%%%%%%%%%%%%%%%%%%%%%%%%%%%%%%%%%%%%%%%%%%%%%%%%%%%%%%%%%%%%%%%%%%%%%%
```